Master's thesis

NTNU
Norwegian University of Science and Technology
Faculty of Engineering
Department of Geoscience and Petroleum

Carlos Alexandre Pereira de Macedo

Trap style characterization of the Paleocene Egga Member across the Ormen Lange Field

Implications for Hydrocarbon volumetrics

Master's thesis in Petroleum Geosciences
Supervisor: Ståle Emil Johansen, IPT
Co-supervisor: Carlos Aizprua Luna, Phd
June 2022

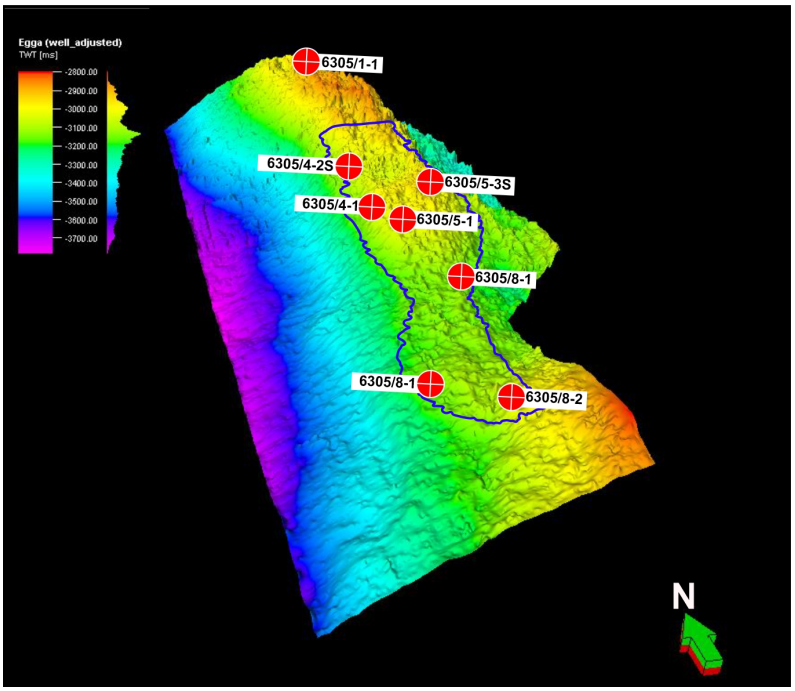

TWT 3D Structure for the Egga Unit

NTNU
Norwegian University of Science and Technology

Carlos Alexandre Pereira de Macedo

Trap style characterization of the Paleocene Egga Member across the Ormen Lange Field

Implications for Hydrocarbon volumetrics

Master's thesis in Petroleum Geosciences
Supervisor: Ståle Emil Johansen, IPT
Co-supervisor: Carlos Aizprua Luna, Phd
June 2022

Norwegian University of Science and Technology
Faculty of Engineering
Department of Geoscience and Petroleum

NTNU
Norwegian University of
Science and Technology

Abstract

The Ormen Lange field is one of the largest gas reservoir offshore mid-Norway, developed as a combined structural-stratigraphic trap. The reservoir type consists of deep marine deposits of excellent quality with a facies deterioration trend towards the fan fringe at its northern margin, coincident with the crest of the structure. Residual gas saturation at the apex of the structure and an overpressure aquifer has led previous authors to propose a hydrodynamic aquifer concept to explain the fluid distribution. However, previous works seem to discuss different observations separately, without direct integration.

Thus, this work focuses on integrating different results to better explain fluid distribution in the field. By looking into the details of each well's stratigraphy, this work further brings the subtle linkage between the underlying structural configuration and the observed reservoir distribution. Furthermore, such configuration may have controlled the facies distribution across the field, with an apparent increase in shale content to the north of the field. A higher shale content may have been prompted to develop polygonal faults through dewatering.

The analysis derived from this work suggests that polygonal faults baffle fluid flow and segment the field, while thin cemented sandstone layers limit the water column's vertical extent. Also, pressure in the field is related to the inflow of over-pressured water from dewatering underlaying smectite-rich shales. Given its origin, water inflow rates are relatively low and localized and do not sustain the premise of a hydrodynamic setting and a subsequent tilted contact. Instead, the polygonal faults serve as a baffle to fluid flow, which in addition to the decrease in pressure to the South, suggests an apparent tilted contact and, therefore, the proposal of a hydrodynamic setting. A hydrostatic setting, where stratigraphic and structural components shift the GWC across the field, is a more plausible concept to explain the fluid distribution.

(This page was meant to be left blank)

Acknowledgements

First, I would like to thank my family for their continuous support during my time at NTNU. Without them, I would not have been able to reach this milestone. I would also like to extend my most profound regards for those who directly or indirectly helped my time in Norway be memorable.

I would also like to thank advisor Ståle Emil Johansen for the support and guidance during my thesis. I am grateful to Carlos Aizprua Luna for the support, guidance, and understanding and for being a source of new ideas and inspiration during this project. More importantly, for giving his time to read, comment and help improve this thesis. Thank you for always being available and making time to help me.

I appreciate NTNU for providing the resources for my success. Thanks to Equinor for providing the topic idea and support. I wish to express my gratitude to NTNU-NPD-SCHLUMBERGER PETREL READY Database for prividing the data needed for the completion of this project

Table of Contents

List of Figures

1 Introduction

The Ormen Lange field is one of the largest gas-producing fields in the Norwegian Continental shelf, with relevant economic impact even after years of production. A trap style characterization and its implications for HC volumetric is essential. The paleocene Egga member is the primary reservoir unit, and its lithostratigraphic outline is the preceding delimiter of net-pay.

Structurally, the Ormen Lange field presents a relatively simple structure. Underlying Jurassic faults and periods of uplift during the Late-Cretaceous and Early-Paleocene have the most significant influence on the structural outlook of the field, which can be defined as an asymmetric syncline. Relative to the reserves estimation, the structure of the field comes into play in the areal extent of the field, and has little to no influence in other aspects. This is because no major structural components affect the main reservoir unit.

Lithostratigraphy, on the other hand, proves to be crucial. The Egga reservoir unit is defined as a turbidity deposit. Furthermore, the turbidity currents were deposited in two primary directions, separating the field into two main zones - North and South. In virtue of its deposition style, the Egga reservoir unit presents sands interbedded with shales, with a downwards trending increase in degree. In this sense, the trap style can be mainly defined as a lateral pitchout, but the north termination is more closely related to faulting and facies degradation. Facies degradation increases towards the North and is closely linked with the depositional setting of the sands. Even though tectonic-related faults are not prevalent in the field, extensive polygonal faults associated with shale distribution are common. The lithostratigraphic relevance arises with thin calcified sandstones in the main reservoir unit, which help delimit the GWC and the lateral/vertical extent of the field. Consequently, being the defining factor for calculating the Net-to-gross ratio, porosity/permeability distributions, and water saturation.

Polygonal faulting is the second most relevant factor for HC volumetric calculations. Facies degradation defines the areal extent of polygonal faulting, which is prevalent in the northern part of the field. Polygonal faulting helps segment the main reservoir units since they are predominately syndepositional, and uplift events helped extend them across the main reservoir unit. Within the field, polygonal faults showcase dynamic sealing properties that influence the flow of gas/water and the leakage rates of the reservoir. However, the properties of these faults are not clearly defined in the literature, and their impact can only be inferred by interpreting different geophysical data sets.

Differential pressures across the field, primarily between the North and south sections, help understand the overall influence of polygonal faulting on the estimation of reserves. Seismic interpretation reveals that the reservoir base is also subject to polygonal faulting with a similar North trend observed at other depth levels. Additionally, the Egga reservoir unit overlays smectite-rich shales, which are de-watered due to a fast deposition mechanism, and serve as the primary source of water inflow to the reservoir. Water from these de-watering shales enters the reservoir with relatively high pressure, sustained by reservoir heterogeneities and a dynamic outline of the polygonal faults. Consequently, with a decrease in facies degradation and polygonal faulting due South, the water column in this region is related to an artisanal flow of the inflowing water in the North. Such effect is also related to the reservoir's proximity to the underlying smectite-rich shales since, at the South of the field, an additonal shale unit separates the sands from the smectite-rich-sales. Consequently, the water inflow is more predominant in the northern section and negligible in the South, based on the observations above.

In situations where the water column is over-pressured relative to the gas column, a hydrodynamic setting is observed. However, this is dependent on the water inflow velocity and its ability to compress the gas. For the Ormen Lange field, water inflow rates are low and do not justify a hydrodynamic setting. This is further highlighted when we account for the lithostratigraphic disposition of the field. A classic flat contact does apply as well since it does not justify the observed gas distribution in the well logs. Literature suggests that the former is the predominant hydraulic setting of the field; the context of the polygonal faults, in addition to the segmentation of the reservoir unit, paints a different image. The contacts are flat within each segment but have slight shifts proportional to the decrease in pressure and heterogeneity due south, giving the perception

of a tilt when the contact is flat. This becomes more evident by separating the field into sections, as the impacts of local heterogeneity become evident, as oscillations in the GWC can be traced to these changes.

Even though the Ormen Lange is a stratigraphic trap predominately characterized by a lateral pitchout, the stratigraphic and structural components introduced by its lithology are the main factors for consideration during reserves estimations. On the one hand, lithostratigraphy helps understand the depositional system and outlines the extent of the main reservoir sands. Subsequently, delimiting the net-to-gross ratio and the parameters for fluid distribution across the field. On the other hand, it is the combination of the stratigraphy and polygonal faulting that ultimately delimit the net pay.The Ormen Lange field is one of the largest gas producing fields in the

1.1 Previous Work

Extensive research exists about the Ormen Lange field. Different authors have modeled the depositional system of the field in an attempt to better understand hydrocarbon distribution across the field. The unique structural and lithostratigraphic disposition of the field makes introduces different uncertainties to the existent models. Additionally, seismic data does not provide enough information to strengthen such models, and a reliance on well data and analogue modeling further increases some of the inferences. Dalland et al. (1988) lithostratigraphic scheme for the Mesozoic and Cenozoic sucessions for offshore mid- and Northern Norway was one of the first introduction to some of the concepts used for the Ormen Lange field.

Dalland's work serves as a cornerstone for some of the more recent models of the field. Furthermore, it was the introduction of the informally named Egga member of the Våle formation that allowed for a different outlook. The introduction of such concept allowed for a better stratigraphic outline, relative to that based on the North Sea terminology. Furthermore, more recent works combine both approachs to depict the overal geologic disposition of the area.

Nicola Møller in his 2003 [Smith and Møller (2003)] and 2004 [Möller et al. (2004)] papers introduces a more detailed overview of the sedimentology and modeling aspects of the field. Here he outlines the different mechanisms behind the observed patterns in the field, such as a depositional model, impacts of faulting and ovearging lithologic considerations of this turbidite system. However, Møller's work serves as an overview and does not expand upon specific oberservations.

Moreover, it is the work of Gjelberg [Gjelberg et al. (2005)] that solidifies previous knowledge about the field. Gjelberg expands upon sedimentation patters and compares the Ormen Lange system with more common examples, to highlight important details and trends. Nevertheless, Gjelberg work serves to consolidate previous knowledge and strength previous modeling postulations.

The work done by Grecula et al. (2015) introduces different concepts and build upon the work done by Dalland, Møller and Gjelberg to paint a more concrete image of the field. Grecula focuses on explaining the development of the field as a combined structural, stratigraphic and hydrodynamic trap. Given the long production history in the field Grecula is able to introduce new finds and solidify the understanding of the reservoir development and outlook.

Notwithstanding, the work done by the aforementioned authors, their findings focus on outlining field and reservoir characteristics. However, little information is given relative to trap styles and their subsequent impact on hydrocarbon volumetric calculations.

1.2 Project Objectives

Previous work in the Ormen Lange field focus on the definition of the geologic, strucutral and lithostratigraphic outline of the field. However, there is scarce information regarding trap styles and their impact on volumetric calculations within the Ormen Lange field. Therefore, this project aims to address/produce the following points:

- Make an in depth seismic interpretation of relevant formations, and use different seismic attributes/well information to outline relevant reservoir properties
- Compare results with existing research, as to assess their reliability and new information
- Analyse trap styles in the field to expand upon the existent knowledge of reservoir architecture
- Assess field connectivity
- Understand the impact of the structural, lithostratigraphic and hydrodynamic setting of the field on hydrocarbon volumetric calculations.

2 Geologic background

The interpretation of stratigraphic traps and their subsequent impact on volumetric calculations relies on a clear and expansive outline of the geology. The primary geologic considerations for the Ormen Lange field relate to reservoir extent/nature, internal sedimentary facies, heterogeneity, and relevant structures (faulting and folding). Figure 1 demonstrates the location of the Ormen Lange field, which lies approximately 100 km offshore Norway within the Møre Basin, and below the Storegga Slide scar. The stratigraphic definition for the relevant facies within the oil field changes. There are two main definitions, one posed by Dalland in his 1988 paper [Dalland et al. (1988)] and the other conforming to the North Sea terminology (NST). For this paper, I will interchangeably use both definitions to convey pertinent information about the reservoir. Moreover, the first step to understanding the geologic disposition of the field is a clear outline of the geologic setting as it pertains to its structural configuration.

Figure 1: Ormen Lange location relative to mainland Norway [Smith and Møller (2003)]

The reservoir is primarily defined by a single seismic reflection, which ties to the Early Paleocene Egga Sandstone member of the Paleocene Tang formation [Dalland et al. (1988)], also called the Våle formation in the NST. The Egga member is underlain by the Springar formation (Jorsalfare in NST) [Smith and Møller (2003)]. Both formations are interpreted as deep marine systems deposited during the Cretaceous/Tertiary transitional period, more specifically between the Maastrichtian and the Danian periods [Möller et al. (2004)].

2.1 Structural Setting

The Ormen Lange structure appears detached from an organized fold system [Möller et al. (2004)]. However, it appears alongside several Cenozoic dome structures, which onset closely coincides with the Early Eocene onset of seafloor spreading in the Norwegian-Greenland Sea [Smith and Møller (2003); Gjelberg et al. (2005)]. Nonetheless, the dome structures are compression features of Cenozoic age, including simple anticlines, domes, reverse faults, and broad-scale inversions [Möller et al. (2004)]. The combination of the spreading in the Norwegian-Greenland sea (ridge push) and the distant effects of alpine tectonics outline the overall compressive stress that gave rise to the Mid-Norway dome structures. This is a weak compressive regime, and it is postulated to still be in play today Möller et al. (2004). Through Borehole breakouts, drilling-induced tension fractures, and hole ovalization, mainly on well 6305/5-1, it is established that the maximum present-day field stress lies between NW-SE to NS [Möller et al. (2004)].

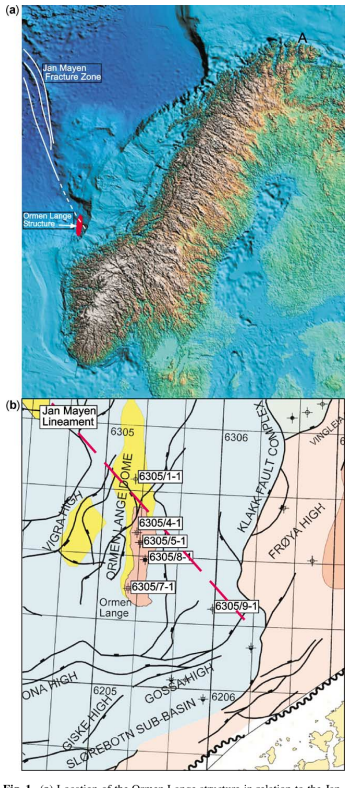

Figure 2: (a) Ormen Lange's position relative to the Jan Mayen Fracture Zone. (b) Jurassic structural elements at the eastern margin of the Møre Basin, including the position of the Ormen Lange field and the Jan Mayen lineament extension towards mainland Norway [Gjelberg et al. (2005)].

The evolution of the Ormen Lange structure is likely to be controlled by the underlying and adjacent structures [Möller et al. (2004)]. For instance, the base Cretaceous unconformity follows the resulting basin configuration controlled by a Jurassic extension with NE-SW oriented faults south of the Trøndelag platform and the Halten terrace [Möller et al. (2004)]. Seismic reflection data demonstrate fault reactivation during the Cretaceous, which, combined with a relative lack of coarse-grained sediments and low sedimentations rate, helped sustain fault-related relief for long periods. The prevalence of fine material sedimentation prevented the development of a smooth topography. The underlying control from the Jurassic structures of the basin extends up to the Early Paleocene, which suggests the presence of several minor sub-basins between the Norwegian mainland and the Møre basin.

However, it's only by looking at turbidity current data and mass flow deposits that such assertion becomes plausible since their distribution is closely linked to slope inclination and topography [Möller et al. (2004)]. Figure 3 demonstrates the distribution of mass flow deposits for the Ormen Lange field and some relevant structures for the field as per Gjelberg et al. (2005) work.

2.2 Lithostratigraphy

Posterior to the definition of the structural settings of the area, a comprehensive stratigraphic outlook is important. The reservoir of the Ormen Lange field is primarily composed of sandstone successions of the Maastrichtian and Danian age. Furthermore, sediments of the Rogaland group, including the reservoir units, have been referred to as the Springar, Tang, and Tare formations[Dalland et al. (1988)]. However, there are no significant sandstone units, which prompted the introduction of the Egga member as an informal name to refer to the Paleocene age sandstone unit found in the area. Further units were introduced to better describe the area, which is the Våle shale, Våle Hetherolithics, and Våle tight at the member level [Grecula et al. (2015); Möller et al. (2004)] (Fig. 4).

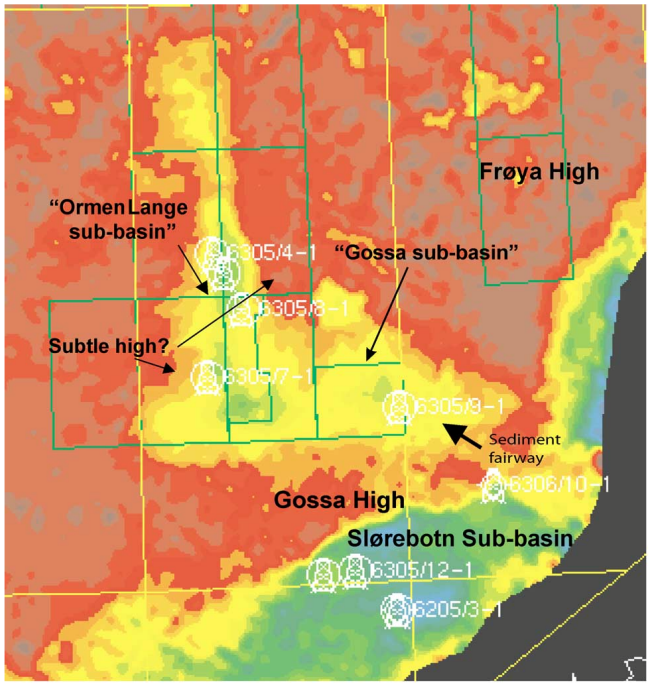

Figure 3: Definition of the sub-basinal areas at the astern margin of the Møre basin, suing time a time isochore map for the Maastrichtian/Lower Paleocene succession [Gjelberg et al. (2005)]. Well location, better represented on Figure 2.

Looking at the Springar Fm, primarily to the Josalfare Eq Member that constitutes the lower reservoir in the field, we observe sandstone, mudstone, and limestone alternations with an increase in sand content upwards. Also, predominate high-density turbidite sands interbedded with thick beds of highly bioturbated mudstones. There is a consistent amount of carbonate sedimentation and the presence of a chalk unit, marking a period of low siliciclastic accumulation [Grecula et al. (2015);Möller et al. (2004)]. This trend contrasts with overlying tertiary rocks, demonstrating minor carbonate cementation and defined extension. Furthermore, the early carbonate cementation of the Josalfare Eq Member increases its susceptibility to brittle deformation [Möller et al. (2004)].

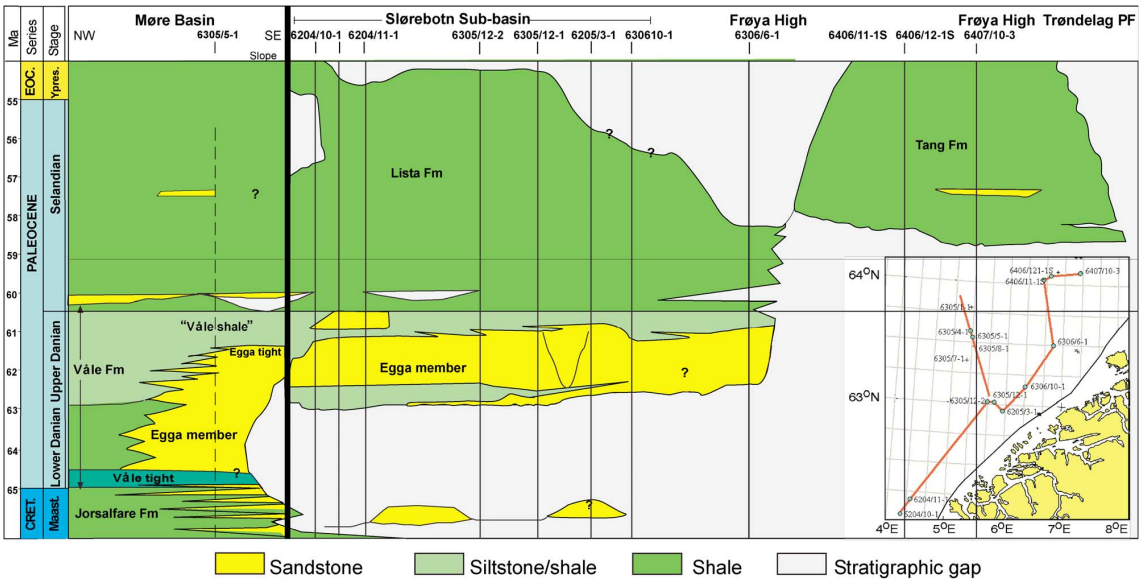

Figure 4: Stratigraphy of the eastern margin of the Møre Basin - Uppermost Cretaceous to Paleocene [Gjelberg et al. (2005)].

Moving to the upper parts of the Maastrichtian units, the increase in sand content becomes more evident as mudstones become progressively thinner, less bioturbated, and turn from a greenish to dark grey color. The recorded mudstone changes are related to external causes, such as climate change, ocean bottom circulation changes, or even bolide impact; there is an additional increase in sedimentation rates relative to underlying and overlying sediments, which resulted from a combination of hemipelagic suspension settling and frequently deposited mud-rich low-density turbidites [Grecula et al. (2015)]. In this sense, stratigraphic development of the Cretaceous reservoir (Maastrichtian units) suggests slow background sedimentation from suspension fallout within a well-oxygenated, open marine basin. Moreover, turbidity current deposition interrupted this prominent trend, allowing for the deposition of sand units [Möller et al. (2004)].

The transition from Cretaceous (Maastrichtian) units to Paleocene (Damian) introduces a different context to the field stratigraphy. Fig 4 showcases changes in stratigraphy across the periods mentioned above. Here we progress from the Springar FM into the Våle FM, where we draw attention to the Egga member. Sandstones in the Egga member have good reservoir qualities (average porosity 26-30 % and permeability 500-1000mD) and present themselves as massive amalgamated or weakly separated sandstones, which may be poorly lithified. Relative to its extent, we can find the Egga member across the field. However, there is a shalling-out trend towards the North of the field, which is further corroborated by a northward decrease in sand fraction to only 40 % around well 6305/4-1 [Gjelberg et al. (2005); Grecula et al. (2015); Möller et al. (2004)]. Thus, significant vertical variations within the Paleocene reservoir warrant a division of the turbidite-dominated Egga member [Gjelberg et al. (2005); Grecula et al. (2015); Möller et al. (2004)]. For this report, we will focus on the following subdivisions of the Egga member (further outlined in Figure 4):

- **Egga Reservoir Unit (ERU):** primary section of the Egga member
- **Våle Tight (VT):** intra reservoir shale
- **Våle Heterolithic Unit (VHU):** composed of sand/shale alternations

Before continuing to the stratigraphic definition of the ERU, it is essential to address the context of the VT and the VHU. The VT contains dark mudstones, siltstone stripes, and very fine sand (pin-striped mudstone) with a low degree of bioturbation and replaces the greenish/grey mudstone observed at the end of the Maastrichtian as the background sedimentation. Nonetheless, the degree of high-density turbidites remains constant between the Maastrichtian and the Danian [Grecula et al. (2015)]. VT thickness increases northward of the field with a correlation between wells 6305/7-1 and 6305/8-1, suggesting a local removal in the southern and southeastern parts of the field due to erosive turbidity currents. However, a 10 m thick section on well 6305/4-1 suggests the possibility of excellent lateral continuity. The VT is postulated to represent the base of gas-bearing sands [Möller et al. (2004)].

Through a biostratigraphic correlation, we can assess the accumulation rate for the ERU to be lower than those observed across the Ormen Lange depositional system. This' starved nature' is consistent with the fringe of the fan located north of the field. Together with the gradual northward thinning of the sand beds and a decrease in the net-to-gross ratio defines the distal pinch-out style of the field as a feathered turbidite system. In this sense, the presence of the VHU is likely to negatively impact reservoir development by reducing oil-in-place volumes at the margins and effective permeability and connectivity. This becomes relevant as fluid fill is linked to depositional patterns via permeability; thus, in zones with decreased reservoir qualities, viscous forces control aquifer behavior and cause an elevation of the free water level (FWL) [Grecula et al. (2015)].

The depositional patterns of the ERU vary. For instance, the ERU is prominent across the eastern margins of the Møre basin and Slørebotn sub-basin, where an unconformity defines the unit's base with the Danian succession, which is usually above Campanian age strata. However, it differs significantly towards the Trøndelag Platform and the Halten Terrace, where no sand is found above the unconformity [Gjelberg et al. (2005)].

Nonetheless, the sand/mudstone alteration is consistent across the field, suggesting that the generation of turbidity currents was sporadic and occurred after long periods of quiescence; however, no breaks in stratigraphy are observed between the Maastrichtian and lower Paleocene successions[Gjelberg et al. (2005); Grecula et al. (2015)]. Furthermore, the ERU has a radial pattern of thickening in the southern part of the field and further represents the depositional outline of the field [Gjelberg et al. (2005); Grecula et al. (2015)].

2.3 Depositional Model

Before expanding upon the deposition disposition of the ERU, we need to first address the sediment supply system. As mentioned, the ERU can be considered a feathered turbidite system that presents itself as " starved. " The definition of the supply system is difficult to reconstruct as it is not preserved due to erosion or uplift-related events. Nonetheless, Smith and Møller (2003) outlines two main observations for the definition of the Ormen Lange field: 1) sand and mud grade material ratios in the deep-water deposits, and 2) sediment accumulation rates relative to vertical aggradation and volume accumulation rates. Moreover, there is a decrease in sand percentage from South to North, suggesting a mud-poor supply system, albeit one delivering mud to distal parts of the field. Smith and Møller (2003) use bulk rate accumulation rates across different wells to delimit the following trends:

- Wells 6305/7-1 and 6305/8-1 showcase a lateral compensation effect
- Increased bulk sediment accumulation rates between early to late Danian times]
- An overall weak decay in accumulation rates from South to North
- Extremely low bulk sediment accumulation rates, relative to similar turbidite systems

The latter point demonstrates the 'starved' nature of the ERU and the Ormen Lange field. A possible explanation for such behavior is the Sløre botn sub-basin acting as a filter, leading to reduced sediment transportation into the basin. While a significant amount of sediments translated into deep-water deposits, they were sequestrated in the perched basin, with low-frequency resedimentation (sporadic turbidity deposition) transferring sediments basinward towards the Møre basin floor [Smith and Møller (2003)]. Looking into volume and run-out characteristics of sediment gravity flows beyond the Sløre botn sub-basin, we see that they deposited a laterally expansive fan despite low sediment accumulation rates [Smith and Møller (2003)], which a few key points can justify:

- Low sediment yields from adjacent subaerial drainage basins
- The presence of subsiding "sediment traps" close to the early Paleocene coastline
- A sand-dominated supply system originated from surf zones of sandy spits built along the shore

Notwithstanding the above suppositions, any evidence supporting them has been erased. However, if we gather the above information relative to the geologic setting, lithostratigraphy and supply system information we arrive upon the depositional system described on Figure 5, which elements are outlined in Figure 6 and expanded upon in Figure 7 [Grecula et al. (2015); Möller et al. (2004)]. These models include three main depositional elements:

- **Channel zone deposits:** not common within the Ormen Lange field but is prevalent within the sedimentary fairway to the east. Proximally located relative to the system and is characterized by thick beds of amalgamated high-density turbidites, which present themselves in a fining - and thinning upwards pattern,

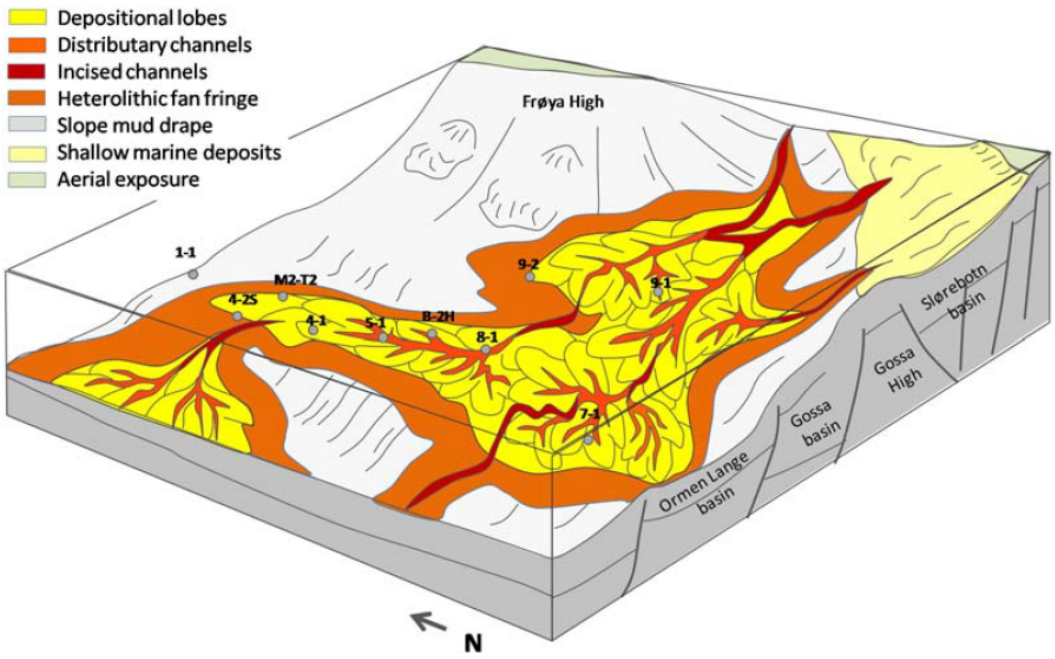

Figure 5: Conceptual model for the Ormen Lange deep-water fan system [Grecula et al. (2015)].

- **Channelized Lobe deposits:** relatively common within the field, consisting of amalgamated high-density turbidites in alteration with classical turbidites occasionally draped by a mudstone package. Mainly dominated by shallow branching channels and sandy overbank deposits. Furthermore, separating both in-channel and overbank deposits is difficult since thick high-density turbidites dominate both.
- **Frontal splay or fan fringe deposits:** consists of low-density and high-density classical turbidites, in alteration with fine-grained, thin turbidites and hemipelagic mudstones. Usually laterally connected to the previous facies.

The Ormen Lange sub-basin is the main target of investigation since it is of Cretaceous-Paleocene age, north-south oriented depression extending toward well 6305/1-1, and most Paleocene aged sands pinch-out. Towards the NW, the fan expands downdip of topographical confinement due to a topographical high west of the field. In addition to the field reorientation from East-West to North-South, there is evidence of a thickness change towards the west, which highlights subtle topographical confinement during the deposition of the ERU [Grecula et al. (2015); Möller et al. (2004)].

Seismic interpretation of the Josalfare Eq Member is limited. However, quantitative observations across the field suggest that the thickness of the sub-Egga units presents an excellent spatial correlation to the ERU, mainly in the south of the field. Overall the depositional models (Fig. 5 and Fig. 7) suggest that through the presence of a series of linked slope depocenters, the sand-rich Ormen Lange sediment supply system evolved around underlying extensional faults (potentially reactivated Triassic aged faults).

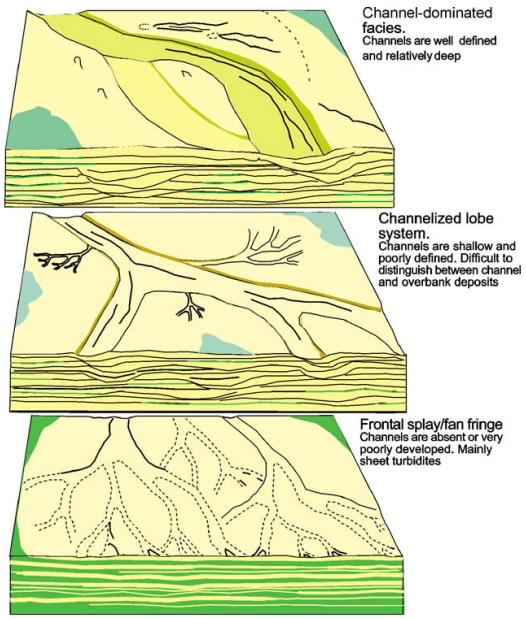

Figure 6: Depositional elements of the Ormen Lange field [Gjelberg et al. (2005)]

Additionally, sediment transportation depends upon accommodation locally at a high angle to the regional dip direction. Finally, steeper slopes might have led to local incisions and bypass or steeper slope ramps where spills from the up-dip confined fan are observed [Grecula et al. (2015)]. The main point of the demonstrated models is to showcase the feathered turbidite deposit along the Ormen Lang field. Also, it serves as a baseline understanding of sediment supply, transportation, and disposition.

2.4 Reservoir Outline

2.4.1 Reservoir Facies

The depositional model outlines the geologic context for the reservoir. However, delineating the impacts of stratigraphic traps on volumetric calculation requires a finer delimitation of reservoir characteristics. Sedimentary facies serve as building blocks for reservoir architecture [Grecula et al. (2015)], and their definition defines our understanding of the reservoir. Gjelberg et al. (2005) uses an extensive definition of the sedimentary facies. However, a more simplistic yet encompassing definition is better suited. Thus, Möller et al. (2004) definition will be used henceforth and is as follows:

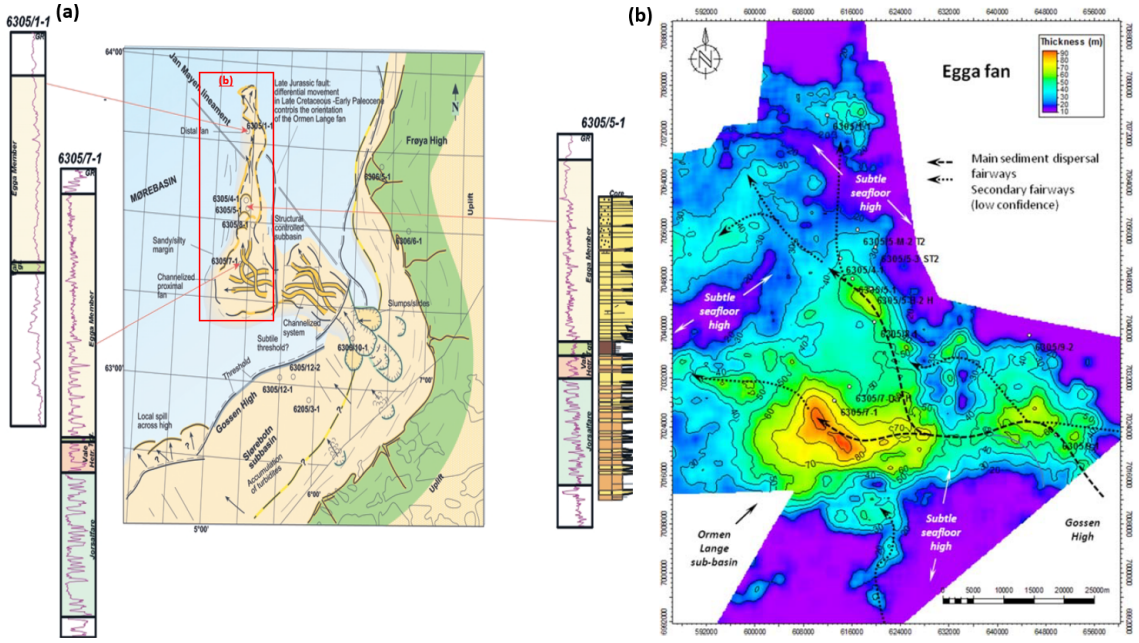

Figure 7: (a) Depositional model and characteristic well observations [Möller et al. (2004)]. (b) ERU regional thickness map showcasing sediment transport fairways [Grecula et al. (2015)]

- **C-sands:** vary from moderately to well-sorted sub-arkosic sandstone with 29% average porosity and 870 mD average permeability (ranging from 300 mD to 3000 mD) accounts for the majority of the ERU and the basal parts of high-turbidity currents, and to a lesser extent low-turbidity deposits [Gjelberg et al. (2005))]. Moreover, encompasses water escape-related structures with an overall uniform grain size distribution. Coal fragments are also frequent, primarily along the upper part of the beds.
- **G-Sand:** contains water-bearing greenish/grey clay-bearing sandstones with a 26% average porosity and 277 mD average permeability (ranging from 1 mD to 3000 mD). Generally associated with the higher part of turbidity deposits, its clay content is related to waning flow, bioturbation, or diagenesis. The preservation of these units is assumed to be low across the ERU due to topographic confinement and high energy of coarse-grained turbidity deposition. Has an estimated volume fraction below 15%

- **Shales:** these facies include shaly and silty sandstones. It is assumed to have no recoverable HC due to low permeability and high water saturation. Has a variable lateral extension from a few meters on the channel facies to several meters in the lobe facies. Ranging from highly bioturbated greenish sandy mudstones, green, greenish-grey, and grey mudstones to pin-striped mudstones.
- **Carbonate cemented rocks:** carbonate cemented sandstones, with reduced thickness (generally below a meter in thickness). The occurrence of this unit is rare on the ERU, but its frequency increases as we move towards the underlying upper cretaceous. It is considered to be non-permeable and fully water-saturated. Overall, its occurrence does not present a barrier for gas flow, except for inner ERU occurrences, which might mitigate vertical fluid flow.

2.4.2 Reservoir Architecture

From seismic attributes and similarities across the wells in the field, we can define Ormen Lange's geometry as being tabular. This is further supported by a lack of strong lateral segmentation across the reservoir. More importantly, seismic data does not clearly define the architecture of the field, and we need to rely on stratigraphic trends to define reservoir architecture [Smith and Møller (2003)].

Lateral variations for sand and mud percentage amalgamation relative to the proximal/axial to distal/lateral subenvironments are evident [Smith and Møller (2003)]. Ormen Lange is a mud-poor system with a high occurrence of turbidity deposits. Therefore, erosional amalgamation towards axial positions rather than lateral ones is frequent and helps delimit the reservoir structure [Smith and Møller (2003)]. Within the reservoir, mudstones extend from proximal/axial to distal/lateral settings and decrease with the upwards increase in amalgamation. Thus, mudstones are assumed to become less continuous upsection and more continuous in a down-paleoflow direction [Smith and Møller (2003)].

Additionally, the thinning rates across the field are low and do not exceed half a degree, suggesting that the termination of the field depicts subtle onlaps. This is further corroborated by the avoidance pattern of Danian sandstones relative to buried Upper Triassic/Lower Cretaceous structural highs [Smith and Møller (2003)]. These structural highs might have influenced paleobathemetry through differential compaction of the mudstones, thus, leading to the postulated onlap terminations [Smith and Møller (2003)].

Relative to topography, it is proposed that it leads to a gradual decrease in sand content, bed thickness, and vertical amalgamation in areas with subtle topography. However, within steep bounding slopes, there is a more abrupt change. Looking at Figure 8 we observe that the axial depositional subenvironment is traced into the lobe-dominate part of the fan, which demonstrates vertical amalgamation despite the presence of well-defined channels. Furthermore, Figure 8 exhibits the overall ERU palaeo-transport direction to have a wide spread from North to south, but with a dominant NW component [Grecula et al. (2015)].

The ERU thickness map (Fig. 8) demonstrates the presence of two depocenters oriented NW-SE and a lateral shift. For this unit, there is a disconnect between seismic and well thickness trends as we approach well 6305/7-1, potentially due to off-axis deposition, which would indicate the deposition of additional lobe complexes in this area. In opposition to the Egga and Jorsalfare units, the Våle heterolytic shows a different orientation and character, suggesting it is part of a different fan system relative to the overlying and underlying units [Grecula et al. (2015)].

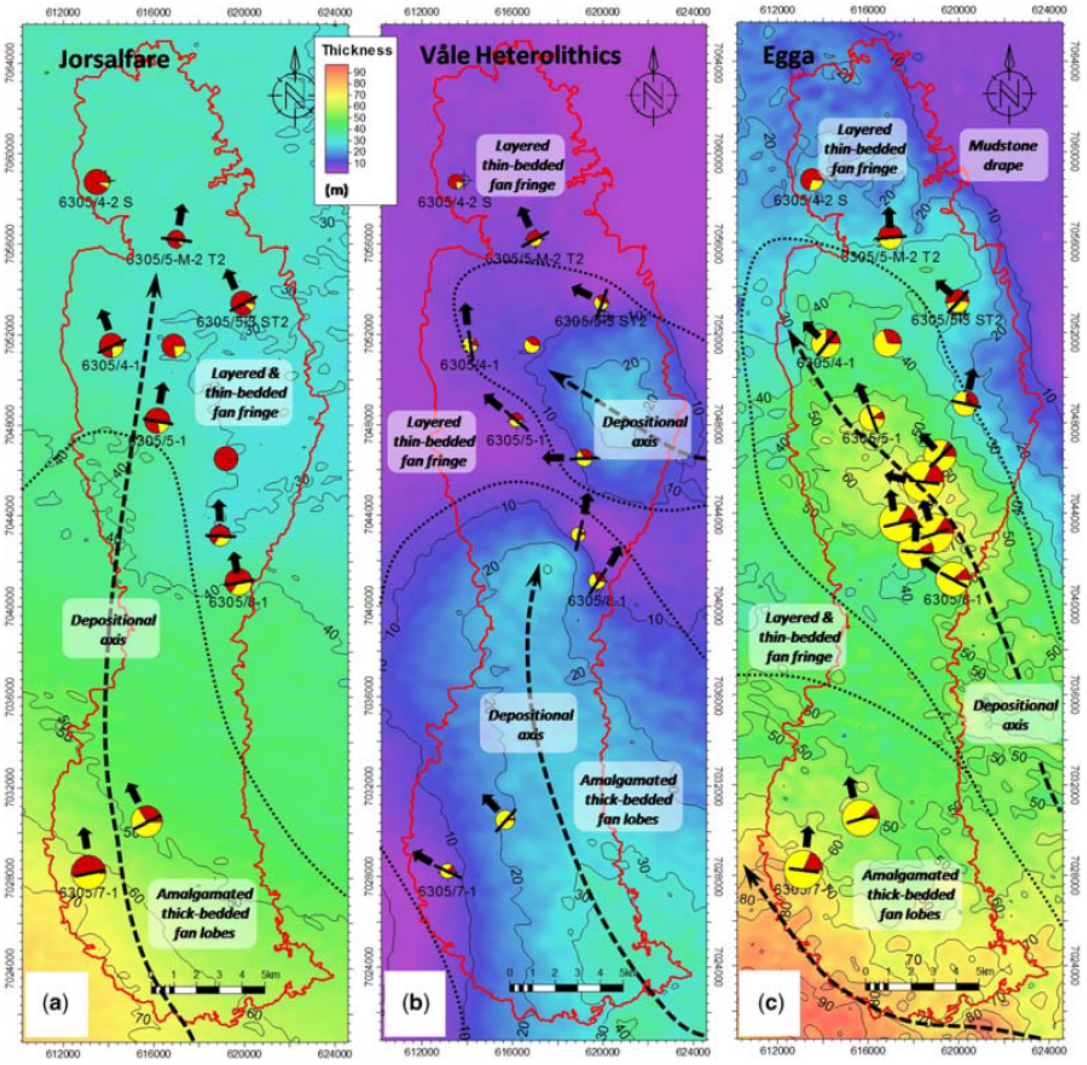

Figure 8: Thickness maps for three units of interest in the Ormen Lange field showcasing depositional environments and composite depositional axis. Pie charts indicate the well proportion of clean sand to hetherolithics, while the size indicates the gross thickness. The thin black lines over the pie charts indicate the average strike of the residual bedding. The dashed black lines indicate the interpretation of the average paleocurrent direction. (a) Jorsalfare thickness map ; (b) Våle hetherolithics thickness map; (c) Egga member thickness map. [Grecula et al. (2015)]

2.4.3 Reservoir quality trends, connectivity and fluid fill

After defining the architecture of the reservoir, we need to analyze its intrinsic properties. For the Ormen Lange field, the definition of clean sand fraction (CSF) presents a more reliable approach for reservoir quality trends. Additionally, permeability is sufficiently high in most of its rocks for gas flow, with effective permeability being dependent upon the variation of CSF in different parts of the field (Fig 9). Reservoir quality uncertainty can also be related to petrophysical evaluations of permeability [Grecula et al. (2015)]. Nevertheless, the Ormen Lange field presents an overall good reservoir quality, and its geologic setting warrants an exploration of formation connectivity.

Faults and drapes are expected within the field and increase in frequency and intensity as we move North. For the Ormen Lange field, reservoir connectivity is linked to the size of depositional bodies, continuity of heterolithic intervals, and the frequency and throw of reservoir faults. Grecula et al. (2015) suggests that combining the above parameters makes true stratigraphic compartmentalization impossible. Nevertheless, the field contains above 400 highly linked NE-SW-oriented normal faults. Fauls are prevalently polygonal and strata-bound and are related to sediment de-watering at shallow depths.

Furthermore, faulting is syndepositional for at least the early parts of the deformation. Looking at pressure data, it is possible to infer that the Omern Lange field is locally baffled but overall well connected [Grecula et al. (2015)]. Moreover, the fluid fill within the reservoir is postulated to follow a hydrodynamic regime, which dictates fluid distribution based on two forces:

- Gravity forces
- Viscous forces created by hydrodynamic flow

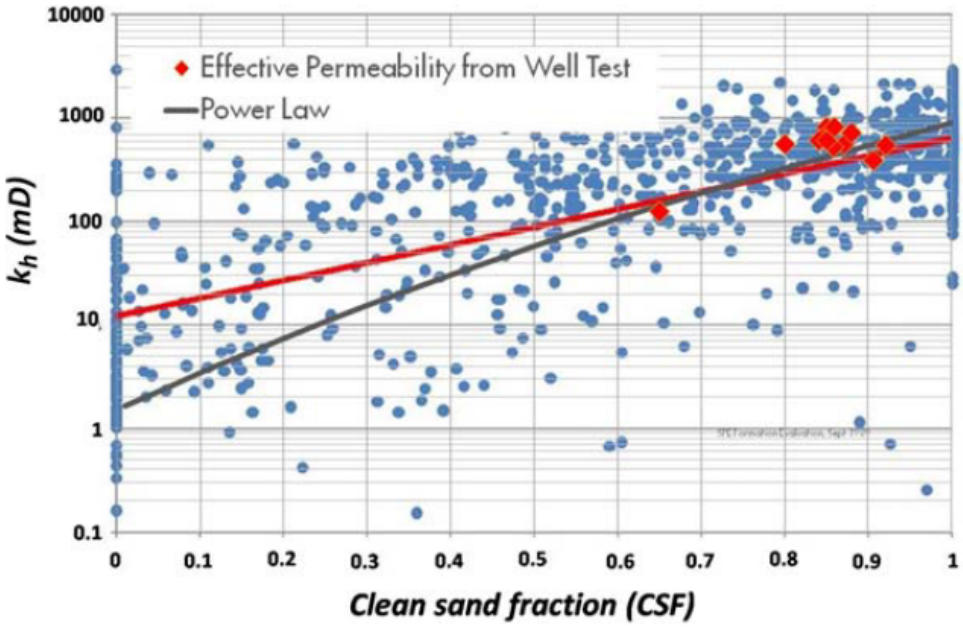

Figure 9: Relation between CSF and horizontal permability accross the Ormen Lange field. Blue dots represent upscaled core-derived horizontal permeability in the reservoir model, and red diamonds horizontal permeability from well tests. Average horizontal permeability decreases along side CSF, which is lowest towards the findges of the fan. . [Grecula et al. (2015)]

Under a hydrodynamic regime, the gas-water contact is proportional to the aquifer pressure gradient and inversely proportional to permeability. Thus, with the differential distribution of CSF across the field, the base of the hydrodynamic column varies in response to the field heterogeneity. Consequently. The FWL is likely to be related to the geology of the field, which would increase towards the edge of good sands within the overarching trend dictated by the water source [Grecula et al. (2015)]. The hydrodynamic model explains the observed fluid distribution on the field, but a more concrete delimitation is necessary.

3 Important Considerations

The previous sections focus on outlining the geologic disposition of the field. However, an outline of key concepts is essential as we progress forward. This serves to guide our interpretation and contextualize observations. For instance, the literature often refers to the DHI area within the Ormen Lange field but does not expand on which indicators are present or how they impact the data. Therefore, this section guides future observations as we progress toward our findings and subsequent discussion.

3.1 Direct Hydrocarbon Indicators

Direct hydrocarbon indicators symbolize anomalous seismic responses due to the presence of hydrocarbons. Furthermore, DHIs occurs when a change in pore fluids leads to changes in the bulk elastic properties of the rock. Such changes are marked by variations in amplitude in the seismic data. Nonetheless, not all amplitude anomalies are due to the presence of HC and need to be analyzed within the geologic context of the field.

Generally, DHIs are caused by a reduction in impedance due to a substantial lowering of the bulk modulus of pore-fluid. Nevertheless, the rock and fluid properties in conjunction with the geologic setting define the DHI as they directly impact the elastic properties and density of the rock and, subsequently, the seismic data ([Nanda (2016a)]. Three common amplitude anomalies are associated with gas saturation in a reservoir - bright, dim and flat spots.

Bright spots are more commonly linked to sand reservoirs capped by shale. When the rock is filled with gas, its velocity is reduced, which causes a negative contrast at the interface. Consequently, a bright amplitude is evident at the top of the gas sand. If a gas-water contact is present, a weak reflection with weak polarity at the flanks, while the gas-filled section provides a bright reflection with reverse polarity [Nanda (2016a); Wiki (2020)]. Dim spots follow a similar stance but present weak amplitudes with positive reflection coefficients.

Additionally, these effects are common for gas-saturated carbonates but can also be linked to high-impedance older sandstones capped by lower velocity shales [Nanda (2016a); Wiki (2020)]. Flat spots are more closely linked with gas water contacts and present as moderate to high amplitude, horizontal reflections with positive polarity. In this instance, the reflection is not influenced by lithology but by fluid contacts, and impedance is related to the fluid density difference between gas and water [Nanda (2016a); Wiki (2020)].

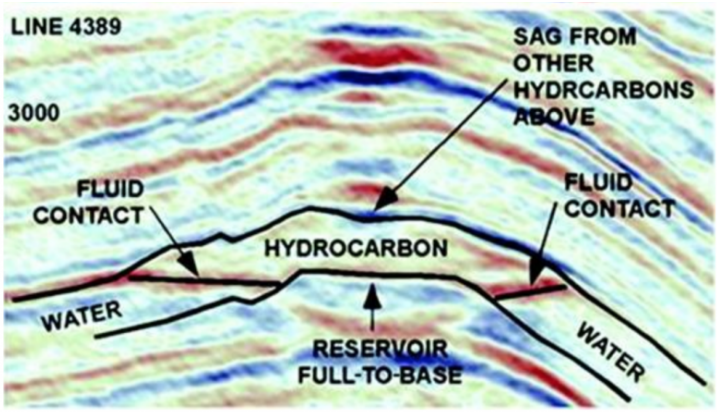

Figure 10: Example of different DHI's [Wiki (2020)]

Furthermore, the interpretation of amplitude changes is valuable and serves as a first-order indication. However, amplitude anomalies alone are unreliable indicators and require more information to outline relevant information. Velocity analysis, polarity, sagging effects, and shadows are additional mechanisms to validate DHIs. Velocity analysis of seismic NMO (normal move out) velocities is useful to identify significant lowering of internal velocities caused by gas within the reservoir. However, this technic is limited by its ability to resolve the top and bottom reflection of the reservoir [Nanda (2016a)]. Polarity delimitation is crucial as the DHI mentioned above is directly linked with distinct reflection coefficient criteria. Additionally, polarities are reliable indicators of reservoir lithology, but their delimitation is difficult due to limitations in the seismic data [Nanda (2016a); Wiki (2020)]. Furthermore, sagging is more concrete compared to the validation technics mentioned above. Sagging is an artifact caused by lower velocities due to the presence of gas. Consequently, the arrival times for reflectors are delayed and may indicate a local depression below the gas zone. This depression is called a 'sag' or 'pull-down' effect [Nanda (2016a); Wiki (2020)]. Figure 10, illustrates some of the aforementioned effects.

Another validation method is low-frequency shadows below bright spots, which are often associated with energy absorption due to the presence of gas. However, this is an occurrence with low reliability, as its mechanisms are not well established, and its occurrence is not adequately explained. Nonetheless, its recurrent occurrence in many gas reservoirs makes it a DHI, but its analysis must account for its low reliability [Nanda (2016a)]. DHIs are important during seismic interpretation, but the intrinsic limitation of the data and the mechanism themselves require a more profound outlook.

Understanding the limitation of DHI is essential. For instance, the presence of gas is not the only cause of bright spots; volcanic sills, calcareous sands, coal beds, and over-pressured sands, among others, can cause the same effect [Nanda (2016a)]. Furthermore, polarity would be a suitable validation mechanism, but its implementation is not practical and often yields incorrect results. Additionally, DHIs are not sensitive to saturation variations, which can be misleading while interpreting [Nanda (2016b)]. However, some DHIs, such as gas chimneys, are easier to identify since they have a particular signature and are associated with specific circumstances. The main takeaway is that DHIs are not all-encompassing and require a careful analysis of the lithological, stratigraphical, and morphological analysis to validate any observations. Modern techniques such as AVO, shear wave analysis, and inversion help mitigate the shortcomings, but cation during interpretation is vital while using DHIs.

3.2 AVO and Velocity Analysis

DHIs, serve as a first-order indication for HC accumulation. Therefore, we need to discuss some modern validation techniques for these indicators, which in this case are AVO and velocity analysis.

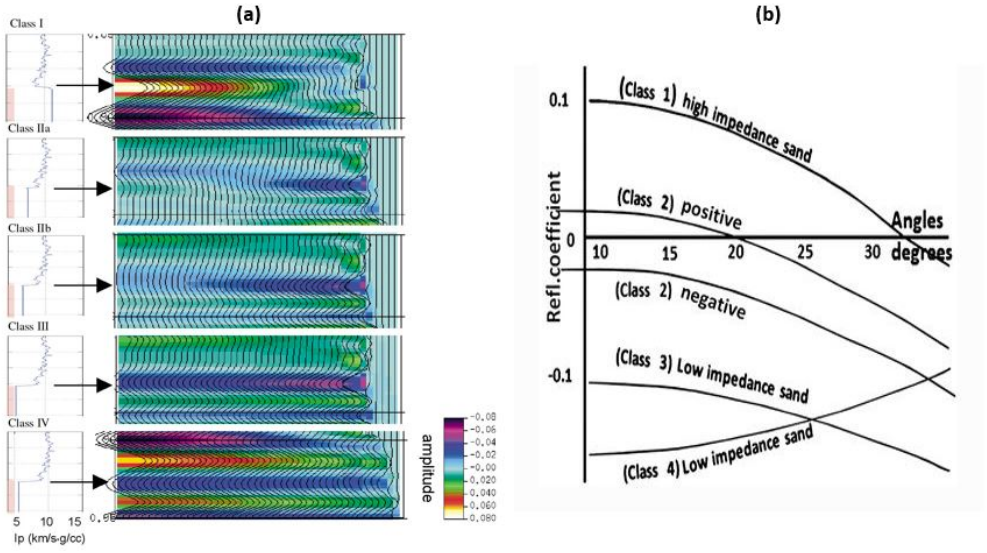

Figure 11: Different AVO classes. (a) Illustration of different types of AVO for gas charged clastic reservoirs [Yongyu Li and Xu (2003)]. Illustration for the four classified P-amplitude variation with offset from top gas-saturated sand reflections [Nanda (2016b)].

3.2.1 AVO Analysis

AVO stands for amplitude variation with offset, which outlines changes in reflection amplitude due to a change in distance between source and receiver (offset). The AVO analysis is a more robust way to validate bright spots relative to traditional P/S-wave stacks [Nanda (2016b)]. Nonetheless, AVO primarily focuses on P-wave amplitudes with offset, but as a phenomenon, it includes shear waves and their velocity. As a phenomenon, AVO arises as the P-reflectivity for inclined incident waves vary with the angle of incidence. This is because a mode conversion of energy generates S-waves, which are more prevalent at larger offsets [Nanda (2016b)]. P-amplitude variations with

offset associated with shear wave generation are directly linked to contrasts in physical properties, such as V_p, V_S, and density [Nanda (2016b)]. AVO effects are closely related to DHIs because they can be quantified and classified based on impedance/reflectivity contrasts [Nanda (2016b)]. Figure 11 demonstrates the different AVO classes based on changes in impedance/reflectivity with offset.

Class I AVO corresponds to high impedance gas sands, and the top of the reservoir showcases a peak that decreases with offset and a change in polarity. The interface between sand and shale has a positive contrast for V_P and density but a negative V_P/V_s [Yongyu Li and Xu (2003)]. Additionally, the amplitude reaches a maximum value at normal incidence and changes polarity (becomes negative) after a certain incidence angle due to the negative gradient of this class [Nanda (2016b);Yongyu Li and Xu (2003)]. Furthermore, indicating high amplitudes at the Near offset followed by a decay with offset, as illustrated in Figure 11(a). However, such effects are hard to find as near and far offset traces with opposite polarities are summed up over the gather, resulting in poor or no reflections [Nanda (2016b)]. A similar trend is observed in Class III AVO, which describes low-impedance gas sands.

For Class III AVO, we observe large negative normal incidence reflection coefficients, which are directly proportional to offset. This class of AVO represents classical bright spots, where P-impedance contrasts with velocity, density, and V_P/V_s ratio at the interface. Different from Class I, Class III AVO showcases an increase in amplitude with an increase in offset in real models (Figure 11(a)) [Nanda (2016b); Yongyu Li and Xu (2003)].

Class II AVO represents near-zero impedance gas sands, where a weak peak or trough showcases the top of the reservoir. Thus, we can observe an increase (Class IIa) or decrease (Class IIb) of the peak/through with offset. Class IIa anomalies are likely to be missed in the normal stack section, while Class II b anomalies are more noticeable (provided large offsets and adequate AVO record). The classification of this class of AVO needs close inspection, as an increase in amplitude may indicate both water or HC depending on the setting [Nanda (2016b); Yongyu Li and Xu (2003)].

Class IV AVO is related to low-impedance gas sand with a hard top seal, where a trough represents the top reservoir, and its amplitude is inversely proportional to offset. Here we see a positive gradient due to the impedance contrasts and V_P/V_s between the hard seal and the gas sand. In this instance, the V_S of the hard seal is higher than the gas sand creating a strong negative contrast, but reflectivity follows the same trend as amplitudes, decreasing with offset [Nanda (2016b); Yongyu Li and Xu (2003)]. Nanda (2016b)], summarizes the AVO responses as follows:

- **Class I:** Positive reflectivity at normal incidence (R_0), high amplitude decreasing with offset and negative gradient
- **Class III:** Negative R_0, high amplitude increasing with offset, negative gradient
- **Class IV:** Negative R_0, high amplitude decreasing with offset, positive gradient

As a method, AVO assumes that the observed effects are associated with isotropic and homogeneous layers. Therefore, the presence of thin-beds, composite events, multiples, noise, overburden anisotropy, and heterogeneity introduces variables not fully covered by AVO. Also, it is not suitable for all types of reservoirs and depths, being more appropriate for shallow siliciclastic reservoirs within the AVO window [Nanda (2016b)].

3.2.2 Velocity Analysis

AVO's lack of dependability (in some circumstances) lies in its reliance on amplitude. Therefore, a more direct and reliable approach is necessary to exclude different factors impacting amplitude and directly access rock-fluid properties. Velocity analysis is a more dependable approach to DHI validation. Sedimentary rocks have different properties that affect P/S-waves differently. Generally, P-waves are more sensitive to these changes and are more commonly used for reservoir property prediction, while S-wave sensitivity to fluid allows us to detect fluid-bearing zones [Nanda (2016b)]. Therefore, we can better describe different rock properties by joining both waves within a more encompassing parameter, the V_P/V_S ratio [Nanda (2016b)].

Furthermore, the difference in propagation between compressional and transverse waves offers predictable outcomes. For instance, the compressibility of fluids affects P-waves but does not impact S-waves. Consequently, rocks with gas will show lower P-wave velocities than those containing water, meaning that we should expect the V_P/V_S ratio to showcase significant differences between both examples [Nanda (2016b)]. V_P/V_S ratio is an excellent indicator of pore fluid and helps access lithologic differences between formations. Its relative ease of application and effectiveness makes velocity analysis a more dependable method to validate DHIs. Nonetheless, both AVO and velocity analysis have their drawbacks and should be accessed within the context of the area.

3.3 Trap Styles

DHI allows us to locate potential HC accumulation within our seismic data, but they need to occur in a coherent setting to allow for such correlation. Oil traps are usually related to either stratigraphic or structural traps. The Ormen Lange field is primarily linked to stratigraphical traps, with some structural elements. Thus, a proper definition of stratigraphical traps allows for a better interpretation and definition of field properties.

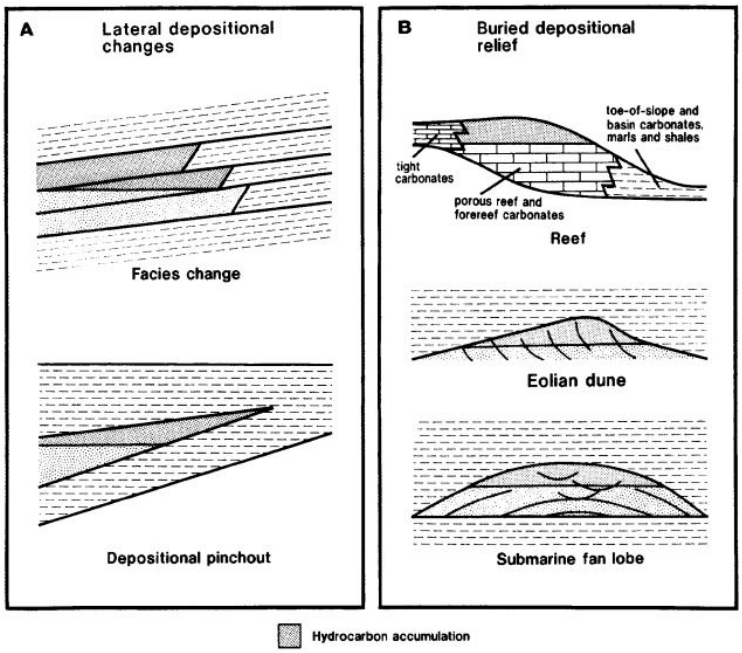

Figure 12: Example of primary or depositional stratigraphic traps. (a) Illustration of depositional traps associated with lateral changes. (b) Illustration of stratigraphic traps associated with buried depositional relief [Biddle and Wielchowsky (1994)].

There are three main stratigraphic traps suggested by Biddle and Wielchowsky (1994) - primary or depositional traps, stratigraphic traps associated with unconformities, and secondary stratigraphic traps. Depositional traps are subdivided into two - one is associated with lateral changes and the other with depositional relief. For traps reliant on lateral depositional changes, it is common to have either abrupt or gradual transition between reservoir and seal, a structural component, and are associated with combined traps (structural-stratigraphic) [Biddle and Wielchowsky (1994)]. However, traps associated with depositional relief tend to have less structural dependence and are more closely linked to the mechanism of deposition (e.g., submarine fan deposits)[Biddle and Wielchowsky (1994)]. Traps associated with unconformities are primarily linked to the deposition of reservoir/seal rocks and have a small structural dependence [Biddle and Wielchowsky (1994)]. On the other hand, secondary stratigraphical traps occur due to post-depositional alteration, which leads to the formation of reservoir-quality rocks from non-reservoir rocks or the creation of seals from previous reservoirs [Biddle and Wielchowsky (1994)].

Stratigraphic traps are, to some extent controlled by the structural disposition of the area, albeit

pre- or syndepositional. Structural elements and topography directly impact reservoir distribution and depositional geometry [Biddle and Wielchowsky (1994); Stirling et al. (2015)]. Stirling et al. (2015), defines the controlling structural elements into three types (Fig 13):

- **Pre-existing:** elemets that help shape the basin physiography prior to deposition
- **Syndepositional:** elements that are contemporaneously forming with reservoir deposition and help with reservoir distribution
- **Post-depositional:** elements that form after the deposition of the reservoir and may change its distribution.

In this context, the structures' origin is irrelevant, and definitions are purely descriptive. Nonetheless, when it comes to basin-forming mechanisms, there are two pertinent classes, flexural subsidence in response to loading and extensional rifting. The latter is of particular importance for the Norwegian Sea and allows for subdivision of the basin deposition relative to the rifting event [Stirling et al. (2015)]. It is worth mentioning that traps can also be defined as combination traps or hydrodynamic traps. Combination traps encompass characteristics of both structural and stratigraphic traps. However, hydrodynamic traps are more related to fluid contact and their distribution in the reservoir rather than a concrete stratigraphic/structural component. This section serves as a small summary of the different styles of stratigraphic traps and what to expect for each one.

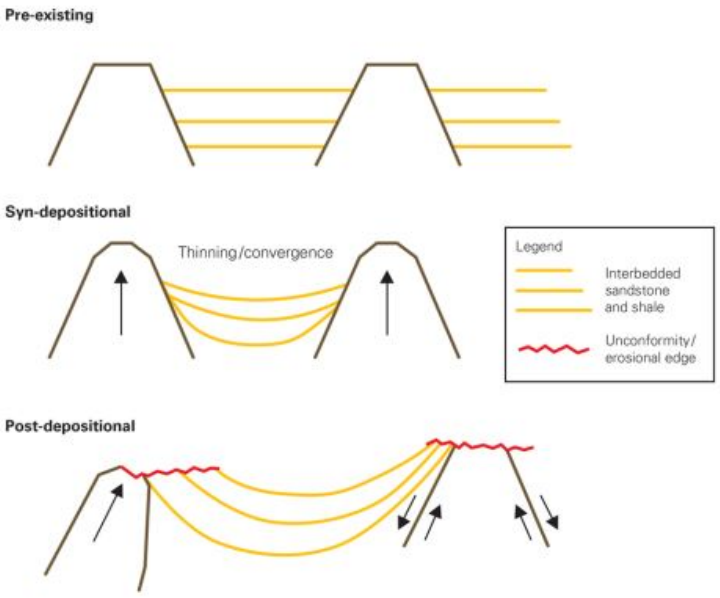

Figure 13: Structural element control on the development of edges [Stirling et al. (2015)].

3.4 Hydrodynamic Aquifers

The project aims to access the trap styles of the Egga member of the Ormen Lange field and its subsequent impact on HC volumetric calculations. Furthermore, to determine the impact of trap-style on HC volumetric, we need to talk about GWC (gas-water contact)/OWC (oil-water contact) and how they related to the intrinsic properties of the field and volumetric calculations.

In a general sense, OWC/GWC are often depicted as linear. Such assumption is sound when assessing reservoirs with minor heterogeneity, which have a small or negligible impact on the tilt of such contacts. Realistically contacts vary with depth across the reservoir as a direct response to structural, stratigraphic, and geomorphological.

Contact variation with depth can indicate barriers to fluid flow within the reservoir or a hydrodynamic aquifer. Furthermore, such changes may be linked to spatially varying pressures or temperatures. The presence of an underlying hydrodynamic aquifer also leads to continuous tilting of the OWCs. Therefore, the implementation of coherent interpretation is a stepping stone to understanding contact variations as results can be conflicting since compartmentalization and the presence of a hydrodynamic aquifer yield similar results. Problems in differentiation arise with the relationship between rock/fluid properties and the hydrodynamic head to the final steady-state inclination of the oil-water contact [Muggeridge and Mahmode (2012)].

Muggeridge and Mahmode (2012), presents a numerical approach to access the time it takes for contacts to reach a steady-state and how different components subsequently impact it. In her approach, she uses Hubbert's (1953) original work to develop two equations to assess the angle of dip of the contact (Eq. 1) as well as the time to steady-state (Eq. 2). Muggeridge and Mahmode (2012), outlines Hubbert's equation to assess the angle of dip of the contact as follows:

$$\tan(\theta) = \frac{h_2 - h_1}{L_{12}} = \frac{k_{eff}}{k_{12}\Delta\rho g}\frac{\Delta P_{aq}}{L} \tag{1}$$

Where θ is the angle of dip of the contact, h is the contact measured depth in meters below the reservoir top (subscripts refer to the well), L is the distance between two wells, k_{eff} is the effective reservoir permeability, k_{12} is the effective permeability between well 1 and 2, ΔP_{aq} is the difference in aquifer pressure between well 1 and 2, $\Delta\rho$ is the water-oil (or water-gas) density difference, and g is the acceleration due to gravity. Moreover, this equation describes Hubbert's steady-state analysis and is used by Muggeridge and Mahmode (2012) to model changes in contact angle. Furthermore, Muggeridge and Mahmode (2012) uses England et al. (1995) to outline the time in seconds required for the contact interface to become approximately horizontal (steady-state) as follows:

$$t = (\frac{L}{H})^2 * \frac{25\phi\overline{\mu}H}{4k_h g\Delta\rho} \tag{2}$$

where t is time in seconds, H is the reservoir thickness in meters, ϕ is the porosity, k_h is the horizontal permeability, $\overline{\mu}$ is the arithmetic mean viscosity of the two fluids. Both equations serve to outline the main properties affecting the estimation of the OWC/GWC. The implementation of Eq. 1 and Eq. 2 by Muggeridge and Mahmode (2012) is congruent with the previous results for homogeneous reservoirs and allowed for an extension to heterogeneous settings.

As a whole, heterogeneities will increase the time taken for OWC to reach a steady-state, often by as much as an order of magnitude. However, there are scenarios where the OWC for the heterogeneous contact reaches a steady-state faster than its counterpart. Nonetheless, Figure 14 illustrates how different heterogeneity impacts the development of a tilted OWC. Muggeridge and Mahmode (2012) models highlight the importance of a good delineation and data interpretation while looking at tilted OWC. This is because different heterogeneities introduce variability on the pressure-vs-depth graphs, which might be misleading. Therefore, with differential permeability due to heterogeneity, the determination of the OWC in the region becomes cumbersome [Muggeridge and Mahmode (2012)].

When dealing with hydrodynamic aquifers, we must understand that heterogeneity substantially impacts pressure distribution and fluid flow, requiring a close inspection of the data during interpretation. It is important to note that observation posed by Muggeridge and Mahmode (2012) might not be applicable for GWC, as gas is more compressible, and the steady-state time delineation may not be applicable when significant pressure drops occur [DENNIS et al. (2005)].

DENNIS et al. (2005), paints a more direct application of hydrodynamic aquifers for our project, as he focuses on tilted OWC in the North Sea, which are often recognized in Paleocene, Cretaceous, and Triassic fields. For the North Sea, potentiometric gradients conveniently refer to lateral changes in overpressure. In this instance, the presence of potentiometric gradients leads the OWC to tilt in the direction of diminishing pressure (hydrodynamic tilting). Consequently, aquifer pressures decrease in the direction of OWC dip while the oil pressure remains constant. DENNIS et al. (2005)

diverges from Muggeridge and Mahmode (2012) in his delineation of dip on an OWC, as he uses the following expression to model the hydrodynamic environment:

$$\frac{\partial z}{\partial x} = \frac{\partial \rho / \partial x}{\partial \rho / \partial h_{w-h}} \tag{3}$$

where $\partial z/\partial x$ stands for the dip per unit length , $\partial \rho/\partial x$ is the horizontal component of pressure gradient in the aquifer, and $\partial \rho/\partial h_{w-h}$ is the difference in vertical pressure gradients between the aquifer water and HC phases [DENNIS et al. (2005)].

(a)

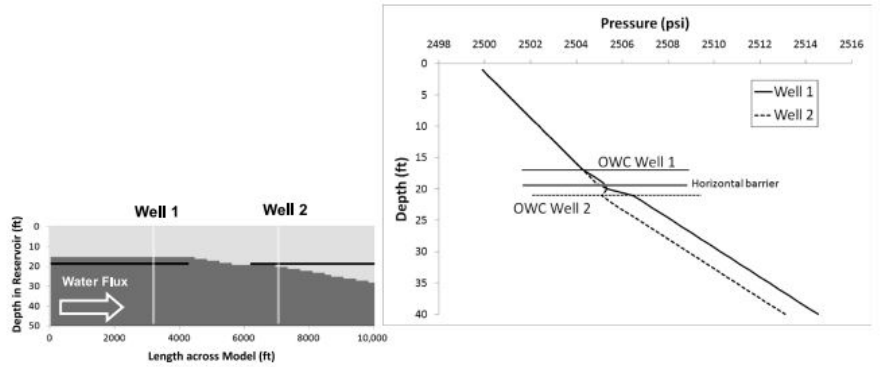

(b)

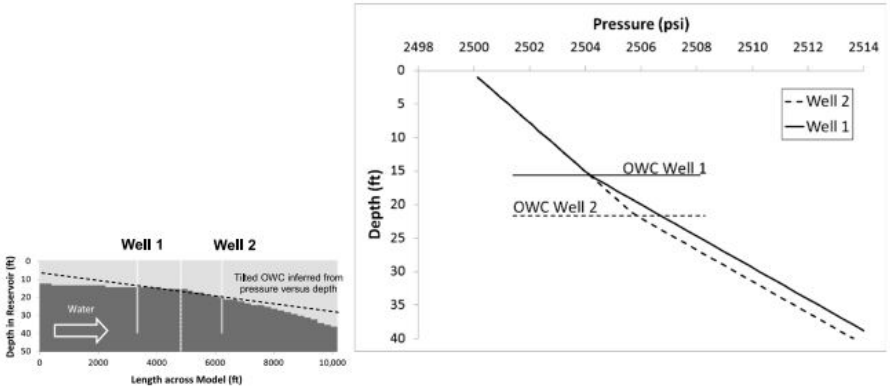

Figure 14: (a) Demonstration of the impact of a horizontal barrier at the initial OWC on the final contact tilt. Here we see that the tilt is restricted to the area below the upstream side of the gap. (b) Demonstration of the effect of a reduction in reservoir quality on the OWC. In this scenario, the modeled tilt does not match the pressure-vs-depth plots. [Muggeridge and Mahmode (2012)]

Models created through the implementation of Eq. 3 present a more direct representation of what to expect when interpreting hydrodynamically tilted contacts. Figure 15 showcases differences between hydrostatic and hydrodynamic contacts and serves as a baseline for interpretation purposes. Moreover, DENNIS et al. (2005) presets relevant observations for the interpretation of tilted contacts, which are as follows:

- The tilting o flattening of the OWC is directly proportional to aquifer thinning, and permeability changes
- Under a hydrodynamic setting, OWCs tend to steepen over the crest of structures.
- If a high permeability reservoir overlays one with lower permeability, the OWC tends to follow the bed boundary

- If a fault acts as a partial permeability barrier, the illusion of sealed compartments is created under hydrodynamic conditions
- Hydrodynamic steps are created due to short, lateral discontinuous faults
- Under the presence of reservoir layers with different permeability, the OWC will undulate as it moves through the different horizons.
- If the OWC moves from a tight reservoir to one with higher permeability, an increased OWC dip is observed on the tight section, while a flattening is observed on the more permeable zone

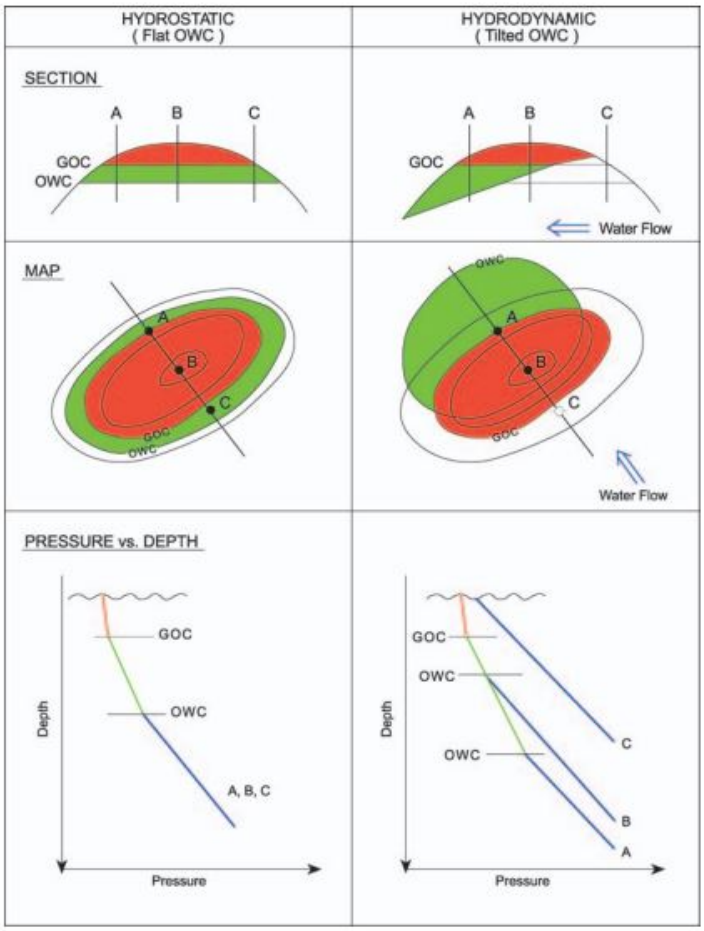

Figure 15: Comparison between hudrostatic and hydrodynamic OWC contacts.

Furthermore, DENNIS et al. (2005) observations give a more concrete delineation of events connected to hydrodynamic OWC. It is important to note that the close connection between potentiometric gradients and hydrodynamic conditions is a powerful tool for understanding the areal distribution of the OWC. Nonetheless, such observations serve as a baseline, and the interpretation of OWCs/GWCs should consider the different heterogeneity's of the field and their impact on the areal distribution of HC. Also, the listed observations are for OWCs, and their extension to GWC needs close attention as the higher compressibility of gas might introduce variables not accounted for by the literature above. In all, a diligent delineation of OWCs/GWCs is crucial as a misrepresentation might lead to an under/overestimation of HC volumes.

3.5 Hydrocarbon Volumetric Calculation Methods

The calculation of HC volumes for a given reservoir is a debatable topic due to the nuances involved during its calculation. Here the definition of net pay is the most controversial, as it is difficult to accurately define how much of the reservoir is oil/gas. The two main points of contingency for volumetric calculations (at least for the scope of this report) are the definition of Gross and Net Pay [Cobb and Marek (1998)]. First, for an interval to be considered Net Pay, it must contain HC, be reasonably permeable, and to a lesser extent, be continuous. However, the thickness of the interval is defined by a permeability cutoff, where the net pay is the part of the reservoir above the cutoff [Cobb and Marek (1998)]. However, the definition of permeability often depends on log analysis, which extrapolates permeability through porosity. In this sense, permeability cutoffs are defined by the porosity cutoffs, which is inherently misleading as there is often no relationship between the two quantities [Cobb and Marek (1998)]. A correct definition of permeability cutoffs should instead reflect its dependent variables: fluid viscosity, permeability distribution, reservoir pressure differentials, and reservoir driving mechanisms. Such an approach allows for an encompassing analysis of the areal distribution of permeability and an outline of the impact of heterogeneity on Net Pay [Cobb and Marek (1998)].

A subsequent problem with volumetric calculations is the definition of Gross Rock Volume (GRV). Generally, GRV is defined as the volume of rock between the top and base reservoir or above a known/postulated HC-water contact [Mahmud Butt et al. (2015)]. The issue arises with the definition; as per our previous discussion, the definition of HC contacts is not necessarily accurate due to its dependence on different factors [Mahmud Butt et al. (2015)]. Additionally, accurately defining the principal structure responsible for HC entrapment can be challenging. Consequently, the areal and depth definition may carry significant uncertainties associated with the data and the inherited geologic setting. The impact of such is observed in exploration, as the models often overestimate reserves.

Nonetheless, the Oil Initially In Place (OIIP) or Gas Initially In Place (GIIP) at standard surface conditions is given by:

$$OOIP = 7758Ah_v\phi(1 - S_w)/B_{oi} \tag{4}$$

$$GIIP = 43,560Ah_v\phi(1 - S_w)/B_{gi} \tag{5}$$

where A is the area in acres, h_v is the net pay, ϕ is the porosity, S_w is the water saturation, and B_{oi} and B_{gi} is the initial oil or gas formation volume factor, respectively. Furthermore, recoverable reserves are given by the multiplication of Eq.4 or Eq.5 by the recovery factor (RF).

The geologic outline of the Ormen Lange (Section 2, showcases the presence of thin shale layers within the reservoir (Egga 1,2 and 3). Therefore, the implementation of Eq.4 or Eq.5 should account for that. Masoudi et al. (2011), presents both a deterministic and probabilistic solution for such a problem in a gas reservoir. However, implementing such a mechanism falls beyond this project's scope. Here the implementation of Eq.4 or Eq.5 within the interpretation nuances above provides sufficient information for interpreting the impacts of stratigraphic traps on HC volume calculations.

4 Data

For this report, seismic, well, and pressure data will be the central guides for the results. The different data sets have nuances that need to be analyzed before outlining any results and expanding upon a discussion.

4.1 Seismic Data

Here we used a three-dimensional (3D) seismic data set resulting from survey NH9602. The seismic data covers the Ormen Lange East block and was collected in 1996 by Norsk Hydro A/S. Furthermore, different data migrations were used to create Full, Near, and Far offsets. The total inline extension is 1500 - 2060, while the Xline extension is 2000 - 8570. Relative to the geodetic datum, the data follows ED50 International 1924 datum, and the projection is UTM Zone 31 North. However, the processing flow plays a more significant role as we assess data quality and resolution.

The survey relied on six streamers of 512 channels each, creating a nominal fold of 39. A minimum-phase signature deconvolution, multiple attenuations, true amplitude recovery, 3D DMO stacking X deconvolution, FD migration, time-variant filtering, and AGC scaling were used. This information is provided by the file header and corroborated by Bünz et al. (2005). Moreover, the central frequency lies between 40-50 Hz with a nominal vertical resolution of 10 and a Fresnel radius of 150 at a depth of 1.6 ms under an average velocity of 1600 m/s [Bünz et al. (2005)]. Overall, the seismic data is good, but some noticeable aspects need attention.

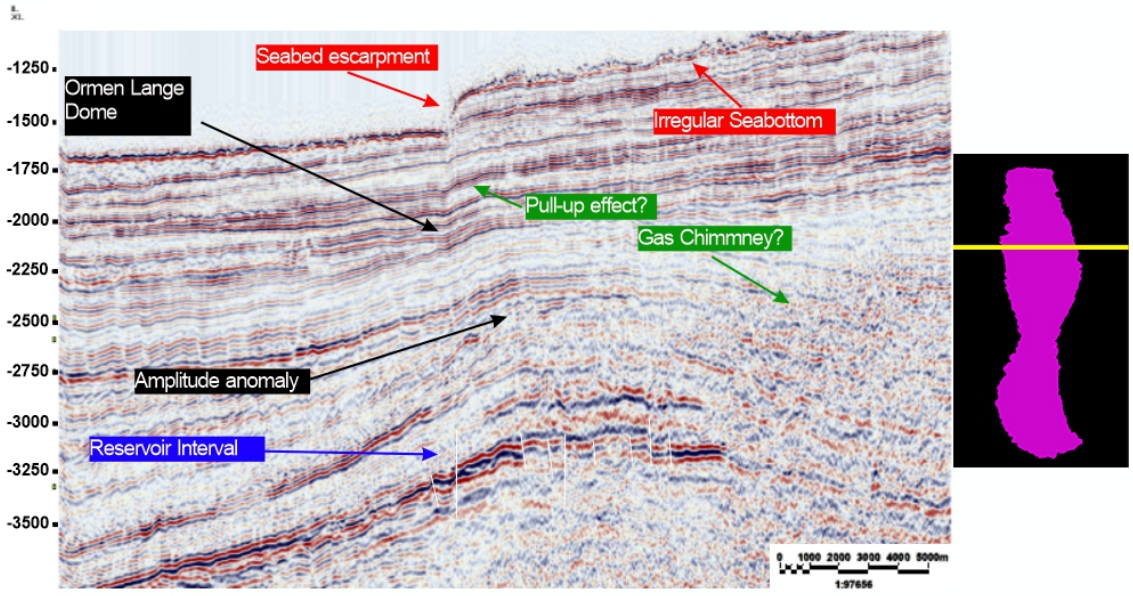

Figure 16: Seismic cross-section (Xline = 5000, Full-Offset) demonstrating some characteristics of the data. Based on Möller et al. (2004) work.

A prevalent feature of the data is the irregular seafloor and seabed escarpment. The presence of a seabed escarpment introduces high horizontal variability at the beginning of the section. Furthermore, such difference could introduce some artifacts if the stacking velocities do not accurately represent such shift; otherwise, pull-up effects might be present as suggested in Figure 16. Additionally, there is evidence of fluid leakage at the seafloor [Bünz et al. (2005)], which would enhance the effects introduced by the seabed escarpment as the definition of stacking velocities would be difficult. The presence of the Ormen Lange dome might further complicate the identification of such effects. Also, it is essential to note that there is no mention of such effects in the literature.

Other noticeable characteristics are amplitude anomalies, multiples, and diffractions. Relative to amplitude anomalies, their presence might be related to DHIs, but more importantly, their presence requires caution during interpretation. The presence of multiples and diffractions is more concerning since they might skew interpretation attempts. Furthermore, the impact of such characteristics is further discussed by Möller et al. (2004) and Smith and Møller (2003) that outline how such events degrade the seismic data quality. Lastly, given that the Ormen Lange is a Gas reservoir, we need to be conscious of potential AVO effects during interpretation. Nonetheless, such characteristics appear to have a negligible impact on the definition of the reservoir section, and the use of well data should help mitigate them and guide interpretation.

4.2 Well-Log Data

For this project, I will use the following wells, which are located according to Figure 17:

- **6305/1-1 :** drilled by Norsk Hydro (NH) in 1998. Drilled close to the crest of the Orman Lange dome. Egga sands were confirmed but with reduced reservoir qualities. Only gas shows were found. Overall the Egga sand is overpressured relative to the other wells. It is a dry well since only formation water and gas shows were found [NPD (n.d.(a))].
- **6305/4-1 :** drilled by NH in 2002, located in the northwestern part of the DHI area of the Ormen Lange field. The well penetrated the ERU at 2774 m MSL, and a Gas Down To (GDT) situation was found within the lowermost part of the ERU. Nonetheless, production tests asserted good reservoir quality and baffles for horizontal gas flow. Well testing showcased, overpressured water-filled sand units after the Egga sands [Möller et al. (2004); NPD (n.d.(b))].
- **6305/4-2 S :** Drilled by A/S Norske shell in 2010. Penetrated the ERU at 2768.3 TVD, the reservoir presented average properties. The ERU was water-bearing and was under high pressure. Testing results helped support the Hydrodynamic model and confirmed the seismic interpretation of the DHI in the area as a paleo-gas/water contact. Considered to be a dry well [NPD (n.d.(c))].
- **6305/5-1 :** drilled by NH in 1997 and served as the gas discovery well for the Ormen Lange field. Here the well found a high-quality gas reservoir with a structure that does not penetrate the FWL but gas a GDT situation within the ERU. Gas-filled units were found within the Cretaceous/Paleocene reservoir unit, as well as within a heterolithic section and a partly cemented Springar FM. However, water-filled overpressured sands were found within the Jorsalfare Eq. Ideal for well-ties and outline of rock and fluid fill properties [Möller et al. (2004); NPD (n.d.(d))].
- **6305/5-3 S :** Drilled by Norske Shell in 2009 on the North-Eastern flank of the Ormen Lange field. Demonstrate a GDT at 2678.7 m TVD. Indicated good reservoir qualities, but the pressure within the egga gas leg suggests depletion relative to the observed values prior to exploration. The Springar formation demonstrated low reservoir quality, and no hydrocarbon saturations were determined. Additionally, gas was found below the gas-water contact. Considered a gas appraisal well [NPD (n.d.(e))].
- **6305/7-1 :** drilled by BP in 1998 within the Møre basin deep-water area and is considered a gas appraisal well. Testing proved the reservoir to be of high quality with no barriers to gas flow. Additionally, a residual gas zone was found below the FWL [Möller et al. (2004); NPD (n.d.(f))].
- **6305/8-1 :** drilled by NH in 200 and is located north of the field's Saddle area. Penetrated a Gas-Oil contact at 2986.5 m MSL. Demonstrated good reservoir quality with a FWL shallower than well 3605/7-1. Considered a oil and gas appraisal well [Möller et al. (2004); NPD (n.d.(g))].

- **6305/8-2 :** Drilled by Norsk Shell in 2014 in the southern part of the Ormen Lange field. Demonstrated good reservoir qualities. An underlying water zone with good reservoir qualities was also found to contain good permeability. All sands below the ERU are considered to be water-bearing [NPD (n.d.(h))]

A comprehensive list of the well logs contained within each well can be found in Appendix A. Relating to uncertainties and error, the varying ages of acquisition introduce undesirable variability. In this instance, method evolution infers a possible difference in resolution that might impact interpretation. Also, there is evidence of interpolation within some logs, which is problematic as the depicted information may skew from reality. Also, some log sections are missing due to problems during drilling. This is not necessarily problematic but may require some attention. For instance, some wells do not possess density/sonic logs for the entirety of the ERU, which makes acoustic impedance calculations difficult and subsequently hinders well-tie attempts. Nonetheless, most wells do not present issues within the ERU and showcase reliable information about the reservoir.

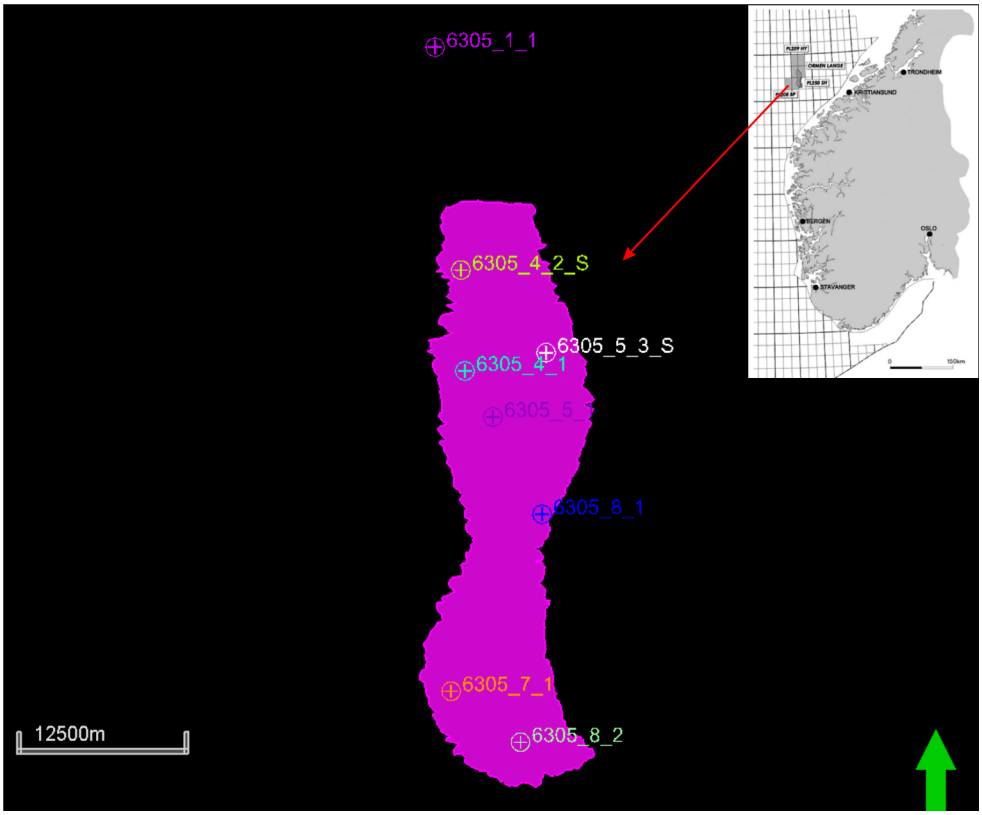

Figure 17: Well location

4.3 Pressure Data

Unlike seismic and well log data, the availability of pressure data is more limited. In this sense, the data used for this report relies primarily on the information well reports provide. Additionally, the availability of such reports is limited, constraining access to this information. Nonetheless, for this project, I will use pressure data related to the wells 6305/1-1, 4-1, 7-1, and 8-1. It is challenging to access the quality of the data, as the presented information has been processed and presented in the report. Also, the representation of information across different reports changes, making data correlation relatively tricky. Nonetheless, I extracted the pressure information from well reports to depict changes in pressure and correlate them with the observation presented by Muggeridge and Mahmode (2012) and DENNIS et al. (2005).

5 Methodology

The approach taken in this work relies on an integrated work linking previous regional observations together with detailed interpretations across the Ormen Lange field. Trap definition is based herein on building a framework consisting of detailed well correlations, seismic geomorphology, and fault interpretation. Trap definition is essential, but it requires a quantitative and qualitative analysis of the reservoir to depict its impact on the volumetric calculations. The first step in this process was to tie the well information with the seismic data to constrain the seismic-derived observations better away from well control points.

5.1 Quality Control

Before performing any interpretation or well ties, we must consider the data characteristics mentioned earlier. For instance, the original seismic is zero phase with reverse polarity (through an increase in acoustic impedance interface). A 180° degree phase rotation was applied to obtain a normal polarity response. Additionally, a structural smoothing of the data to decrease the random noise was performed to improve reflection continuity for interpretation purposes. Relative to the well logs, there were no necessary changes. However, raw data (mainly well head locations and well paths) needs to be cross-referenced with available literature to ensure that there were no mistakes during setup. The final step was to analyze the different partial stacked seismic volumes (near and far offsets) to define an interpretation strategy and identify the area with an AVO effect.

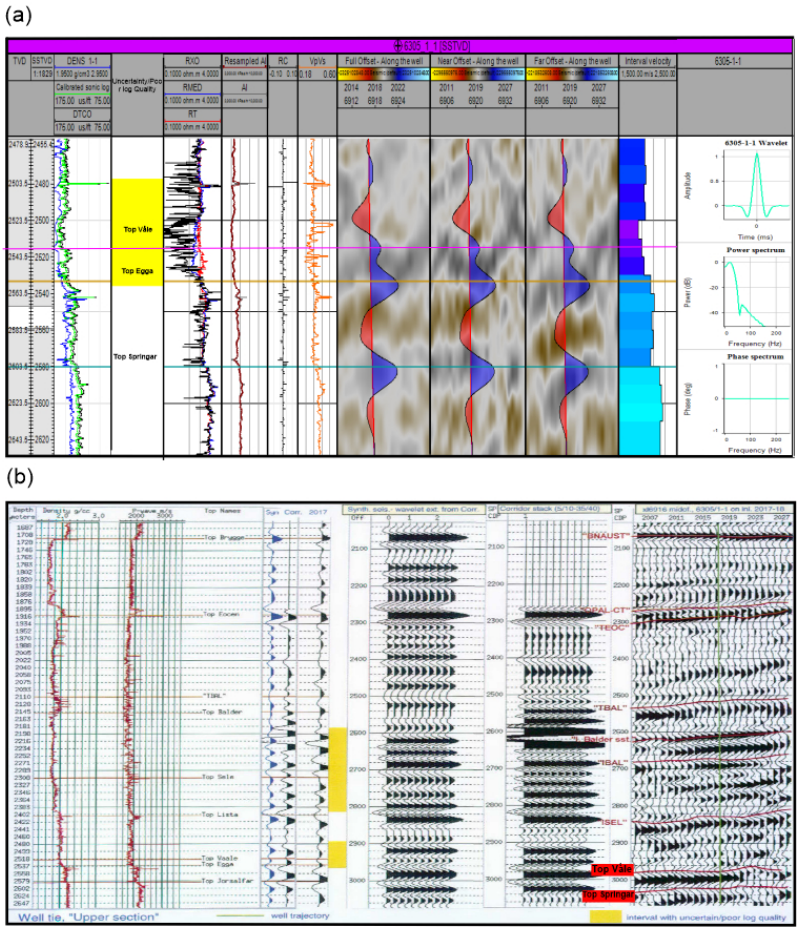

Figure 18: Example of a well tie showcasing the performed well tie in comparison to the one presented by Norsk Hydro [Roe (1999)]. (a) Performed well tie demonstrating main formations - Våle, Egga, and Springar. (b) Well-tied performed by Nork Hydro [Roe (1999)], in this instance, the Jorsalfare are used interchangeably. The Jorsarfare is the name used within the NST, and Dallan introduces Springar, but both refer to the same formation. Norsk Hydro's section uses SSTVD for its depth reference.

5.2 Well-tie

Prior to carrying a seismic horizon interpretation, a seismic to well-tie for all the available wells , which contain checkshot data (6305/1-1, 4-1, 5-3 S, 8-2), was implemented, allowing to calibrate the relationship between depths and calculated times from sonic logs.

Given the field's lithostratigraphic disposition, this is one of the most crucial steps since it will allow us to represent the different formations accurately. Thus, well top position and available literature supplemented any efforts throughout this step. Given that our objectives surround an interpretation of the ERU, the focus of the well ties was to primarily and accurately relate well data to the seismic at the reservoir level. Being associated with a gas field, the seismic data presents some AVO effects, which can be observed during the well-tie process.

Figure 18 showcases an example of a well tie performed using well 6305/1-1. Here we see a good relationship between the well logs and the seismic, even within a section with complex geology. It is worth pointing out that there is no significant amplitude discrepancy across the different seismic volumes in this section (no AVO). More importantly, we see that the performed well tie shows the same trends like the one presented in the well report. Furthermore, a similar approach was implemented for the remaining wells, and similar results were found.

In all, this step aims to correlate the seismic to the well data to guide interpretation and extend the available information about each formation.

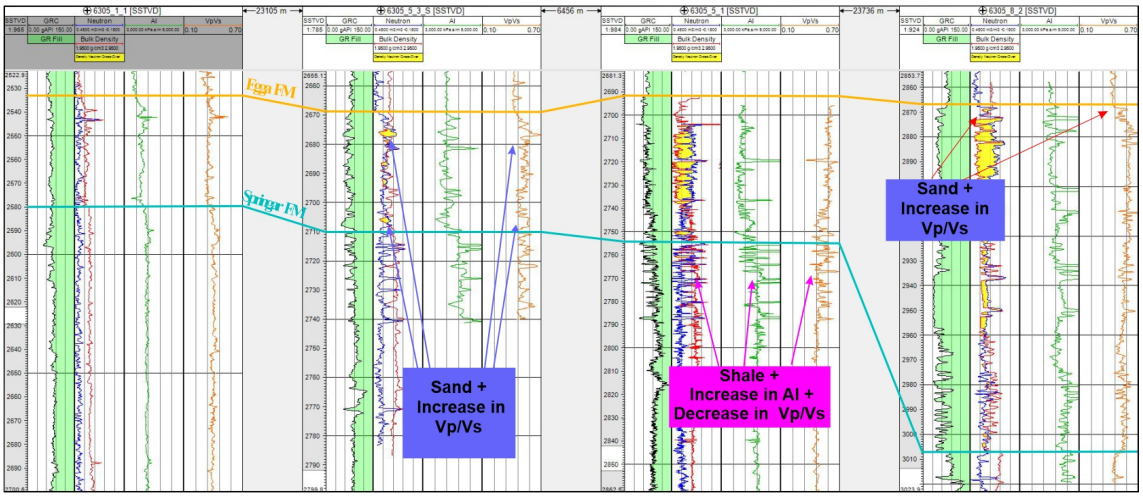

(a) Well logs demonstrating changes in AI and Vp/Vs as across significant well tops

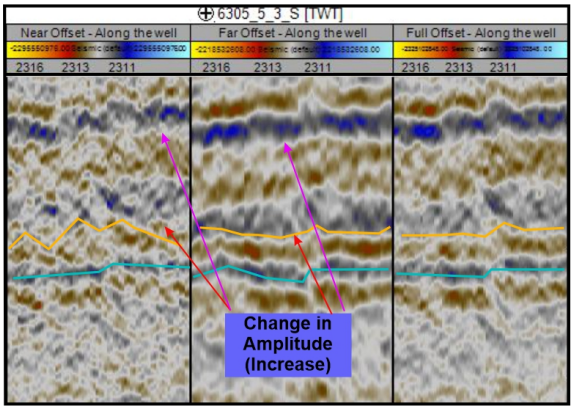

(b) Demonstration of AVO effects for well 6305/5-3S. Orange line represents the top of the EGGA FM and teal color the top of the Springar formation

Figure 19: Outline of changes in AI and Vp/Vs, with an example of resulting AVO effect.

5.3 Seismic Interpretation

After performing the well tie, we have enough information to identify our main zones of interest. In this case, the focus lies on the reservoir. Thus, the primary interpreted reflections are the ERU and the Springar formation since our goal is to understand their disposition. However, the field size is an issue that requires a more focused approach for a detailed interpretation within the project's time frame. Nevertheless, a more refined interpretation of the reflections in areas with complex geology is preferable. The central defining aspect of complex geology was the interplay between the clean sands and the heterolytics found within them.

Moreover, a balance between general trends and detailed information was necessary. The first step was to decide in which offset to pick horizons. Therefore, changes in acoustic impedance (AI) and Vp/Vs helped determine AVO effects and the proper offset for interpretation. Figure 19a outlines the increase in Vp/Vs and decrease in acoustic impedance for sands within our reservoir. Additionally, Figure 19b showcases the AVO effect caused by the presence of gas within the reservoir, which is consistent with the increase in Vp/Vs across top Egga. Consequently, the Far-offset pick provides a better outline of horizons since the AVO effect reduces the amplitude at the Near-offset. The Full-offset represents both the Near and Far-offset, and as such, is impacted by the amplitude decrease of the Near-offset, which further hinders a detailed interpretation of horizons.

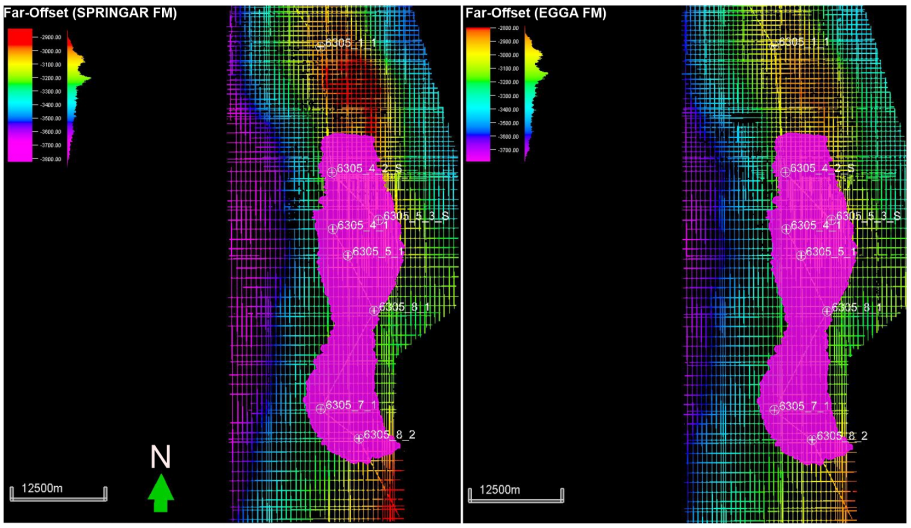

Figure 20: Interpretation grid for the Egga and Springar FM. At the left we have teh interpretation grid for the Springar FM and at the right for the Egga formation

After choosing to pick horizons on Far-offset, a definition of the interpretation grid was necessary. This is important because we must define a grid that provides enough detail to depict significant trends but does not require a line-by-line interpretation. Figure 20, demonstrates the implemented picking grind for the Egga and Springar horizons. Both horizons represent the delineation of the reservoir unit, and as such, a particular emphasis was put on ensuring a coherent interpretation. Section 2 mentions reservoir quality deterioration as we move from South to North. Consequently, a more refined grid was implemented above well 6305/5-3S to account for reservoir depreciation. Figure 21 demonstrates this trend well as we can see the quality of the seismic data decrease as we move northward.

The above steps aim to ensure a good reservoir outline, as any interpretation results are directly linked. It is also important to note that not all the section was interpreted; the northernmost section was not interpreted due to poor data quality and lack of additional information relative to the presented interpretation grind. Also, the areal distribution of the presented interpretation covers enough information to investigate the observations in Section 2 and outline relevant structural, lithostratigraphic, and morphological characteristics of the reservoir.

5.4 Pressure-Data

As per the previous discussion, there is some discussion about the hydrodynamic disposition of the Ormen Lange field and its subsequent impact on the areal distribution of HC. The first step was to digitize the formation pressure data in the reports. The subsequent step is replicating relevant graphics, dependent on the available information within each report. For instance, for well 6305/1-1 [Roe (1999)], the report is not explicit about how the data has been handled to produce pressure-versus-depth graphs. Nonetheless, the main goal is to ensure that any results follow the well reports.

Posterior to quality control of replicated results, one must cross-correlate information across all available wells. This step is crucial, as it draws a parallel between Muggeridge and Mahmode (2012) and DENNIS et al. (2005) observation and their relevance for the Ormen Lange field. The aim is to demonstrate how the field's different fluid contacts and gradients vary. The final step is assessing potential links across the wells and their relation to other observations.

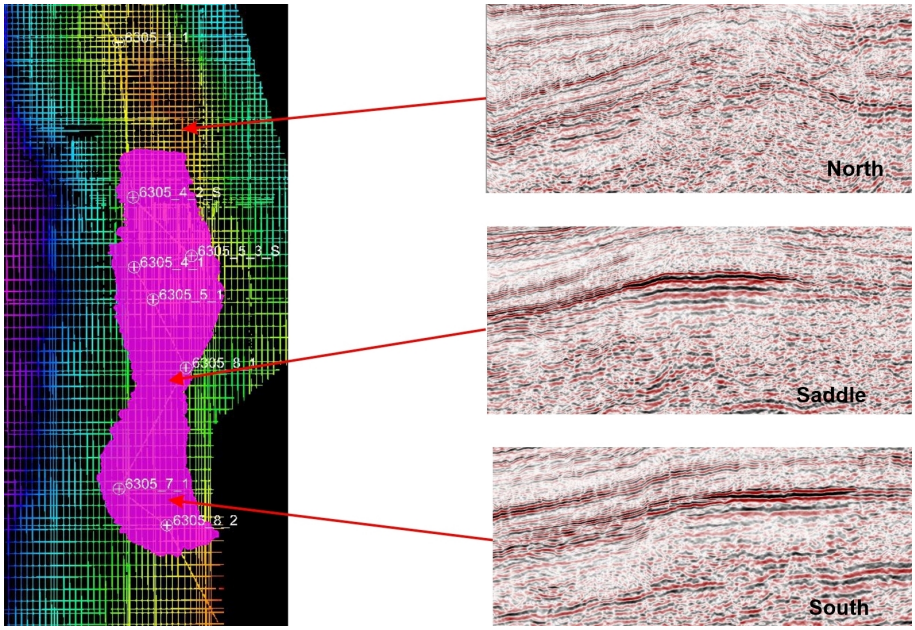

Figure 21: Demonstration of reservoir degradation from South to North.

5.5 Cross-Correlation and Model Definition

Cross-correlation and model definition is the most crucial aspect of this project. The method definition relies on interpreting and connecting information across different data sets and literature. The first step is to outline pertinent information relative to the interpretation of the data. Furthermore, the aim is to showcase seismic and well-log information on relevant trends. Afterward comes the depiction of pressure trends and inference about the geomorphology of the field. Posteriorly we must draw a parallel between the seismic, well-log, and pressure information to ensure that all observations are consistent and demonstrate the same trends. Finally, we compare results with those framed by literature to compose a model.

Model definition accounts for the goals of this project and serves as a means to an end. The construction of a model represents structural, lithostratigraphic, and morphologic trends that showcase the impact of stratigraphic traps on volumetric calculations. Therefore, the model accounts for the area's geologic history to map the HC areal distribution and its connection to the observed trap styles within the field. From here, we default to the volumetric equations present beforehand to depict and predict trends for the amount of hydrocarbons present within the main reservoir unit. In all, cross-correlation connects the interpretation across all data sets, and the model definition illustrates relevant trends for the resolution of the project goal.

6 Results

This section focuses on the outline of the different results of this study.

The Egga RU is divided in different ways in the literature depending on the author and their approach to the issue. For this project, I will use Möller et al. (2004) biostratigraphic division as the baseline for facies definition and overall description of the Egga unit, and the results will expand upon some observations to better define the reservoir unit.

Furthermore, this section will present results about three main data sets, well logs, pressure, and seismic (as per the above descriptions). Well log results will outline different facies of the reservoir and their intrinsic properties (such as density and porosity). The aim is to cross-correlate the information from the available wells to delimit the overall trends of the field. Pressure data aims to explore the literature's hydrodynamic claims and their validity based on the available information. Seismic aims for the structural outline of the field, as results point towards sand distribution, AVO effects, DHI areas, and other prominent trends.

6.1 Well Log Results

Figure 22 depicts the limits of the Våle, Egga, and Springar formations. In this section, all correlations have the same datum (0 m SSTVD); this better showcases the current structure and the areal distribution of facies. Furthermore, we see that the field has a stepping structure, with the northern side being shallower than the southern side. Also, as we look at the Egga unit, we observe a thickening as we move from North to South. Such a pattern indicates that the stepping structure had some influence during deposition as the deeper parts allocate more sediments than their shallower counterparts. Additionally, the Springar formation (blue on Figure 22) follows the same stepping structure but maintains an even thickness until well 6305/4-2S, where there is a northward increase in thickness. The Våle formation follows the same outline as the Egga formation but with smaller variations in thickness.

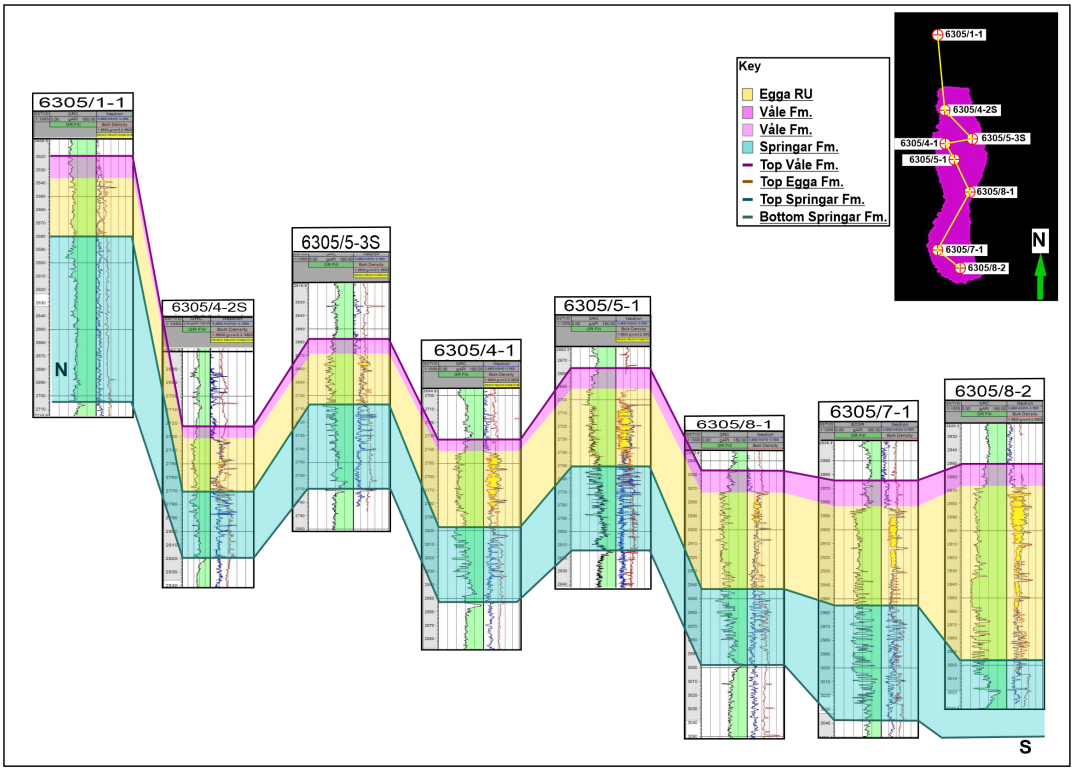

Figure 22: Broad lithostratigraphic correlation for the Ormen Lange field. The image outline the extent of the Våle formation, Egga formation and Springar formation. Datum = 0 m SSTVD

Considering the areal distribution of the wells in conjunction with the broad correlation demonstrated by Figure 22, it is possible to separate the wells into three groups. The southern group is composed of wells 6305/8-2, 6305/7-1, and 6305/8-1, and the middle group is composed of wells 6305/5-1, 6305/4-1, 6305/5-3S, and 6305/4-2S, and the northern group composed by well 6305/1-1. As we progress with the results, group definition becomes more concrete and allows for a better depiction of general trends.

The literature outlines the inter-bedding of sand and shale on the Egga RU, which is more frequent towards the deeper parts of the reservoir. Variations in the type of shale deposited also vary, as per the discussion in Section 2. Consequently, it is essential to subdivide the Egga RU into different sections to describe these changes better. Here we will follow the biostratigraphic division posed by Möller et al. (2004), where the Egga RU is divided into three subsections, Egga I, II, and III. Boundary delineation is based on changes in biological markers associated with shale deposition. The definition of these markers falls beyond this project's scope but is detailed on Möller et al. (2004). Nonetheless, the biostratigraphic markers identify the tops of the different subdivisions, but their areal correlation is implemented using a lithostratigraphic correlation as demonstrated by Figure 23.

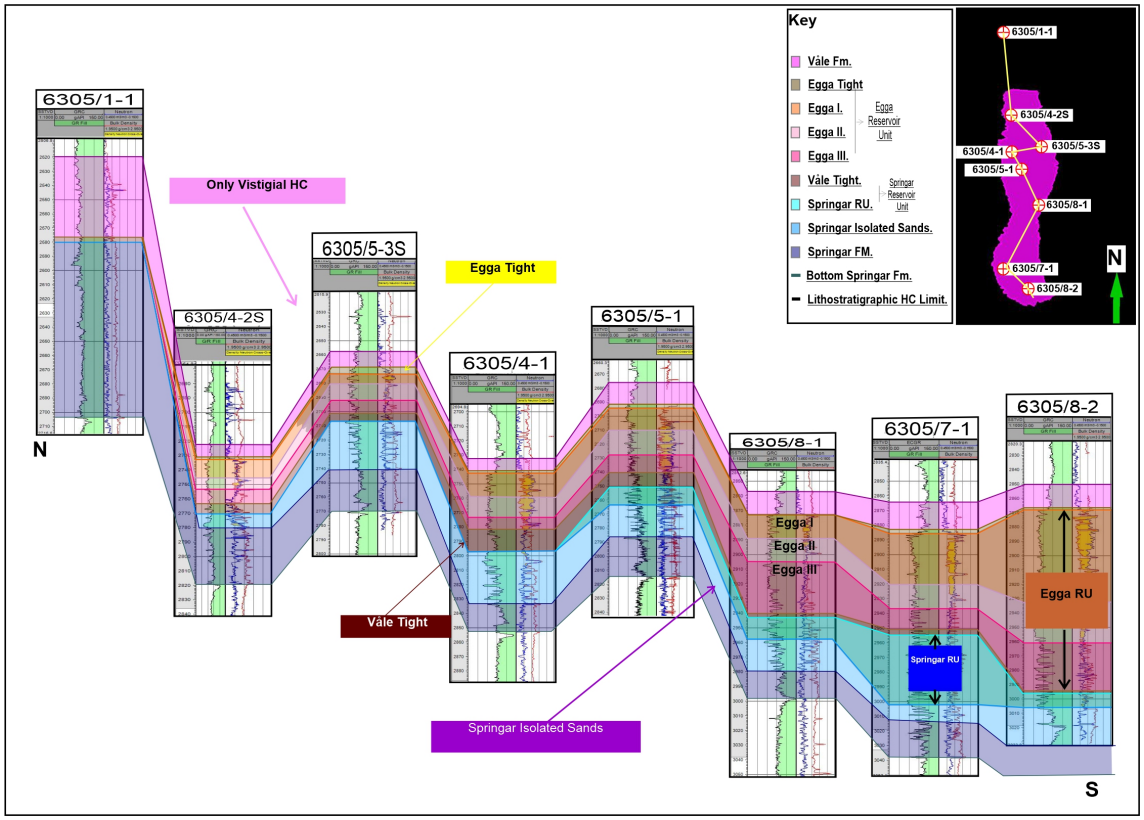

Figure 23: Complete lithostratigraphic correlation for the Våle, Egga and Springar formations. Outline of the subdivision of the Egga RU, HC extent and some relevant features, such as the Våle tight. Datum = 0 m SSTVD

Figure 23 outlines the lithostratigraphic correlation of the available wells across the field. This image uses GR, density, and Neutron porosity to outline essential features. Being part of the Våle formation, the EGGA RU delineation varies depending on the author. Since subdivisions are based on Möller et al. (2004) biostratigraphic division, Figure 23 does not showcase the Egga RU, as the presented facies do not correlate with the rest of the wells. The well report for 6305/1-1 mentions an "Egga member equivalent," which for our analysis will not be correlated with the Egga RU observed in the remaining wells. Therefore, as we move forward, we establish that the Egga RU terminates between well 6305/4-2S and well 6305/1-1. This observation is further comprised by the logs since there is a sharp degradation in facies between the wells, with well 6305/1-1 having no sand indication on the Density-Neutron track and a high GR value combined demonstrating an extensive absence of reservoir sands.

The Springar formation is also sub-subdivided into three subzones, the Springar RU, Springar Isolated Sands, and the Springar Unit. The subdivision of the Springar formation serves to illustrate the overall picture of the reservoir but will not be explored further. Given the limited areal extend of relevant sections (Springar RU and the Springar isolated sands) and lack of data to fully explore this section across all wells, the exploration would not yield valuable results. Nonetheless, an outline of the facies distribution of the formation is vital for future discussions about HC in the Ormen Lange field.

Looking at the Density-Neutron and GR logs presented in Figure 23 there, we observe a few important trends. First, the transition from the Våle formation into the Egga RU is marked in most wells by a tight zone, which is the Egga tight. As a unit, it is relatively thin and has a large areal extent, only missing on well 6305/8-1. Second, Egga I and II hold the bulk of sands in the reservoir. The density-neutron cross-over (indicated by yellow on Fig. 23) outlines this trend. Additionally, there is an increase in GR as we move from Egga II to III. For the Egga RU (Egga I to III), GR has an overall cylindrical shape, depicting the aggradation of sediments, which is common for deep water marine systems. However, as we move towards the end of Egga III into the Våle tight, the GR trend transitions to be serrated or a funnel.

A funnel trend is more evident for our middle wells and 6305/ 8-1, with higher prominence towards the Springar formation. The serrated trend is more evident in the southern wells beginning at the end of Egga III, which can be associated with a distal marine slope deposition. The interbedded deposition of shale and sand across the field leads all wells to present a serrated pattern to the GR, which becomes more prominent in the interval mentioned above. Also, being a turbidite deposited unit, we observe a coarse up and sharp top (funnel trends) GR trend across all wells, which varies in degree and depth from well to well.

While the GR gives us an idea of the location of sand-shale distribution, the density-neutron cross plot gives us a better idea of the sand extent. In this sense, the southern and middle wells present identifiable sand packages correlated with the observed GR trends. Additionally, we see that the thickness of the sand packages is more significant towards the southern wells and decreases northwards with the increase in shale content. Furthermore, as we get to well s 6305/5-3S and 6305/4-2S, the sand packages become more isolated as the shale concentration leads to the sand packages' separation. We also observed a bell shape for the sand packages, a standard response for Gas bearing sands. This trend becomes less evident as we move northward and with an increase in shale content.

Furthermore, a depiction of sand and shale trends requires further exploration to outline other trends outlined in Figure 24. We can explore facies trends by adding resistivity, AI, and Vp/Vs curves. For the southern wells and well 6305/5-1, we observe an "undulating" AI impedance trend. This trend is directly related to thin low porosity layers found across the wells. The presence of such layers leads the AI to increase and decrease; such variation is more evident when we arrive at shalier parts towards the end of Egga III. The impact of such barriers is more evident when looking at the density log since it remains relatively constant throughout the reservoir unit and increases in these low porosity layers. For the remainder of the wells, AI decreases towards Egga III, where we observe a hard shift leading to a gradual increase in AI with depth.

Relative to Vp/Vs, we observe a general increase as we transition from the Våle formation into the reservoir unit. After such an increase, Vp/Vs remains relatively constant until the GWC. This transition is well correlated with the resistivity curve for the southern wells, as the increase in VP/Vs matches with areas with high resistivity. This observation is more predominant in the southern wells, where the separation of sand and shale is more readily identified. Additionally, we observe a standard resistivity response to HC for these wells, which further corroborates the AI and Vp/Vs trends. It is also important to note that the aforementioned low porosity layers are characterized by an increase in AI, density, and resistivity and a decrease in neutron porosity and Vp/Vs. Paring such observation with the possibility of thin carbonate deposits within the Egga unit, we can define these layers as calcified thigh sandstones.

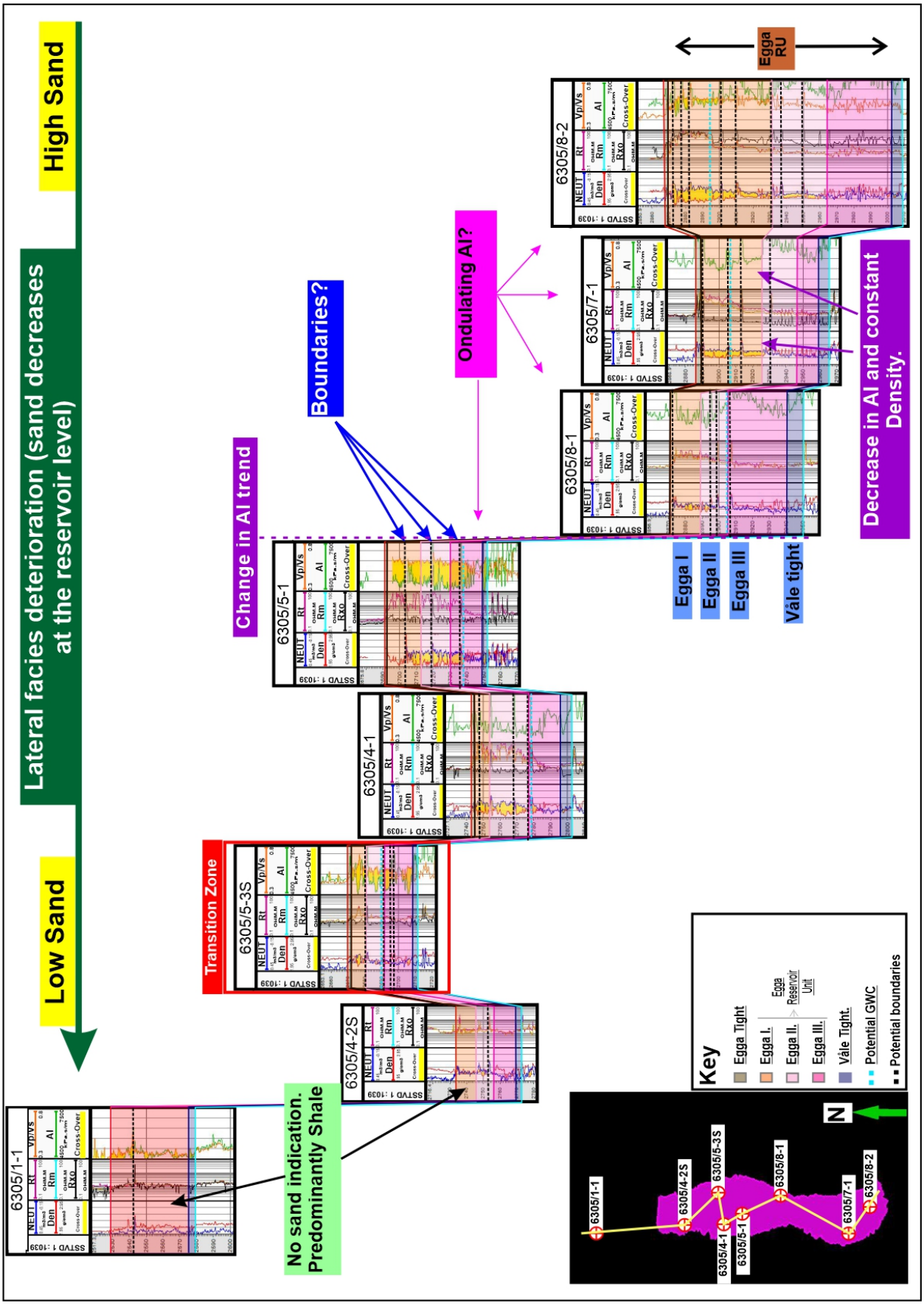

Figure 24: Detailed litostratigraphic correlation, showcasing main trends across the field. The Vp/Vs-AI correlation showcases a differential response as we move North of the field. Additionally, it is possible to see a facies degradation towards North with wells 6305/4-2s and 6305/1-1 having no sand indication

The influence of the tight calcified sandstones on fluid motion is unclear from log analysis alone. Nonetheless, the variations in density, neutron porosity, resistivity, and AI suggest that they might have some influence. However, it is difficult to conclude such a premise confidently without a permeability curve. Another important trend relates to facies degradation. From Figure 23 and 24 we northward facies deterioration becomes evident. Here we see that up to 6305/5-1, our sand packages are relatively thick, and log responses to Gas are standard. However, as we move North towards well 6305/5-3S, the sand packages become more isolated, and the responses to HC become more irregular. Lastly, well 6305/4-2S demonstrates small to no response to HC, suggesting that well 6305/5-3S is a transition zone between HC-bearing sand and water-saturated sands.

The above observation delimits interesting trends across the reservoir but, more importantly, accentuates the aforementioned grouping of our wells. Therefore, we must look at each group in detail. Figure 25 showcases the southern wells in more detail. Here we see two main layers within the Egga RU, a sandy zone marked by the presence of calcified tight layers and a shale layer. The transition between layers is marked by a sharp increase in AI followed by a gradual decrease. This is followed by a dirtying-up serrated GR trend which depicts an increase in the shale content and a decrease in grain size.

Concurrent in the correlation between the tight calcified layers, the GWC, and the shaly zone. Across all three wells, the transition into the shaly zone is marked by the presence of a tight calcified zone. Also, the GWC is located above this calcified tight zone. It is important to note that the calcified layers delimiting the GWC occur relatively at the same depth, suggesting a contemporaneous deposition and variability across the different calcified layers.

With the current data, we can assert that for the southern wells, there is a clear shift in deposition across the Egga RU. Here we have a sandy zone between Egga I and II and where we can find our HC. The tight calcified sandstone appears to have different permeability properties and does not, as a whole, restrict fluid flow. Also, these layers play a role in the transition into the shaly zone, which is mostly restricted to the Egga III unit.

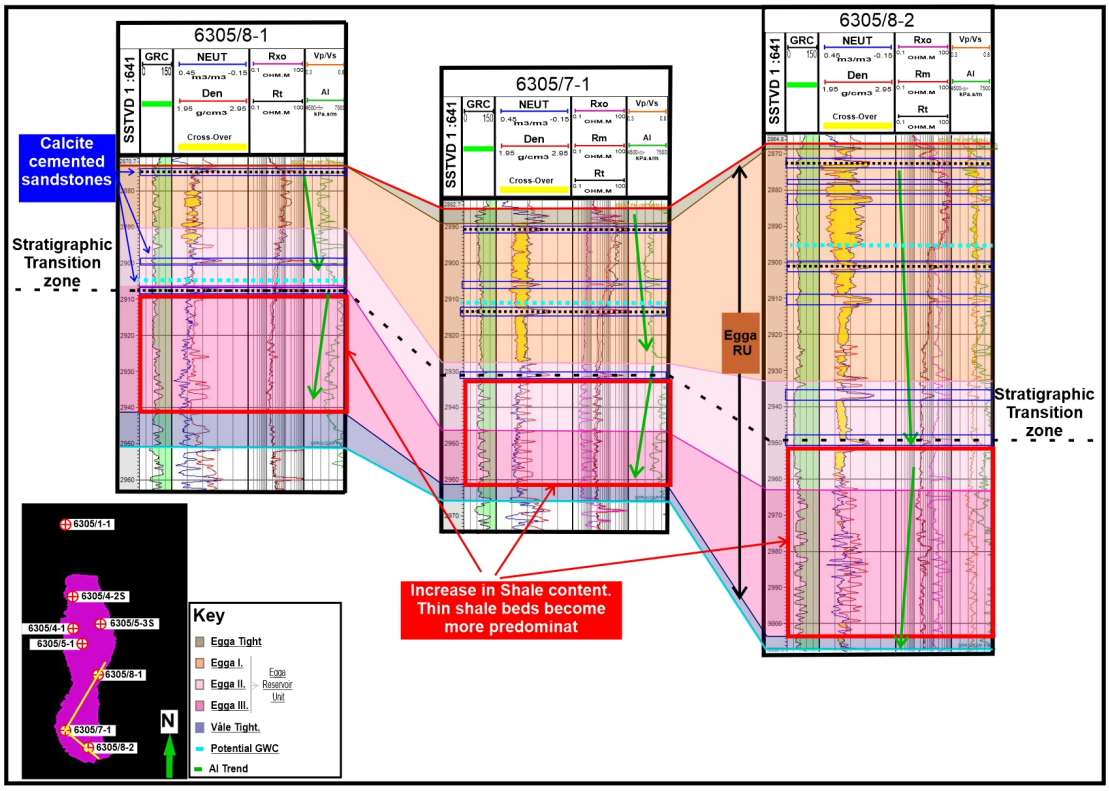

Figure 25: Correlation of southern wells. Detailed depiction of facies correlation, as it partakes to the GWC and distribution of tight calcified sandstone layers.

As mentioned before, there is a distinguishable difference in the trends between the southern and middle wells. The first difference lies in the AI trend, where we see a decrease in AI towards the GWC and calcified layers, followed by a gradual increase. This section does not show a transition into a shally zone within the Egga ERU. Similar to the southern wells, the GWC occurs at a similar depth. However, we see that it occurs below the layer mentioned above. Considering the structural relief between well groups, it is plausible that the calcified layer attached to the GWC is a field-wide event and might have some impact on the areal distribution of the GWC. Consequently, the cemented zones attached to the GWC might serve as a stratigraphic transition zone, where the quality of the sand decreases.

Additionally, we see a localized thickening of the Våle tight at well 6305/4-1, which to this was relatively thin. As mentioned before, the sand units become progressively more isolated in this section, with well 6305/5-3S demonstrating sparse sand pockets. Such progression is related to the overall northern degradation of facies in the field. Relative to Gas, NPD reported findings at 6305/5-3S, but when compared to wells in the same area, there is an apparent decrease in volume. The resistivity curves are one of the leading indicators of this event, as we see a smaller response in our Gas-bearing sands compared to 4-1 and 5-1. relating this observation with the significant facies deterioration of well North of 6305/5-3S, it becomes evident that this week marks a transition zone between Gas bearing to the water-bearing sands.

The overall reduction in thickness of the reservoir is another pertinent trend. South of the field, we see the reservoir reaches its max thickness (approximately 130 m) and reduces its thickness significantly in the middle section, with well 6305/5-3S having a 40 m. Thus, the reduction in thickness may indicate the field's structural outlay, a potential change in depositional patterns, or a combination of both. The absence of a shally zone within the Egga RU may indicate the latter. However, further investigation is needed to confirm it.

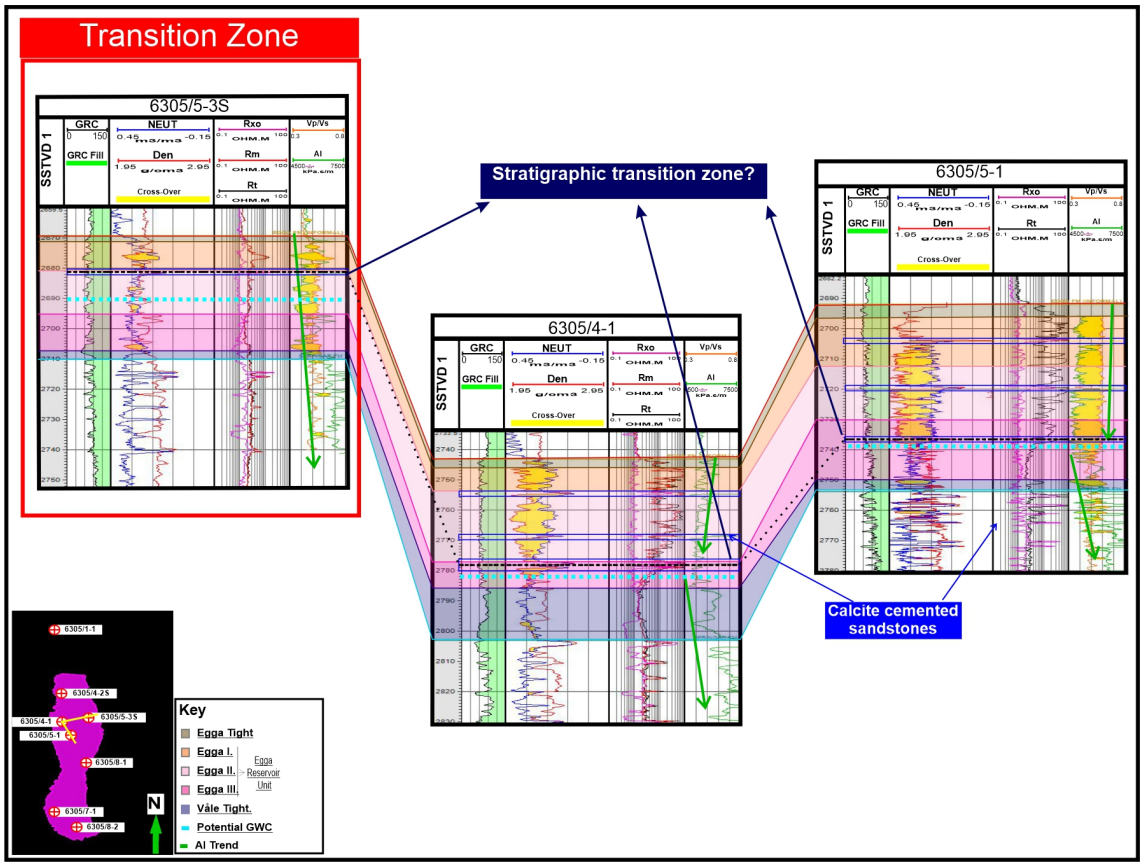

Figure 26: Correlation for the middle wells. Detailed depiction of facies correlation, as it partakes to the GWC and distribution of tight calcified sandstone layers.

The middle and southern well demonstrate some similarities, but their differences pose a more pertinent problem related to the influence of stratigraphic fluid flow variations and subsequent distribution of the GWC. First, we see similar trends in the "sandy zone" dominated by the presence of calcified tight zones. Here we observe degradation in facies northwards which is accompanied by a decrease in Gas in this unit. Such observation is evident in the resistivity logs, which showcase a decrease in the same direction until we get a slight response on well 6305/4-2S. As a whole, the Vp/Vs and acoustic impedance in conjunction with the density-neutron plot depict the evolution of the sands and the distribution of gas/water. From the logs, we can infer that 6305/1-1 sits beyond the limits of the reservoir unit, but further investigation is needed. Additionally, the localized presence of a shally zone within the southern part of the reservoir indicated a differential dispositional mechanism across the field, which the following results will investigate.

The goal of the project is to understand how the trap style of the Ormen Lange field impacts volumetric calculations. In this instance, the well logs depict the differences in stratigraphy across the field and their impact on gas mobility. Furthermore, the literature suggests [Grecula et al. (2015)] a hydrodynamic component in the trap characterization, which requires some investigation to corroborate such findings with our observations.

6.2 Pressure Analysis

To investigate a potential hydrodynamic-controlled aquifer, I used pressure vs. depth graphs to illustrate the variation in pressure across the wells and depth. Here I used formation pressures as they allow to define of fluid contacts by plotting the different fluid gradients and marking their intersection. However, the availability of the information is sparse in some cases because the data was not collected during drilling or because the access to such information is restricted. Nonetheless, using well reports, I could access data for wells 6305/1-1,7-1,8-1,4-1, which areal an extent allows for a good overview of the field.

In figure 27 we can see how the pressure data for the available wells compare. The first observation is the pressure discrepancy between well 6305/1-1 and the remaining well. We observe an 80 bar difference between well 6305/1-1 and 4-1 and a 90 bar difference for wells 7-1 and 8-1. Such difference indicates that well 6305/1-1 lays outside the reservoir system and represents a different setting for water flow.

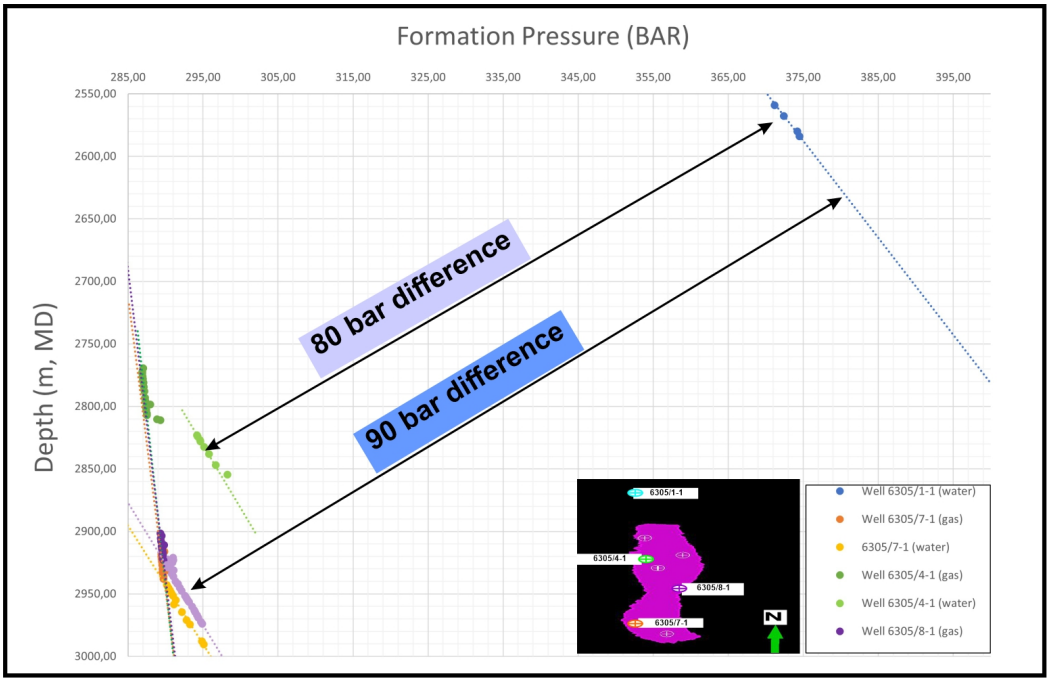

Figure 27: Pressure vs Depth graph for wells 6305/1-1,7-1,8-1, and 4-1. Well 6305/1-1 showcases an abnormally high pressure, which is suggestive of it being in a separate system as the rest of the reservoir.

Adding to the observations for wells 6305/5-3S and 4-2s, it becomes clear that 6305/1-1 cannot be connected with the rest of the field. Also, there are few data points which introduce a high degree of uncertainty to the presented observations. Given that only well 6305/1-1 is located in the north, and there is a significant difference in pressure with the rest of the wells, I decided to exclude it in this section and bring it back in the discussion section. After removing well 6305/1-1 from the pressure plot (figure 28), the results outline a similar trend for wells 6305/7-1 and 8-1 concurrent with the well logs observations. However, well 6305/4-1 presents a significant shift in pressure between the water and gas section. Grecula et al. (2015) identifies this separation as indicative of a hydrodynamic setting

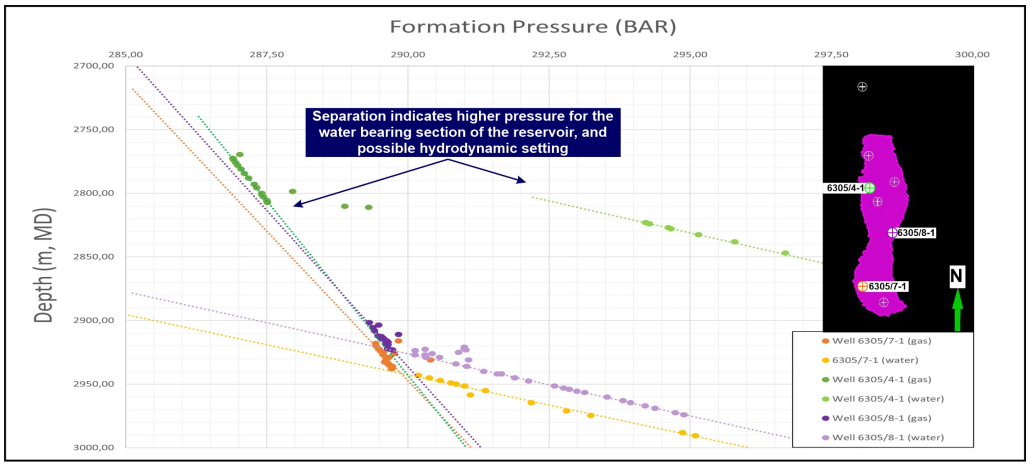

Figure 28: Depth vs pressure graph outlining the changes in pressure for wells 6305/4-1,7-1 and 8-1. We observe an increase in the pressure of the water section of well 6305/4-1, which can be indicative of a hydrodynamic setting

Additionally, we can consider other explanations for the pressure shift by accounting for previous observations. First, if the water pressure trend is shifted to represent a scenario where the water section is not over-pressured, we see that the trend for well 6305/4-1 matched the trends for the remaining wells. This becomes more evident as all three well have a similar gas pressure regime. Therefore, the difference in pressure on well 6305/4-1 is better justified by a local change in stratigraphy/structure. Looking at Figure 25 and 26, we see that the primary difference between the south zone (well 6305/7-1 and 8-1) and middle zone (well 6305/4-1) is the relative position of the tight calcified zone relative to the GWC. In the southern part, the GWC lies above the calcified layer, while in the middle section, it lays above the calcified layer. Furthermore, an investigation of the impact of the layers mentioned above is essential for describing the pressure shift.

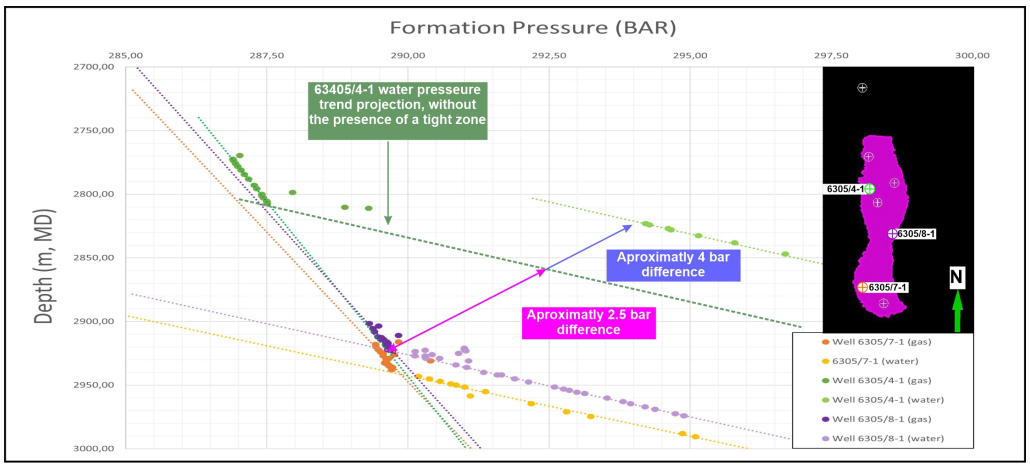

Figure 29: Projection of the water pressure trend for well 6305/4-1. Demonstrates that if the pressure shift was absent the Gas and pressure trends would be conforming to the remaining wells.

Shifts in pressure can be caused by different mechanisms, which include barriers. Previously, we postulated that the tight calcified layer around the GWC could be relatively impermeable. If that is the case, by placing the layer in the graph, we should observe that the layer's placement matches the shift in pressure. For well 6305/4-1, this layer is a few meters thick (less than 5 m, and its top standing at 2800 m MD). Looking at figure 30 we observe a good correlation between the location of the tight layer and the observed pressure shift.

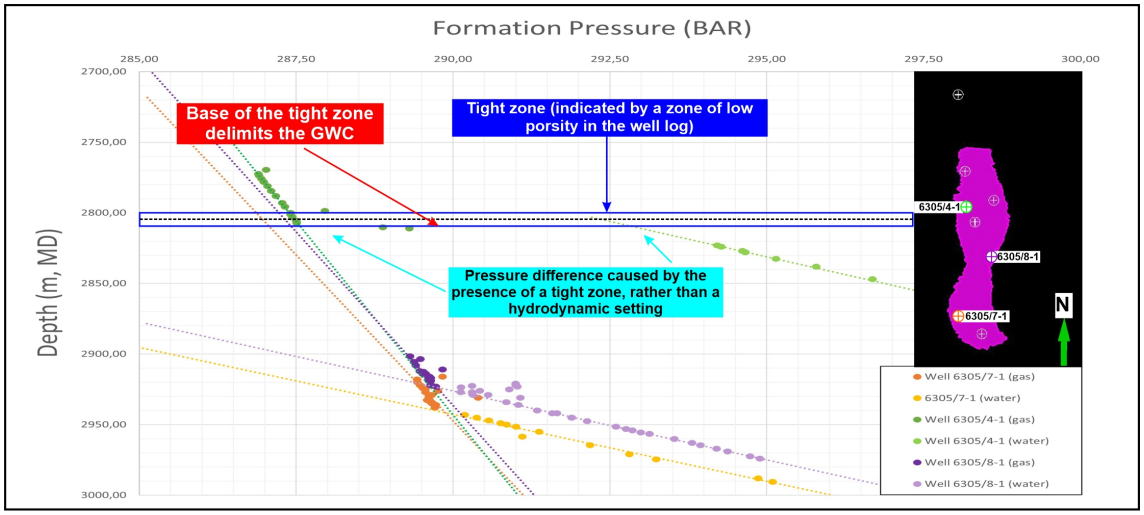

Figure 30: Illustration of the correlation between the calcified tight layer on the shift in pressure observed in well 6304/4-1

Moreover, the correlation between the pressure shift and the tight calcified layer demonstrated in Figure 30 does not necessarily indicate causation between the two observations. However, the proposed relation is plausible considering the trends mentioned above. Adding to this scenario the decrease in reservoir thickness and an increase in the thickness of the Våle tight, the presented scenario becomes more plausible as the changes in thickness towards the well could justify the increase in pressure in the water zone. However, under such an assumption, we should observe a similar trend on wells 6305/5-3s and 5-1, which data is not represented here. Pressure information for well 6305/5-1 is represented on Möller et al. (2004), and it depicts a shift in pressure as well, but to a smaller extent. This could be justified by the increase in thickness of the Våle tight on well 6305/4-1. Nevertheless, it is clear that the tight calcified zone plays a role in pressure and the position of the GWC.

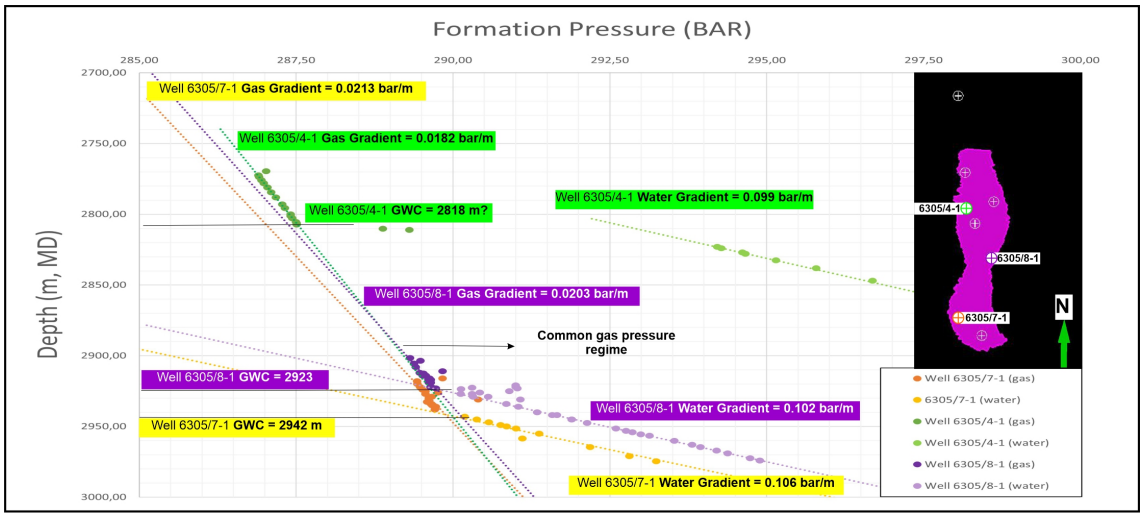

Figure 31: Interpretation of the GWC, gas and gradients for wells 6305/7-1, 8-1, and 4-1

For the remainder of this project, I will work under the assumption that the tight calcified layer significantly impacts the pressure distribution of the field. Also, given the well observations, I will assume that it has a significant areal distribution mainly towards the middle of the field, where wells 6305/5-3s,4-1, and 5-1 are located. Using Figure 31, and the assumptions above, we can interpret the GWC, gas, and water gradient for well s6305/4-1, 8-1, and 7-1 to be as follows :

- **6305/4-1**:
  - Gas gradient: 0.0182 bar/m
  - Water gradient: 0.099 bar/m
  - GWC : 2818 m
- **6305/8-1**:
  - Gas gradient: 0.0203 bar/m
  - Water gradient: 0.102 bar/m
  - GWC : 2923 m
- **6305/7-1**:
  - Gas gradient: 0.0213 bar/m
  - Water gradient: 0.106 bar/m
  - GWC : 2942 m

6.3 Seismic

Notwithstanding the correlation between pressure and well-log observations, it is essential to analyze the seismic data trends before further discussion. Furthermore, the Ormen Lange field has an extensive history of polygonal faulting due to the dewatering of shales. Since there is an extensive presence of shales within the reservoir unit, it is essential to understand the impact of faulting and how they might be related to the abovementioned observations.

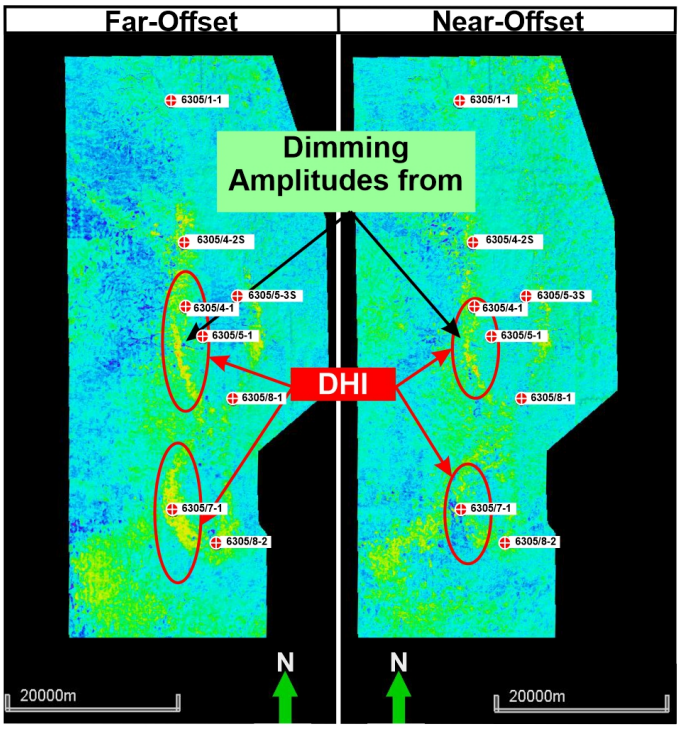

Figure 32: AVO map, showcasing the changes in amplitude from Near to Far offset

6.3.1 Well-ties and AVO

The results above showcase the main observations for the well log and pressure data. This section will explore the main trends held within the seismic. Since the Ormen Lange field is a gas field, exploring the potential AVO effects is essential. Looking at Figure 32 we observe an increase in amplitude as we move from Near to Far offset. This increase in amplitude over the outline DHI areas is connected with potential avo effects caused by gas accumulation throughout the field. Furthermore, identifying these AVO effects using amplitude maps is essential and helps guide interpretation. However, such events should be corroborated by the well ties to confidently decide the overarching type of AVO effect and what is the better way to interpret the seismic data.

Figure 32 demonstrates a trend regarding the DHI areas, which is that we see an increase in amplitudes towards the flanks of the field. Moreover, in the middle of the field, there are no distinguishable increases in amplitudes. Consequently, we need to adjust the wells grouping to better explore the AVO effects throughout the field,g. We will group the wells based on their relative position to the field flanks to showcase the well ties and the AVO effect. For the eastern field, we grouped wells 6305/1-1, 4-2S, 4-1, and 7-1; for the western flank, we grouped wells 5-3S, 8-1, and 8-2, and well 6305/5-1 serves as a single example for the middle of the field.

We have the large well grouping for the East flank and can see a larger variation of the AVO effects. Figure 33 demonstrates that a similar trend as that presented on Figure 32. Here we see that well 6305/1-1 presents AVO indication as the amplitudes remain the same across the different offsets. However, as we move south towards the first DHI area (wells 6305/4-2S and 4-1), we start to see a clear AVO effect. Here we see a significant increase in amplitudes between the Near and Far offset. For well 6305/4-1, we observe some faults across top Egga and some correlation between them and changes in amplitude. As per our previous discussion, we know that 6305/4-1 presents a dynamic sealing for the faults, which can impact how Gas accumulates throughout the layer. Consequently, the observed changes in amplitudes across faults could be related to the dynamic sealing present in well 6305/4-1.

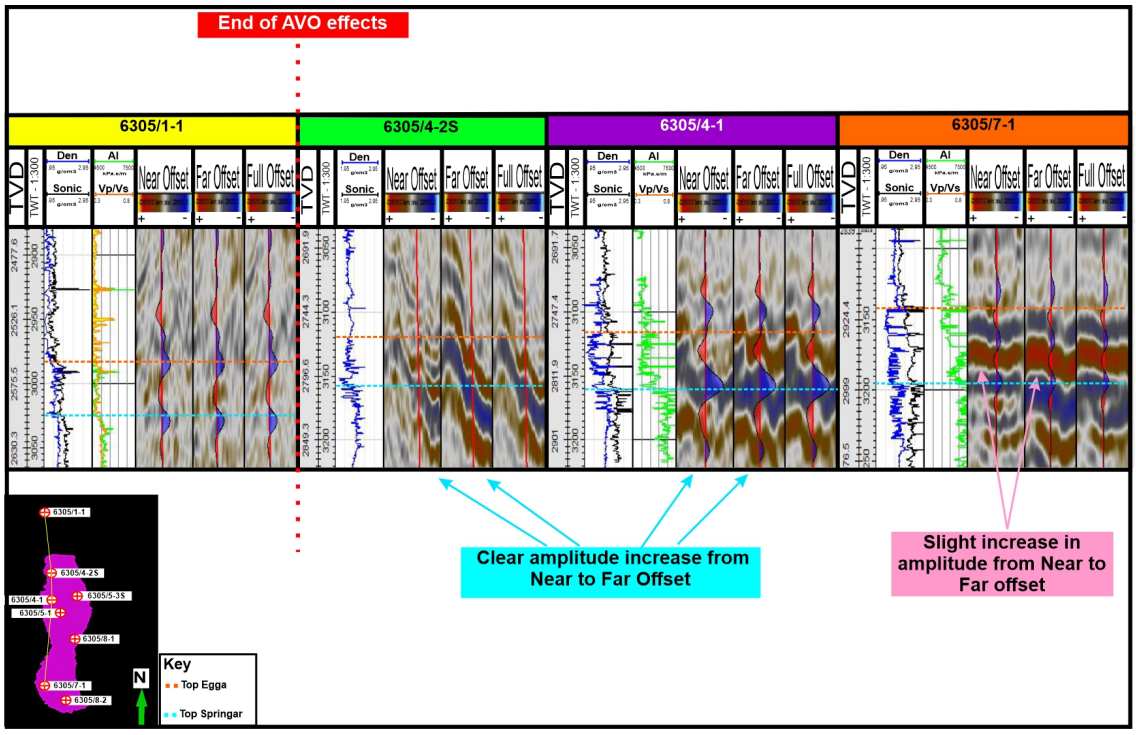

Figure 33: Well tie for wells in the East flank of the field, and demonstration of the AVO effects across the area

As we move the southeastern DHI area (well 6305/7-1), we observe a general increase in amplitude in our reflection. In this position, we observe larger amplitudes across the different offsets, which differs from the observed trend in the previous wells. Instead, we see a slight increase in amplitude between the Near and Far offset, which is more evident in the Springar formation. Moving to the western flank, we observe a similar trend, with a slight increase in amplitudes as we move from the Near to Far offset. However, as we move south (well 6305/8-2), we see that the increase in amplitude becomes more evident (Figure 34).

Well, 6305/5-3S stands out from the other wells on both flanks. We do not see a bright spot for this well as in the rest of the wells in the DHI areas. Instead, we see a relatively fractured reflection at the Near offset that transitions to be more continuous with higher amplitude in the Far offset. Nonetheless, the increase in amplitude is still observed similarly to the other wells. Additionally, well 6305/8-2 presents a similar trend as that observed in well 6305/4-1, where there seems to be a relation between faulting and the increase in amplitude between offsets.

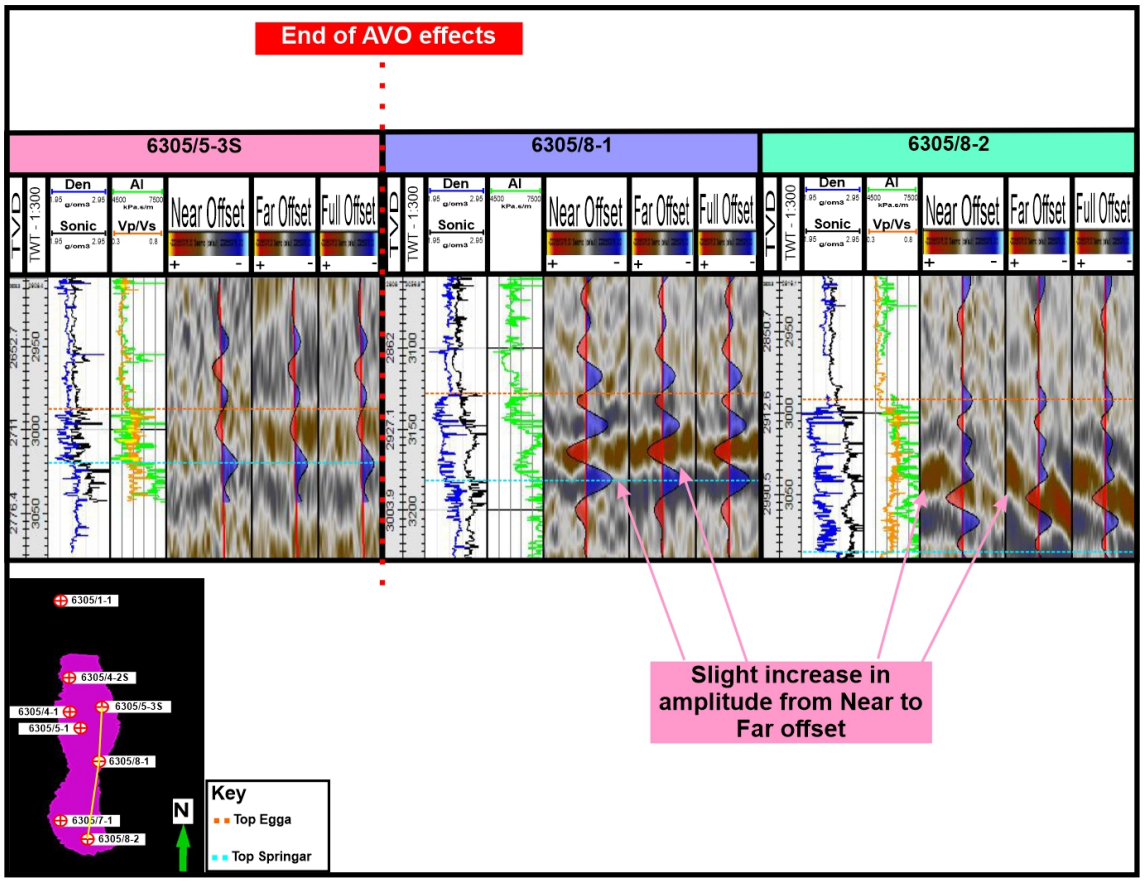

Figure 34: Well tie for wells in the West flank of the field, and demonstration of the AVO effects across the area

Relative to well 6305/5-1 in the middle of the field, we observe a similar trend as that observed in Figure 32. For the other wells, the primary AVO indicator is the reflection between top Egga and Top Springar. For most wells, this intermediate reflection showcases large amplitudes, with a clear to slight increase in amplitude between Near to Far offset. However, in this scenario, there is no apparent change in amplitude, which matches the observed trend in our amplitude map. Nevertheless, when we look at the well-logs, there are clear indications of HC accumulation in this well. Therefore, we would expect to observe AVO effects given the large extent of Gas across the field.

Using Figures 33 to 35 we are able to illustrate the overall AVO effect in the filed. Regardless of Near to Far offsets, all wells showcase the same trends. First, the primary indicator is the reflection between top Egga and top Springar. This reflection is the primary AVO indicator, is generally reresented by a peak, and presents an increase in amplitude with offset. Second, Top

Egga (representing top reservoir) is represented by a weak through in most wells. Also, looking at the AI, we can observe a relatively small change between the overlying formation and the reservoir. Comparatively, there is a more significant change in AI impedance between the RU and Springar formation. Taking the AI contrast between the overburden and the RU, with the increase in amplitude with offset, establishes the AVO effect as a negative class II or class IIb. Class IIb AVO effects are more readily noticeable than its counterpart, but more importantly, they introduce some caution for our analysis. Under this class of AVO, HC indications need a close inspection, as an increase in amplitude may be indicative of both water and HC Nanda (2016a)).

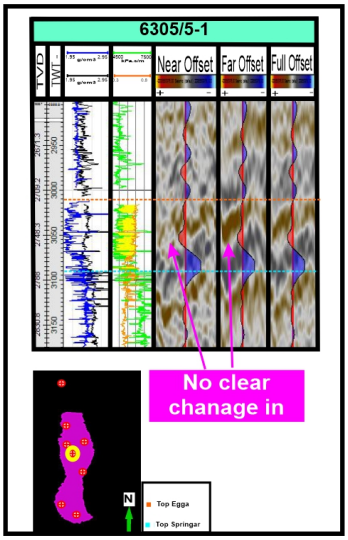

Figure 35: Well tie for well 6305/5-1 in the middle of the field demonstrating of the AVO effect in the area

Furthermore, for the good ties, we see some variation in data availability that hinders the calculation of AI for some wells. Nonetheless, the reservoir section is readily identifiable and, to a more considerable extent, relatively easy to connect to the good logs despite the complex geology in some sections (a more detailed methodology used for well-ties is outlined in Section 5). Considering the observed AVO trends, it is more accurate to interpret the seismic data using Far offset, as general trends are better depicted. To further explore the previously outlined trends, we will use a combination of selected cross lines and inlines (Figure 36). Moreover, log data analysis outlined an apparent degradation of facies towards the North of the field. Consequently, the selected seismic sections will focus more on the Northern part of the field to explore potential causes for facies degradation.

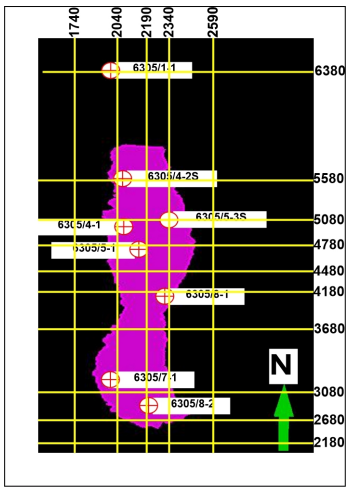

Figure 36: Map of the selected inlines and cross lines for the depiction of main trends in the seismic data.

6.3.2 In Lines

The goal of the following inlines is to outline the North-South trends of the field as they relate to the observed facies degradation in the well logs. Additionally, there is a need to investigate the extent of polygonal faulting across the field and its correlation to trends in facies. Also, it is crucial to see how the different DHI indicators translate from the presented amplitude maps and well-ties to the seismic section. All the images below follow a 1:5 vertical exaggeration.

Our exploration starts at inline 1740, which lies outside the field's eastern flank, allowing us to have an idea of potential transitions from outside to the inside of the field. The more evident trends relate to faulting. We observe extensive polygonal faulting across the section, but some differences in-depth and as we move from north to south. First, until -2000 ms, we see that the seabed topography has some influence on the outline of the reflection, as they follow the same structural outline. Additionally, polygonal faults present a relatively low throw but are extensively present and do not appear to have lateral variations. In other words, we have extensive minor, polygonal faults presenting the same behavior as we move laterally. However, as we gat to shallower parts of the section, mainly towards the scarps, we see an increase in faulting.

As we move into the Ormen Lange dome (bellow -2000 ms), we observe an evident change in the distribution of faulting. Towards the south of the field, we see polygonal faults occurring at specific levels, with no extensive links between different levels. As a result, the southern section is less fractured with more continuous reflections. However, as we move towards the slope of the syncline, we observe a connection between polygonal faults at different levels. Also, there is a general increase in the degree of faulting. An extensive fractured area arises with an increase in the degree of faulting alongside a link between faulting levels. The transition between both types of faulting is relatively easy to identify and is marked in Figure 37. Additionally, as we move towards the surface, there are some sections where the links between polygonal faults reach the surface, creating a long fault that connects the reservoir area to the surface. This is evident in the southern part of the field, where an apparent fault extends from the surface to the end of the section. The presence of scarps at the seabed presents some issues relative to the velocity variation. As per our discussion in Section 5, the horizontal variation in velocity introduced by the scarps may introduce some pull-up effects. However, in this section, such effects are not evident. However, it is possible to observe several bright spots throughout the field. Given the location of the section beyond the field, the connection of these DHIs with the accumulation of gas is unclear.

Additionally, their sizeable areal extent suggests a leakage in the main reservoir area, which would allow gas to move through the network of polygonal faults. In this area of the field, this assumption requires further investigation. More important is the investigation of the signature along the reservoir area.

Looking at the reflections of top Egga and Springar, we can set some observations about the reservoir. First is a correlation between the accumulation of clean sands and the observed amplitudes (at least at the reservoir level). Such correlation is more visible through the correlation of sweetness and the actual section, as showcased in Figure 37. Also, there is an amplitude shut down towards the end of the southern part of the field. This shutdown is marked by a fault and is interpreted to mark the lateral extent of the field. There is also a separation between zones with clean sands. A heavily faulted zone separates the areas with good sand accumulation. Additionally, the overburden layers are thinned, allowing for a connection between the reservoir area and the above layers. Furthermore, if the are HC in this field section, the combination of an overburden thinning and the faulted zone would establish a path for HC movement and justify the observed DHIs.

The observed trends tell the potential influence of faulting in the field. To further investigate, we must investigate the remaining areas of the field. First is the Easter flank of the field, where we observed two distinct DHI areas in the surface maps (Fig. 32). Figure 38 showcases the main observation over the Eastern flank. First, the shallow trends observed outside the field remain, with extensive polygonal faults with low throws dominating sections above 2000 ms.

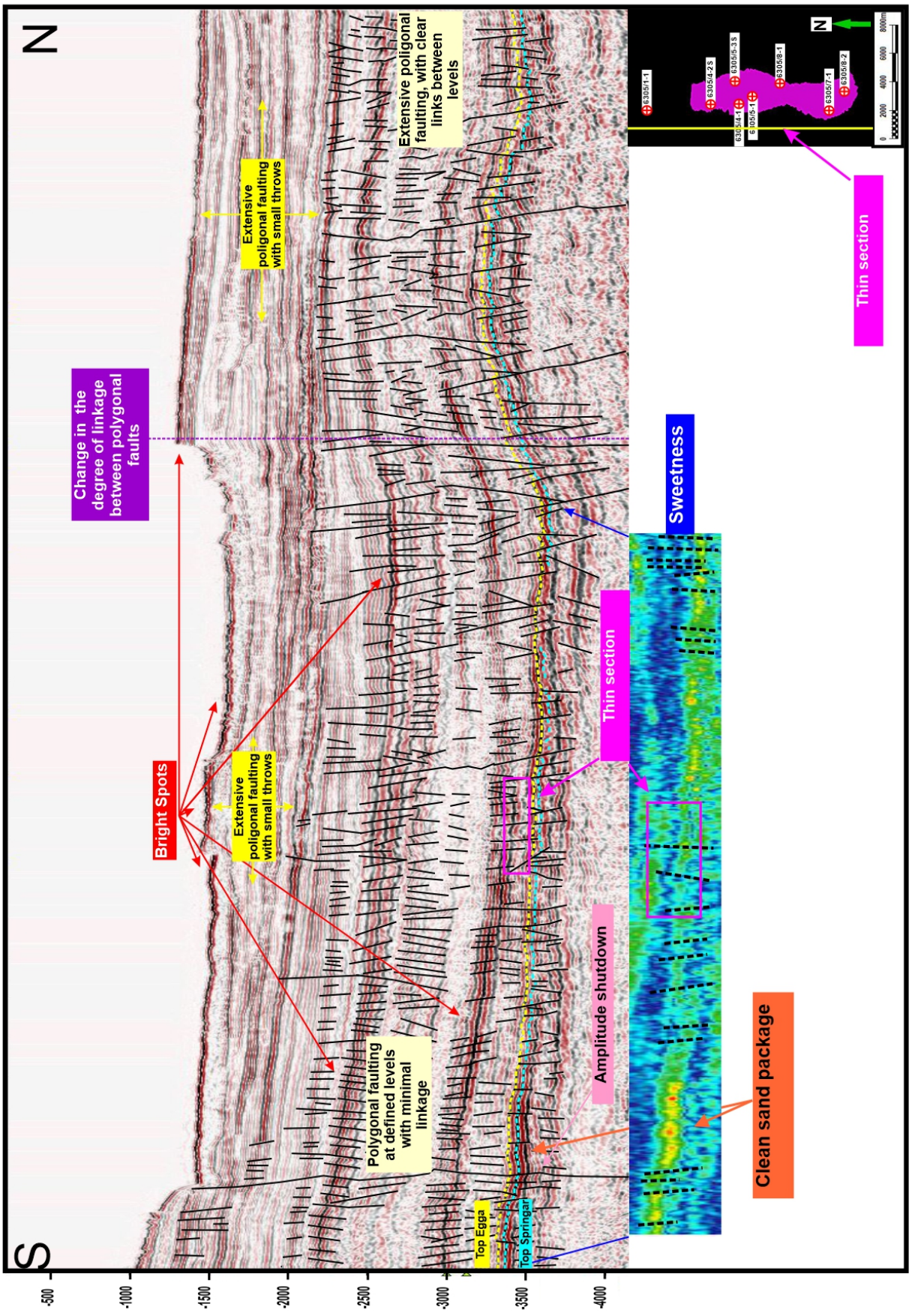

Figure 37: Interpreted inline 1750, showcasing the primary North-South trends in the beyond the western flank of the filed.

Second, the differences in faulting between north and south prevail, with the northern part showcasing extensive links between faults and high deformation levels. Also, the large areal extent of bright spots remains, with more emphasis on the surface, the layer right above the reservoir section, and above the dome.

We have an extensive correlation for this section, allowing for a better investigation of HC distribution. From our logs, we know that gas was found in well 6305/7-1 and 4-1, residual evidence of gas is present on well 6305/4-2S, and there is no evidence of gas. In the seismic section, at the reservoir level, we see that the DHIs are primarily concentrated in the southern flank of the dome. This is consistent with the well information as no gas was observed beyond well 6305/4-2S. Moreover, in this section, we observe two distinct DHI areas separated by a heavily faulted zone, which is coincidental with a thinning of the overburden layers (labeled "thin zone" in Figure 38. Faulting is relatively consistent within the DHI areas but appears to have less impact on the lateral extent gas. Looking at the sweetness, we see that these DHI areas coincide with areas with good sand accumulation.

Both DHI areas are laterally delimited by a fault, which showcases a level of reservoir compartmentalization. This compartmentalization is further emphasized by the clean sand distribution demonstrated by sweetness. Here the clean sand packages are separated by an intermediate area with poor sand quality and extensive faulting, which coincides with a thinning of the overburden layers. In the seismic section, the extent of the clean sands is delimited by amplitudes shutdowns beyond the delimiting faults. Consequently, we can assert that in the eastern flank, the reservoir is compartmentalized by a zone of increased faulting associated with a localized area of facies degradation. More pertinent to understanding the gas accumulation in the clean sand packages is the interplay between present polygonal faults and leakage.

Similar to the trends in the outskirts of the eastern flank, we observe bright sports throughout the section. However, we can delimit areas where HC accumulation is known in this case. Thus, faulting in the clean sand packages may lead to leakage, as we observe bright spots immediately above the reservoir area, which further suggests leakage. For instance, we know that well 6305/4-1 presents a dynamic sealing while bright spots are readily observed above the well's reservoir area, suggesting leaks and gas accumulating beyond the overburden.

Relative to the wide areal distribution of bright spots in the section, the fault distribution becomes essential. While the main reservoir area lies towards the south, the presence of bright spots northwards suggests a connection between the south and north fault patterns, where gas leaks in the south can migrate to the northern parts of the field. Thus, justifying the observed DHI in different parts of the field. However, we must look at other regions of the field to better determine this as a general pattern of a local event.

Figure 39 showcases a cross-section of the middle of the field. Similar to the previous sections, we observe a wide areal distribution of bright spots. However, we observe that the bright spots become more prevalent towards the northward delimitation of the reservoir unit. Here we see our DHI migrating from the reservoir level to the layers immediately above it. Polygonal fault patterns remain the same, with the north part of the field showcasing an increase in faulting and links between fault levels. Unlike the previous sections, we observe higher bright spot amplitudes towards the north, with higher prominence immediately above the northmost lateral termination of the reservoir.

Here the reservoir section does not have any compartmentalization and demonstration of a continuous disposition. Also, it remains located on the southern flank of the dome. Sweetness shows clean sands throughout the reservoir. Additionally, the lateral termination is marked by amplitude shutdowns, after which the quality of the sands decreases. At the reservoir level, we observe extensive faulting of the overburden and the underlying layers. Unlike the previous section, we do not observe a thinning of the overburden as its thickness remains relatively constant, as the lateral extent of the Ormen Lange dome increases in this section. Comparatively to the trends observed in Figure 38, extensive faulting within the reservoir does not lead to compartmentalization and does not affect the distribution of clean sands or the presence of leaks in the middle of the unit. Instead, we see more evidence of leaks in the extremes of the reservoir unit.

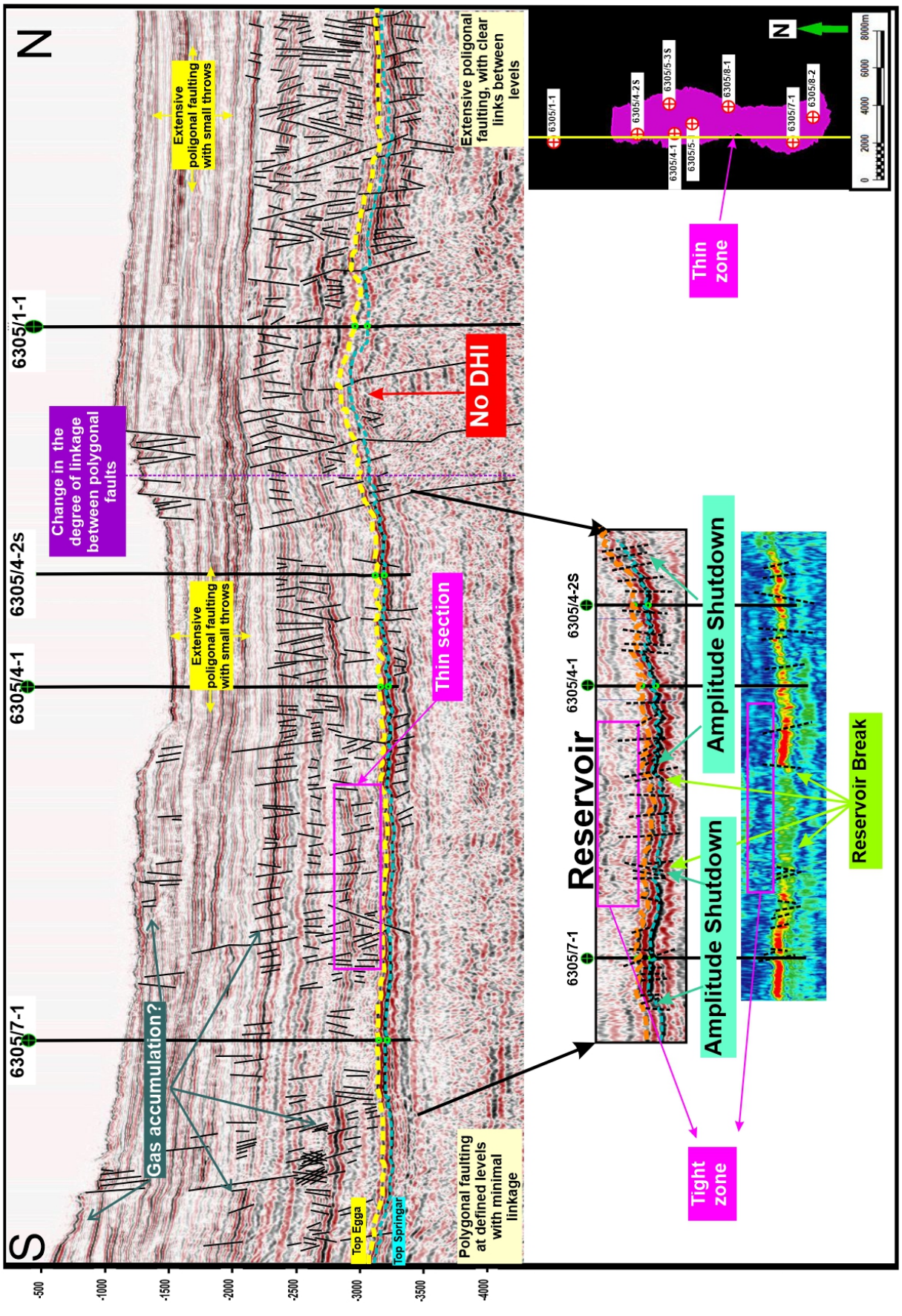

Figure 38: Interpreted inline 2040, showcasing the primary North-South trends in the Eastern flank of the filed.

The reservoir unit's lateral terminations are still delimited by faults but showcase some evidence of a lateral pinch-out. Looking at the sweetness, we see that the thickness of clean sands increases towards the north, even though well logs showcase better HC accumulation southward. Such a trend is better observed by the aforementioned northward facies degradation on the logs. However, if we look at the bright spot distribution in conjunction with the bounding faults at the reservoir level, we arrive at a possible explanation. Even though we observe a bright spot immediately above the south termination of the reservoir unit, the current section has lower amplitudes than those observed towards the north. Also, the polygonal faults tend to be more isolated towards the south than in the north. Consequently, the difference in HC accumulation presented in the logs might be connected with differential leakage rates caused by different fault patterns in the extremes of the field.

Faults in the extremes of the reservoir unit lead to some level of leakage. However, the northward extremity coincides with the transition from an area of low linkage between polygonal faults to an area of more extensive linkage. Consequently, we can assume that the extensive breaks in the north extremity allow for higher leakage rates and a subsequent decrease in gas accumulation in this field area. Therefore, justifying the prominence of DHI above the north end of the reservoir unit and the decrease in gas accumulation showcased in the logs. It is important to note that the difference in accumulation between well 6305/5-1 and 6305/8-2 is not as significant as that of more north wells. The observed facies degradation plays a role in the gas distribution of the field, but the degree of links between different polygonal faults appears to play a role in the trap set.

At this point, we observed a decrease in reservoir compartmentalization as we moved eastward, with the middle of the field showcasing a continuous distribution of clean sands. Polygonal faulting maintains a consistent trend, with the north of the field showcasing extensive deformation due to a higher degree of links between fault levels, with the south presenting moderate deformation as polygonal faults are not as well connected. The transition between both zones appears to migrate towards the south and be linked with the south beginning of the southern flank of the Ormen Lange dome. Furthermore, the reservoir unit appears to be delimited by faults but with some indication of a lateral pitchout as we move towards the field's eastern flank.

More importantly, the South-North facies degradation observed in the logs appears to be connected with the South-North fault change. Consequently, bright spots become more prevalent in the north section as we move towards the field's eastern flank. Figure 41 showcases the primary North-South trends in the eastern flank of the field and the critical trends for the eastern termination of the field. Starting with some similarities, we observe that the polygonal trends remain the same and that bright spots have a large areal extent. However, the outline of the reservoir unit has significantly changed. First, the transition between the South-North polygonal faults trend has significantly shifted southwards and contained the main RU unit to the western flank of the Ormen Lange field. Consequently, we do not observe the reservoir unit in the southernmost sections of the field. This is more evident by a lack of leakage indication in the south of the field and the migration of shallower bright spots towards the northern areas.

We observe a lateral pinch out of the Egga sands at the reservoir level while the Springar formation continues throughout the section. Looking at the DHI at the reservoir level, we observe the same amplitude shutdown and clean sand delimitation as in the previous sections. However, in this instance, we observe an apparent gas migration to layers above the overburden, clearly outlined by a flat spot. Looking at the sweetness, we see that clean sands are primarily localized to the flank of the dome but with some clean sands in the flat spot area. An amplitude shutdown also delimits the lateral limits of the flat spots. Therefore, suggesting that there is gas migration from the reservoir unit to shallower sections.

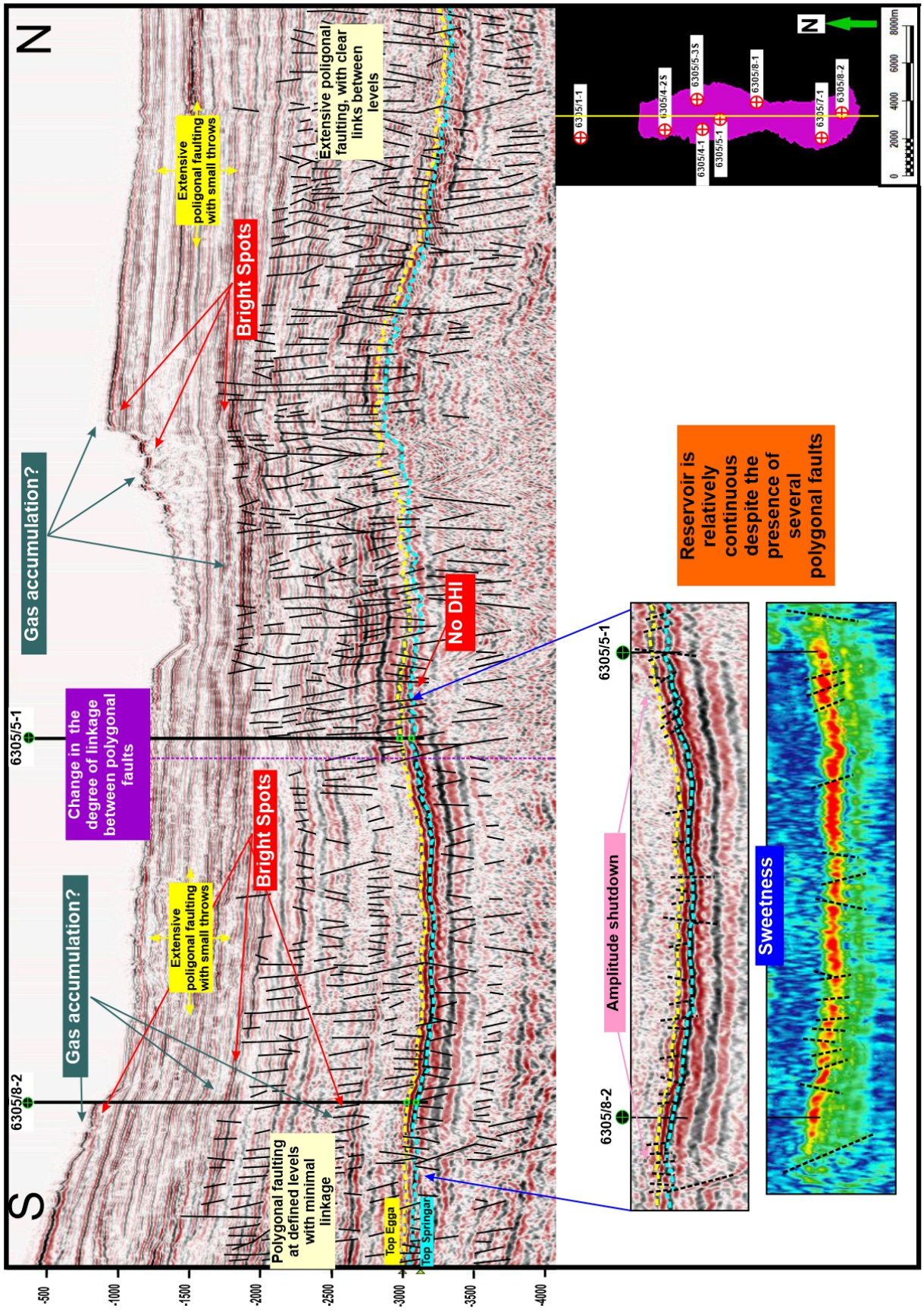

Figure 39: Interpreted inline 2190, showcasing the primary North-South trends in the middle of the filed.

Additionally, faulting is more extensive at the reservoir level in this section, with faults transecting the reservoir section and ending at the flat spot. Placing the polygonal faults and gas accumulation at shallower depths indicate leakage and subsequent gas migration. This assumption is further confirmed by Bünz et al. (2005), as he describes the occurrence of free gas in the shallow subsurface of the northern parts of the Ormen Lange field. Therefore, we can assume that the polygonal faults at the reservoir level lead to gas leakage, migrating through the polygonal fault network north of the field. In this instance, the high degree of deformation allows for both lateral and vertical movement of gas that accumulates at shallower depths.

A more prominent observation is the differential behavior of the polygonal faults. The presented sections outline the link between polygonal faults, reservoir linkage, and delineation. Therefore, the trends in Figure 41 demonstrate that the polygonal faults can seal the reservoir or serve as a mechanism for fluid flow. However, the mechanisms that allow for such differentiation fall beyond this project's scope. For this investigation, we need to outline the influence of polygonal faulting on gas distribution and its correlation to HC trapping. In this instance, polygonal faulting help define the North-South limits of the field, which also has a lateral pinch-out component towards the north of the field as we move closer to the eastern flank.

Looking at the progression from the Western to the Eastern flank, we see a different trend from that observed on the logs. The facies degradation is closely linked with the increase in deformation observed towards the north of the field. However, there are apparent differences between the east and west sides of the field that need exploration. Here we want to observe if there is an East-West deterioration in facies and if a similar polygonal fault trend is also observed in this direction. More importantly, we need to investigate different trends in gas leakage and its connection with polygonal fault distribution. Also, we see that clean sand accumulation has some relation with the structure of the field, as it is primarily concentrated on the western flank of the Ormen Lange field. Thus, if a similar polygonal trend is observed in the East-West direction, it would help describe the relationship between the structural definition of the field and the gas leaks we observed in the inlines.

Lastly, if we look at the area beyond the eastern flank (Figure 40, we observe an apparent change; first, the Ormen Lange dome is not longer visible, and polygonal faults appear to have a uniform distribution; moreover, the reflection appears to be relatively continuous with polygonal faults having small trows throughout the section; nonetheless, we still observe some bright spots at the reservoir level, but the DHI is not as prominent as the sections laying within the field, this emphasizes the presence of East-West delineation of the filed that is closely related with the areal distribution of the Ormen Lange field, the seabed appears to become more fractured, while the scarps become less prominent, as mentioned before, we need to investigate the cross lines to delimit the field better.

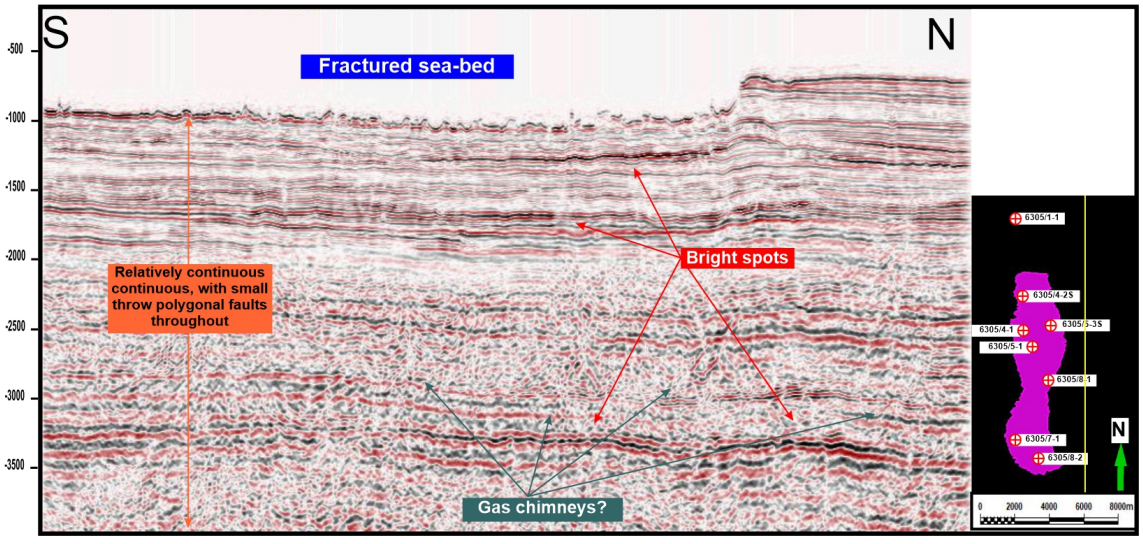

Figure 40: Interpreted inline 2590, showcasing the primary North-South trends in the eastern flank of the field.

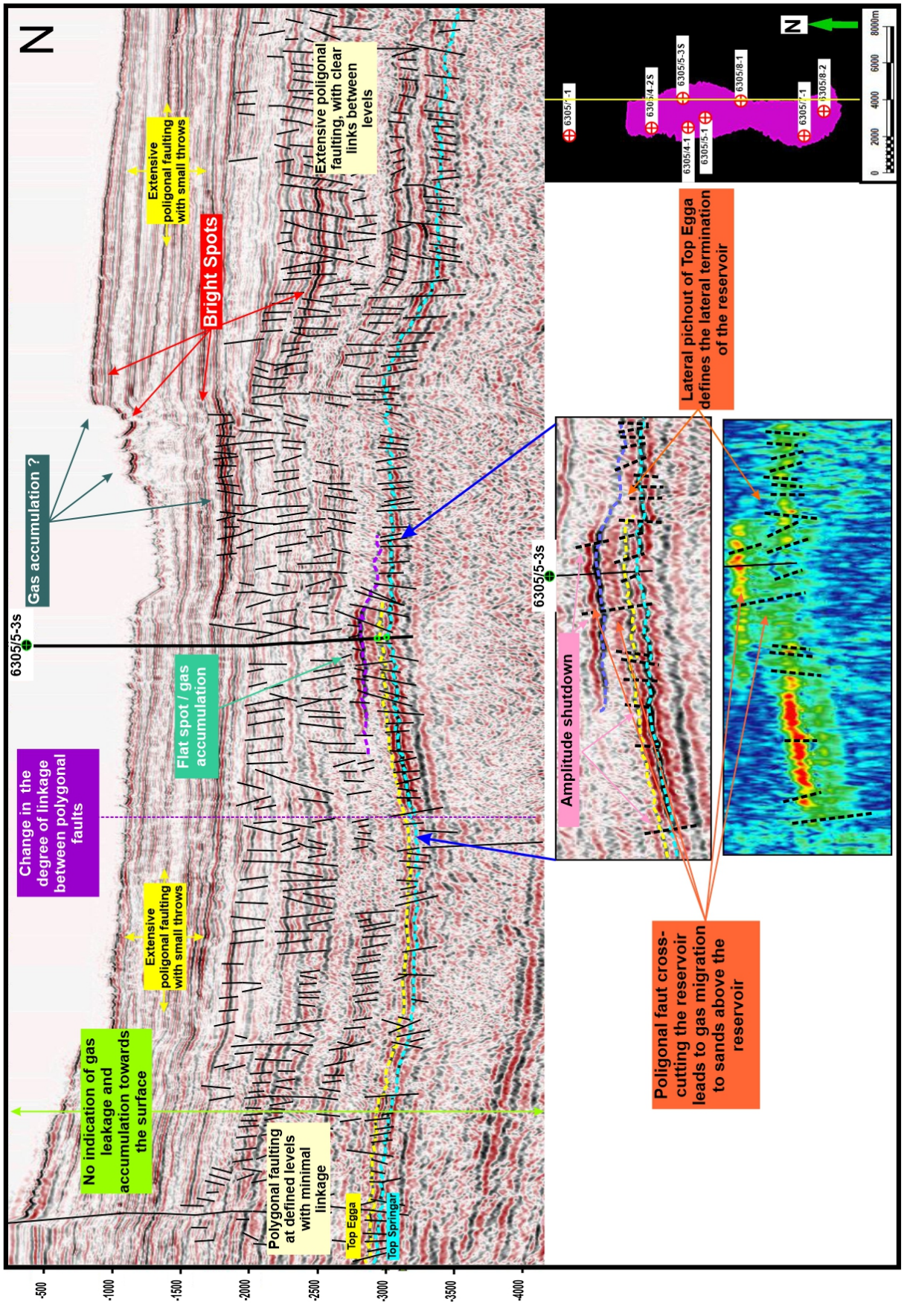

Figure 41: Interpreted inline 2340, showcasing the primary North-South trends in the eastern flank of the field.

6.3.3 Cross lines

For our analysis of the East-West trends of the field, we will start at the southern edge of the field with cross-line 2680 (Figure 42. Here we see some polygonal faulting but with a limited degree of linkage and a subsequent small degree of deformation. This is evident by the relatively continuous reflection throughout the section. Unlike the inline, deeper sections reflect the stepping outline of the seabed but without apparent pull-up effects. Similar polygonal faults appear at set depth levels, as observed in the inlines. Despite the limited linkage between different faulting levels, bright spots are observed at varying depths, with higher amplitudes at shallower depths, primarily due east.

At the reservoir level, we observe some familiar trends. The lateral limits of the reservoir unit are marked by an amplitude shutdown attached by the presence of a fault in the western margin. At this level, the reservoir unit extends to the end of the eastern margin, but there are some indications of a similar pattern as that observed in the western margin. The sweetness over the reservoir unit showcases some facies degradation due west, with clean sands primarily concentrated in the eastern margin. We can also see some faults that transect the reservoir unit and link it to overlaying layers. Sweetness shows some compartmentalization of the clean sands as they correlate well with the present faults. Overall, his section correlates well with the trends showcased in the previous sections.

As we move North, we observe some different trends. Looking at Figure 43 we maintain the same overarching trends, mainly as they partake in the distribution of bright spots and polygonal faulting. However, we start to observe some trends on the western side of the section. First, we observe an increase in polygonal faulting and associated deformation; this is clear by the presence of a gas chimney at the western end of the reservoir unit. Additionally, we observe points of gas accumulation towards the surface. Nonetheless, the polygonal fault remains predominately localized to specific layers.

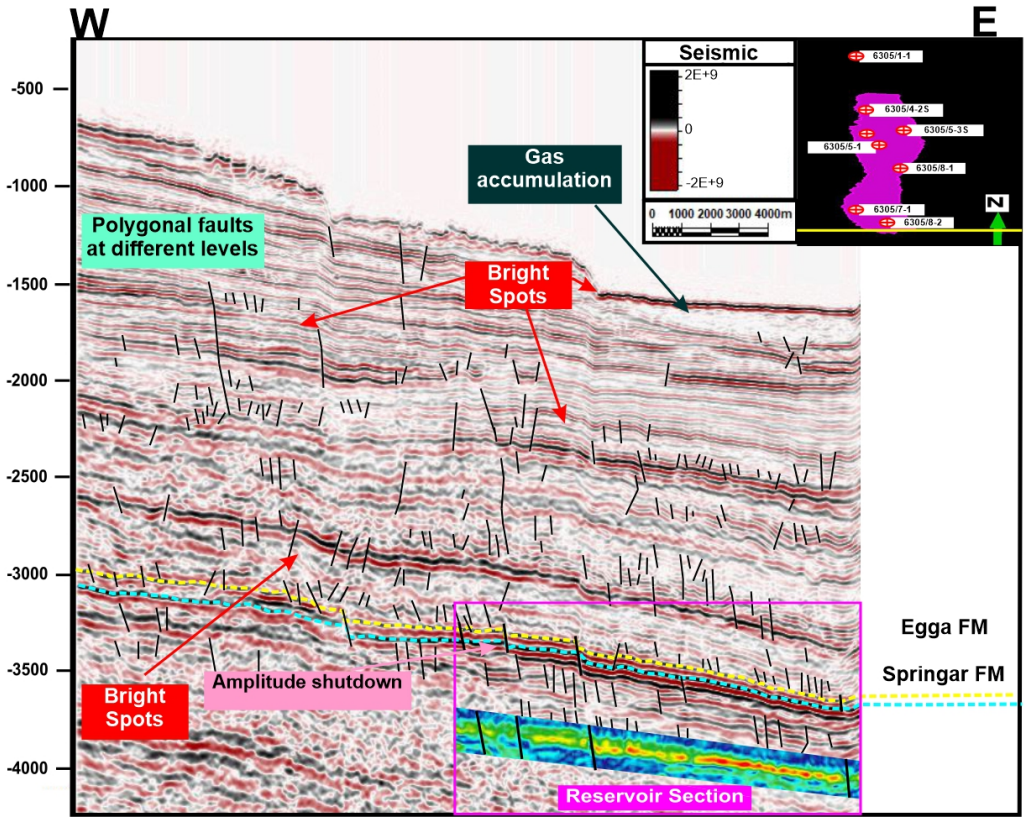

Figure 42: Interpreted cross line 2680, showcasing the primary East-West trends in the southern part of the field.

Furthermore, we see that the main reservoir is primarily contained at the structural high of a monocline. However, sweetness suggests that clean sands that do not extend to flanks and are more localized in the structural high due to a lateral pinch preceding the monocline flank. Despite a clear pitchout of the reservoir sands, we still observe the presence of faults at the extremities. In this case, we can see that faults at the extremes of the reservoir unit lead to leakage as per the bright sports demonstrated at the shallower layer immediately above the faults. We still observe faulting across the reservoir unit that leads to some breaks and minor compartmentalization, which might have small to no effect on the overall distribution of gas.

Amplitude shutdowns remain one of the leading indicators of the lateral extent of the main reservoir area, which maintain a close relationship with the clean sand termination and the faults at the extremes of the field. More evident than the inlines, we observe that some bright spots present the same amplitude shutdown trend, which is often close to a fault. However, we need further investigation to establish this as a filed trend.

Being placed between well 6305/8-2 and 7-1, we know that the section presented in Figure 43 has gas at the reservoir level. Thus, helping link, the observed bright spots with zones of gas accumulation. It is important to note that at the surface, gas primarily accumulates at the structural low at the eastern end of the field. More prominently is the relatively small lateral extent of clean sands delimiting the field, contrasting with the North-South lines that present larger areal extents.

Figure 44 shows the position where in the inlines, we start to transition into a higher level of polygonal fault linkage and an overall increase in deformation. The familiar trend prevails, with shallower faulting becoming relatively more frequent. Bright spots maintain their sizeable areal extent, but we start to observe an increase in amplitude towards the eastern end of the field. Moreover, the deformation at the western flank becomes more prevalent as links between fault levels increase.

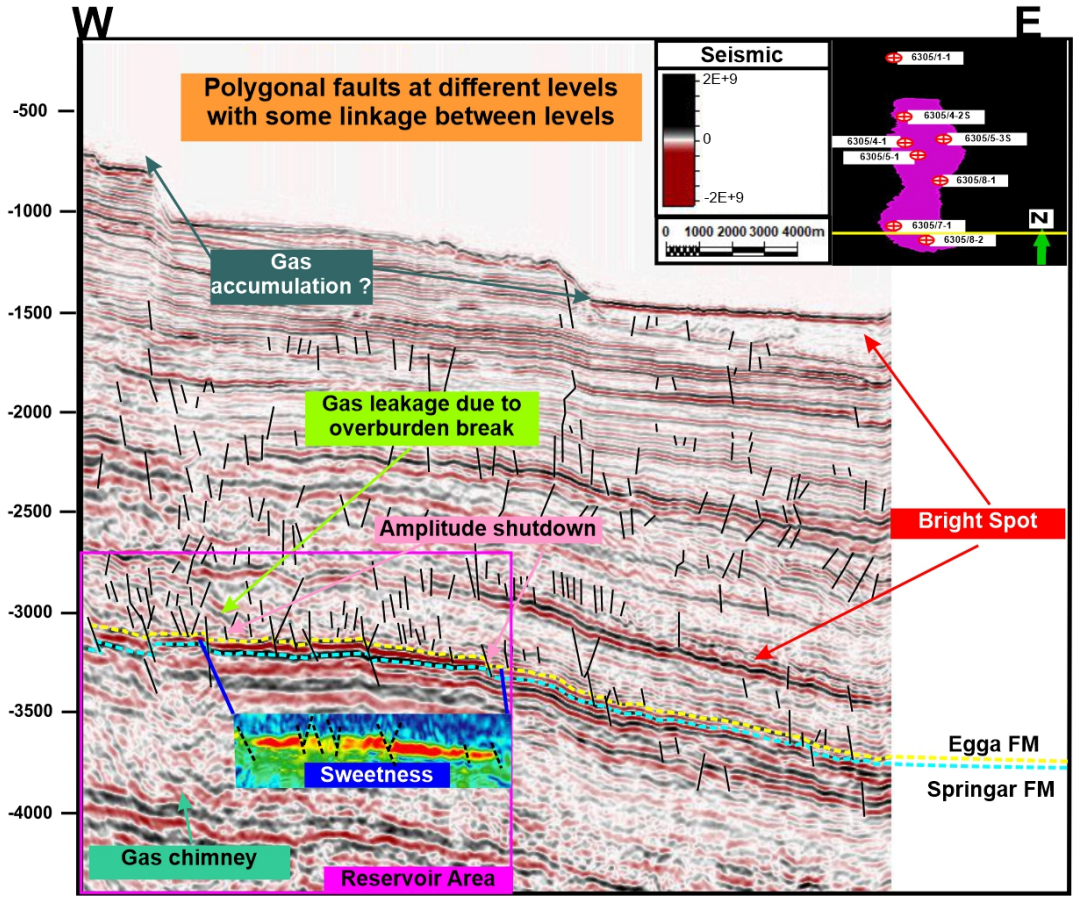

Figure 43: Interpreted cross line 3080, showcasing the primary East-West trends in the southern part of the field.

While in Figure 43 the reservoir unit seems to be delimited by a lateral pinch-out, in Figure 44 the reservoir unit termination appears to be more closely linked to the presence of bounding faults. Remaining located at the structural high of the monocline, the clean reservoir sands terminate with faults and do not extend to the flank. Here the delimiting amplitude shutdown becomes more evident, and faulting within the reservoir unit becomes not prevalent, landing to a higher degree of compartmentalizing.

Nonetheless, the sands appear to be relatively continuous, and compartmentalization should have little to no effect on HC distribution. Looking at the sweetness, there is a facies degradation from east to west until a fault, after which we have a clean sand package and the delimiting western fault. In this case, the fault separating the two clean sand packages might compartmentalize the reservoir. This trend is also observed in Figure 43, where the middle section of the central reservoir unit presents a facies degradation, and the main clean sand packages are on the flanks. Such observation is consistent with the DHI areas outlined in Figure 32 since they tend to be localized at the flanks of the field.

Even though deformation is more readily noticeable on the western flank, we must outline an increase in the linkage between different fault levels in the Eastern flank. This increase in the linkage is outlined by the prominent presence of higher amplitude bright spots in the eastern flank. Connecting the position of high amplitude bright spots and the delimitation of the main reservoir by faults (for Figure 44), we can infer that the eastern delimiting fault allows for a higher rate of leakage relative to the western fault. It is also possible that the higher degree of deformation on the western side allows for lateral fluid motion, preferentially accumulating on the eastern side. The combination of both aspects is also plausible.

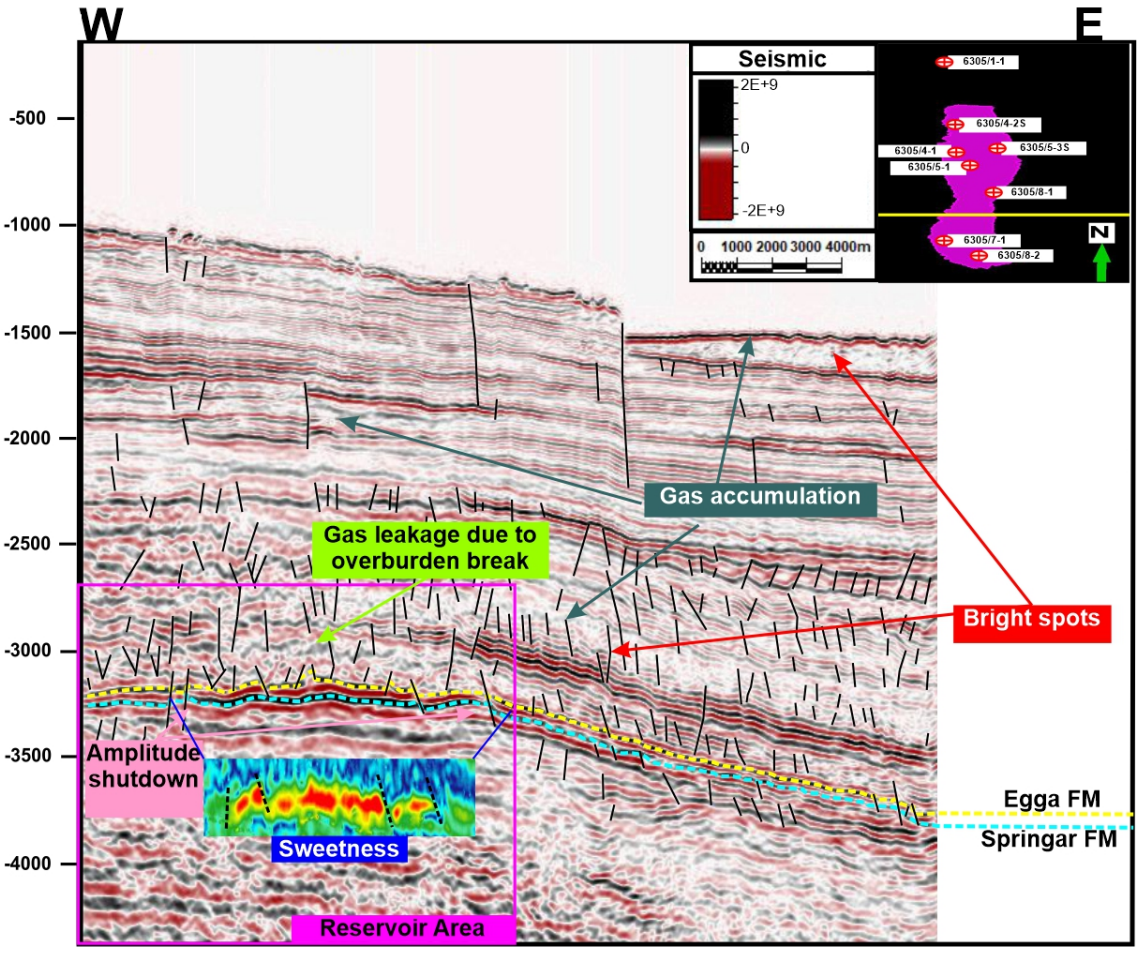

Figure 44: Interpreted cross line 3680, showcasing the primary East-West trends in the southern part of the field.

The transition from Figure 44 to Figure 45 marks the end of the first DHI area marked on Figure 32 and the transition into the northernmost DHI area. This transition also applies to the trends in the well logs as we move from the south well group to the middle. The first change lies in the lateral extent of the field, as it becomes shorter in this section and increases afterward. Consequently, we expect the main reservoir unit to have a smaller lateral extent. Looking at Figure 45 the shortening of the main reservoir unit is evident. Even though it remains located at the edge of the structural high of the monocline, the increase in deformation on the western side impacts the lateral extent of the main reservoir. A lateral pitchout better defines the sand package, but the extremity faults remain.

Unlike the previous crosslines, bright spots are primarily confined to the shallow eastern side of the section. On the western side, deformation subsides at depths shallower than -2000 ms after wish reflections are primarily continuous and show no clear, bright spots. Also, we start to see some dim areas, primarily located east of the central reservoir unit. Deformation also increases eastward by maintaining specific depth levels with some links between them.

At the reservoir level, amplitude shutdowns remain the delimiting factor for the later extent of the reservoir unit, but with a lesser degree of faulting within the sand package. Consequently, we do not see any clear signs of compartmentalization. Nevertheless, the increase in deformation on the eastern side, alongside a localized extent of bright/dim spots, suggests that the eastern termination of the reservoir unit is the primary source of leaks. Consequently, pointing to a differential behavior between the western and eastern faults relative to their sealing capabilities. Nevertheless, it is still possible for the western bounding fault to allow for gas leaks, as the large degree of deformation would justify lateral flow and the preferential accumulation on the eastern side.

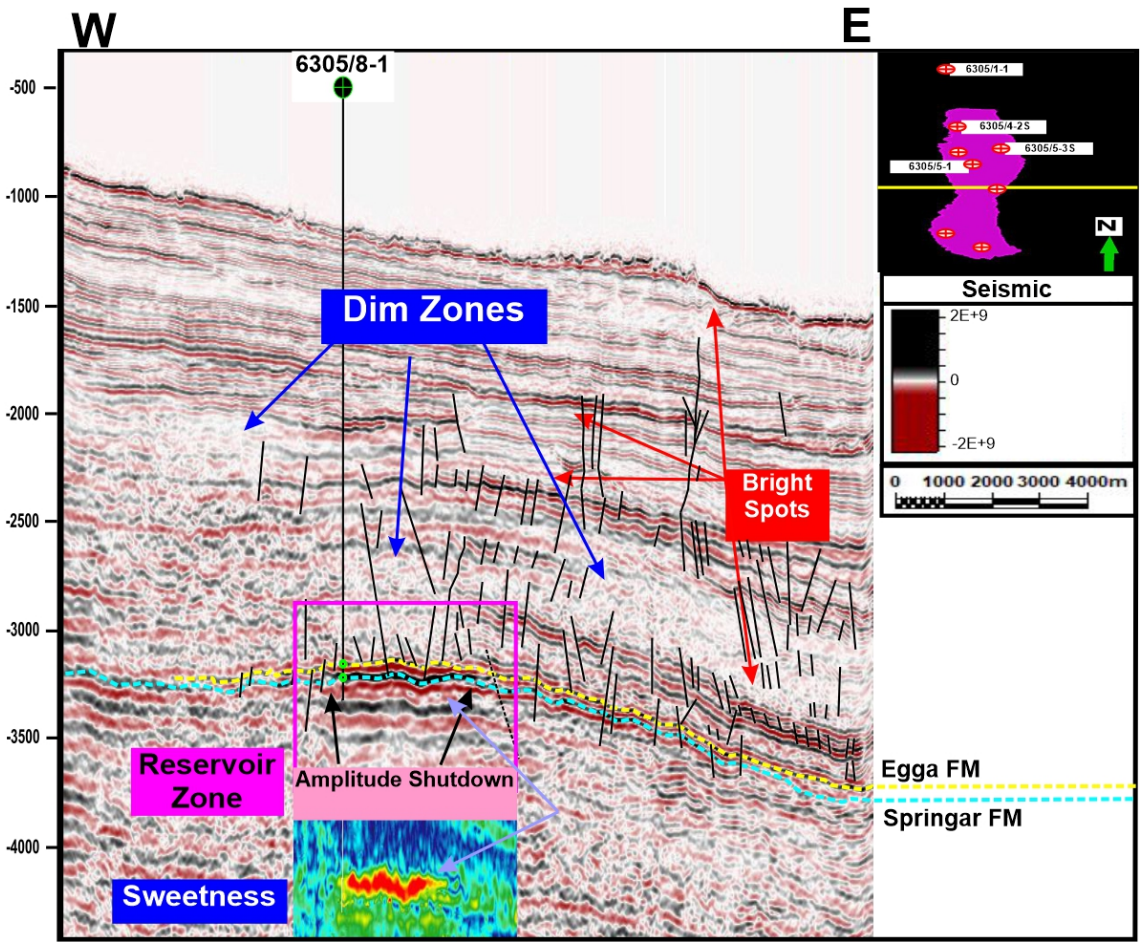

Figure 45: Interpreted cross line 4180, showcasing the primary East-West trends in middle of the field.

Looking at the inline sections above, Figure 45 should outline an overall increase in deformation and fault links. Figure 46 outlines this exact effect as we observe a significant increase in deformation and fault linkage. Nonetheless, deformation remains more prevalent due west, with the eastern margin showcasing different faulting levels with minimal linkage. Despite the higher degree of the formation due west, gas migration and accumulation maintains a preferential migration trend due east, as highlighted by the position of bright spots. Dim zones consolidate immediately above the reservoir area and extend due east.

The increase in faulting is evident at the reservoir level; the fault density increases within it. We observe that the sand package is segmented by the faults, which introduces some compartmentalization. Nevertheless, we maintain a lateral pitchout with faults at the extremes outlining the points with an amplitude shutdown. Different from other observations, we see the presence of some clean sands below the reservoir. At this point, we are still outside the northern DHI area, which is evident by the short lateral extent of the main reservoir area. The Ormen Lange dome is more evident by maintaining a monocline-like outline. Looking at Figure 39 we expect to see an increase in gas migration to overlaying section as we move north from cross line 4480.

Figure 47, introduces some changes in the field. First, the Ormen Lange dome becomes better defined, and the eastern flank becomes steeper. Also, the western flank becomes shorter, which decreases the western deformation zone. Therefore, the section becomes dominated by polygonal faults at specific levels with small links. Looking at the good logs, we expect a significant decrease in facies quality beyond this point, making it important to outline cases for the transition.

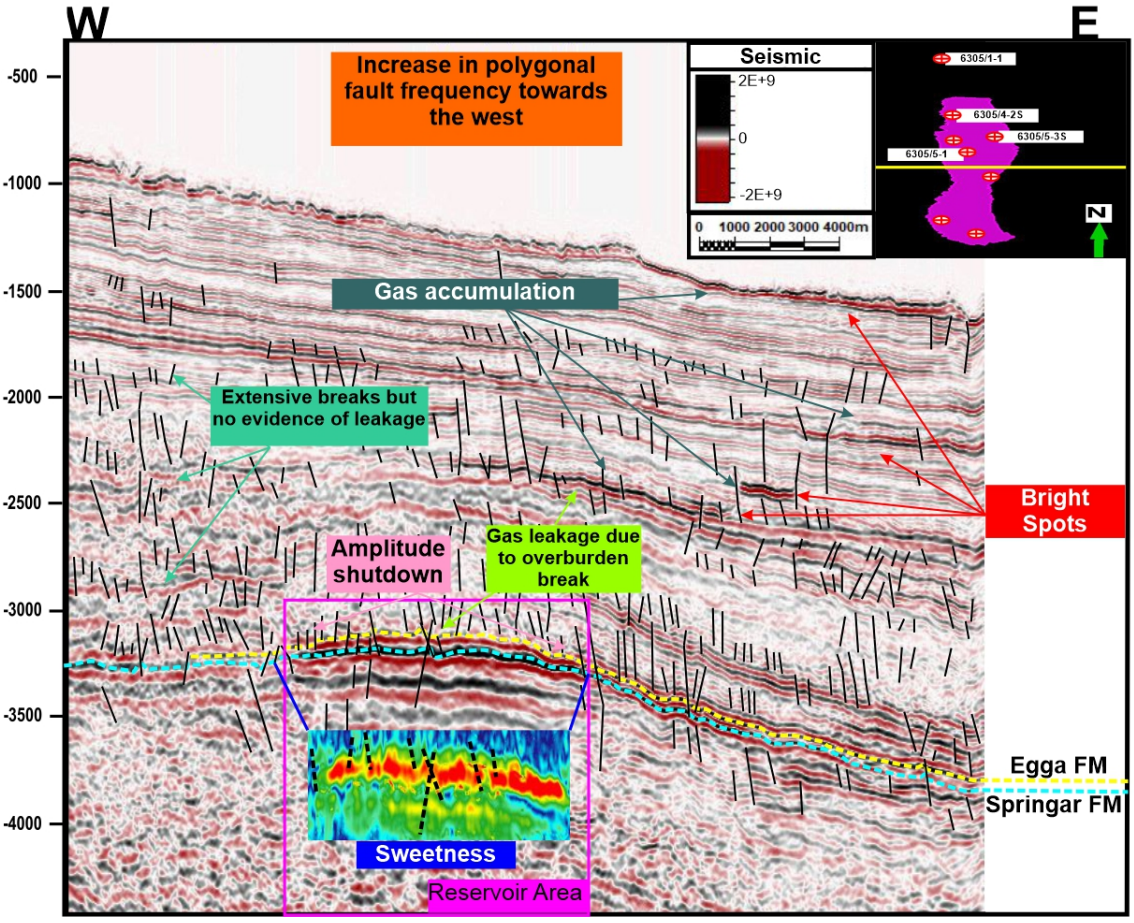

Figure 46: Interpreted cross line 4480, showcasing the primary East-West trends in the north of the field.

First, we see clear compartmentalization of the reservoir unit, with the sand packages migrating to the dome's flanks. Amplitude shutdowns further outline this trend and showcase the localized presence of DHI on the flanks of the dome. At the structural high, we see a degradation in facies

associated with increased polygonal faulting, leading to gas migration to the layer overlying the field. This gas accumulation is marked by the flat spot immediately above the central reservoir unit, indicating that the reservoir compartmentalization is not only lateral but also vertical.

The main sand packages maintained can still be delimited by a lateral pinch out, but the fault zone separating them moves them to two extremes of the field. Accounting for the extensive South-North facies degradation and increase in deformation, separating the sand packages may lead to a differential accumulation of HC in this field section. This is important as it could justify the differential accumulation of gas observed in the well logs beyond this point.

Furthermore, with the general increase in deformation, we observe breaks at different levels immediately above the reservoir. Consequently, we start to observe some bright spots on the shallow western side, suggesting that the faulting in the western side is not responsible for leaks. Instead, the faulting in the eastern side is responsible for gas migration and the observed accumulation of gas in the shallow eastern parts of the field. Such delimitation suggests a weaker sealing capacity for faults due east, while faults on the western side have better-sealing properties. However, the combination of both allows for the observed migration patterns. At the seabed, we see the preferential accumulation of gas at the structural low, and if we follow it in-depth, we observe that bright spots occur within this area and shift towards the reservoir unit at -2500 ms. Further suggests a presence of a fault network on the eastern side of the dome that is directing gas migration.

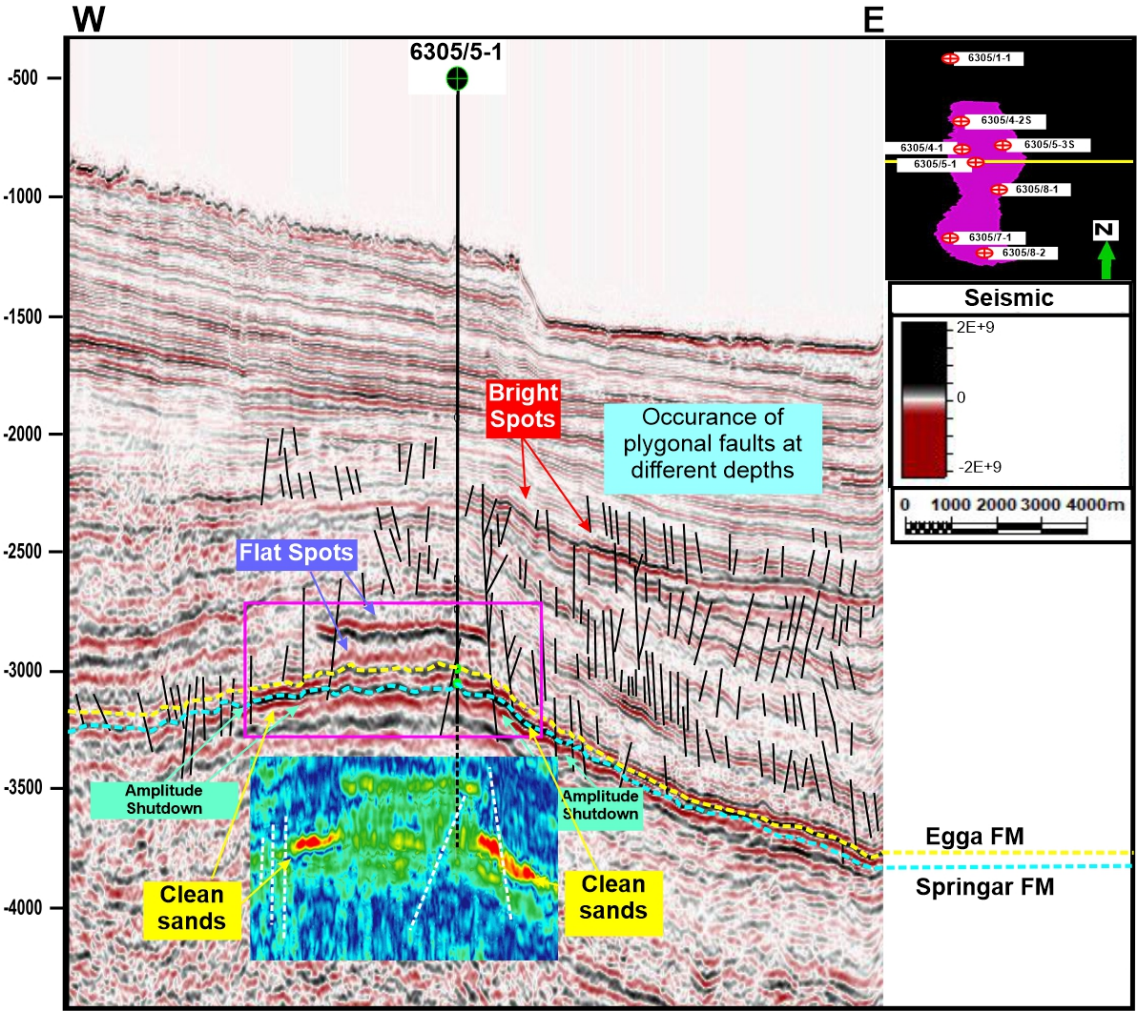

Figure 47: Interpreted cross line 4780, showcasing the primary East-West trends in the north of the field.

Figure 48 defines the sand deposits' transition towards the field's eastern flank. At the reservoir level, clean sand packages are predominantly on the eastern flank, with the sand package on the western flank being negligible in comparison. Here we observe that the sand units at the structural high have a lower sand content and are heavily faulted. Nonetheless, faulting is also prevalent in the eastern flank and compartmentalizes the already small sand package in the eastern flank. Looking at the logs, we expected a sharp decay in facies degradation, which is evident in this section.

Moreover, they also observe an increase in deformation in the eastern side of the field, with faults becoming evermore linked. Deformation at the western side maintains its level of deformation, while no evidence of gas leakage is readily observable. Flat spots overlaying the reservoir unit indicate a continuation of gas migration to overlaying layer due to an increase in faulting at the reservoir level. Gas migration continues to have a preferential migration pattern due east, but with increased faulting, more bright spots appear above the reservoir unit and at some western points. Therefore, there seems to have been a slight adjustment to the gas migration pattern that allows it to accumulate in more expansive, shallower areas.

From the good logs, we expect the reservoir unit to have a higher shale content and some isolated sands until well 6305/4-2, with residual evidence of HC accumulation. From Figure 32, we know that we are still within the northern DHI area. Therefore, we must investigate why we still observe a DHI even though the well logs suggest a vestigial presence of gas in the sections beyond cross-section 5080.

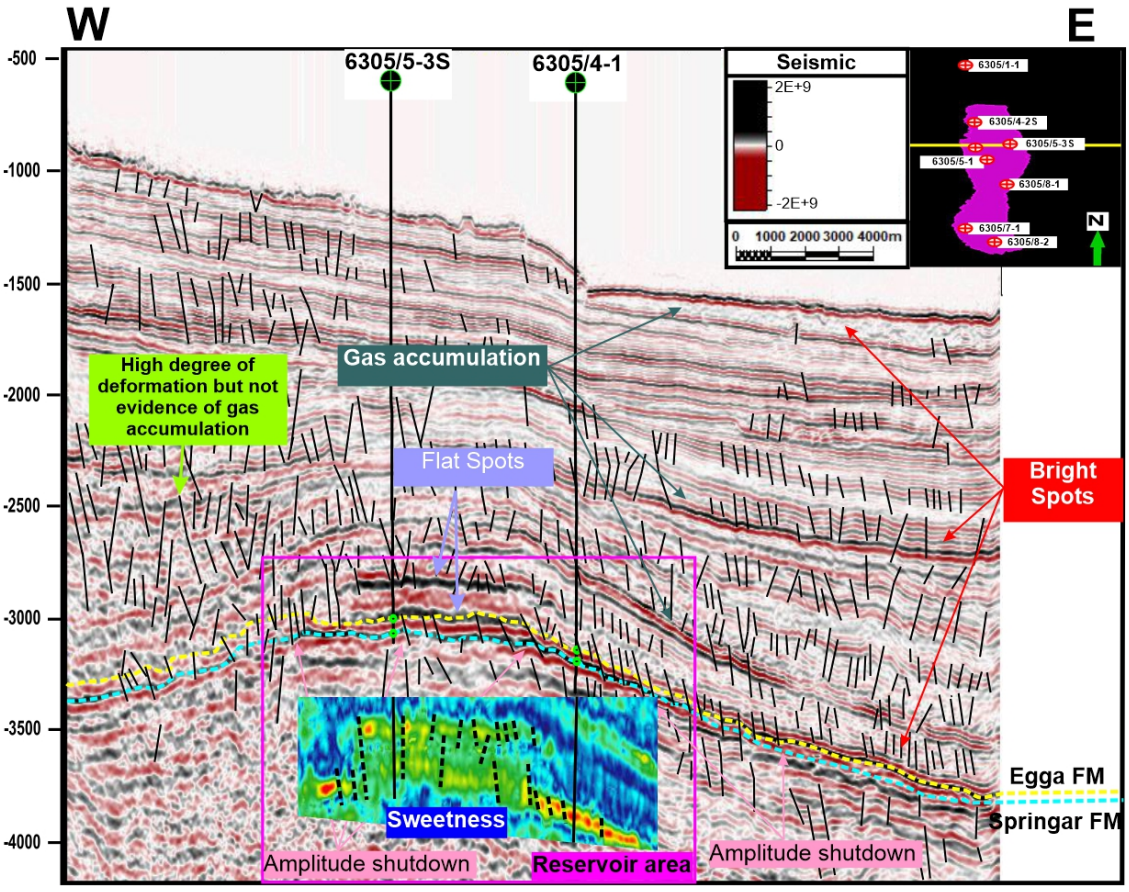

Figure 48: Interpreted cross line 5080, showcasing the primary East-West trends in the north of the field.

From the previous cross-section, we observed an increase in deformation across the field, which led to the separation of the reservoir sands and the overall deterioration of the reservoir unit. With the increase in deformation due to a higher degree of linkage between polygonal faults, the center of the Ormen Lange field became increasingly faulted. In the previous sections, faulting at the reservoir level led to gas migration to the overlying layer and gas's subsequent migration to shallower depths. Looking at Figure 49 (co-insides with well 6305/4-2S), we see a sharper increase in deformation, primarily at the center of the Ormen Lange Dome. Furthermore, we observe a high degree of deformation after -2000 ms throughout the field. Additionally, we observe a shift in the gas migration patterns as gas starts to accumulate due west preferentially and right above the center of the dome, as outlined by the distribution of bright spots.

At the reservoir level, we confirm the trend outlined by the well logs. Sweetness demonstrates the minute accumulation of good sands, with the reservoir unit primarily dominated by low-quality sands. The reservoir maintains its preferential location at the dome's eastern flank, where the deformation increase imposed compartmentalization of the sands and general degradation of the facies. Even though there is no clear DHI at the reservoir level, we start to see a clearer accumulation of gas at different points. Furthermore, suggesting that the extensive deformation below 2000 ms led to a migration of gas, which accumulated at shallower depths where polygonal faulting and deformation is less severe. As aforementioned, gas preferentially accumulated due west, as the deformation allows it to reach a deep fault and accumulate at a structural high at shallower depths.

The final step is to observe, how the trends in cross section 6305/4-2S translated northward. This is important because we need to outline the termination of the trap containing the HC

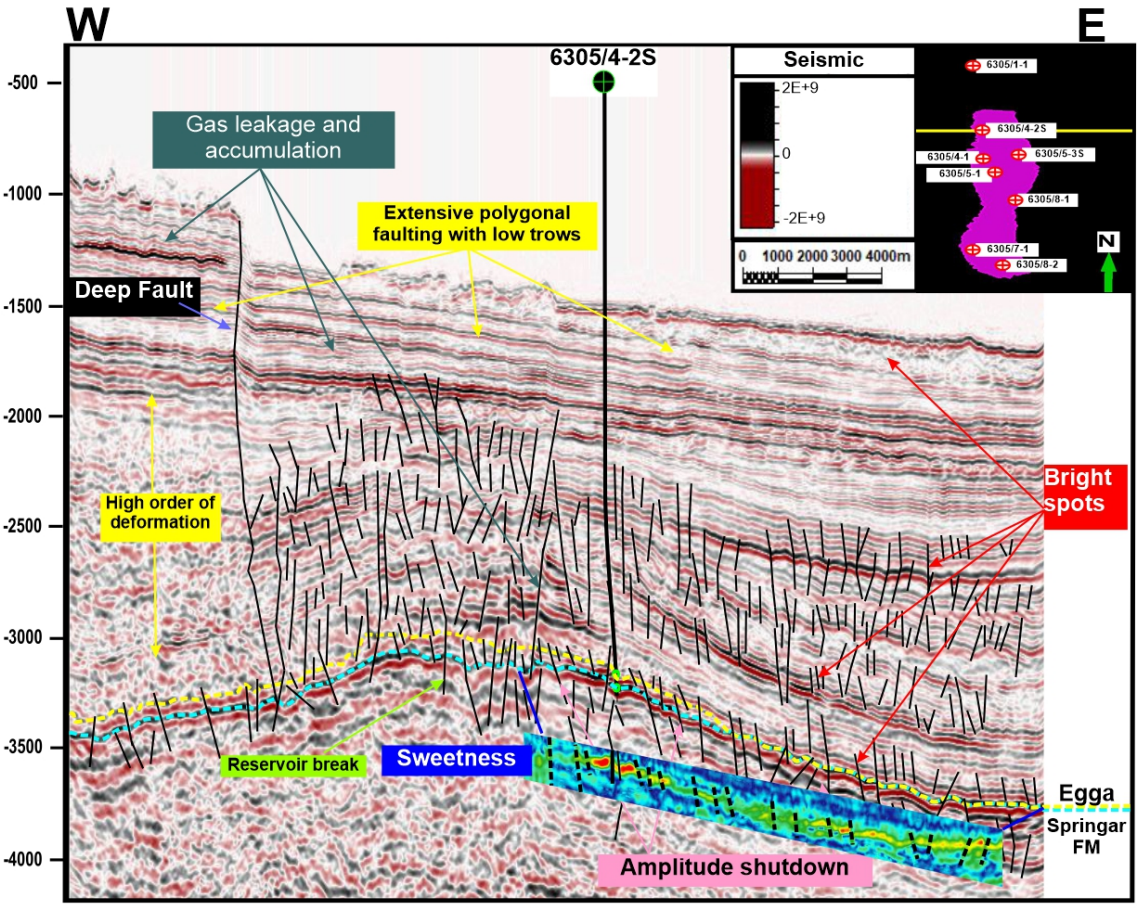

Figure 49: Interpreted cross line 5580, showcasing the primary East-West trends in the north of the field.

Figure 50 showcases a different picture. First, the western margin becomes less deformed as it becomes dominated by polygonal faults at different levels with a low degree of linkage. Also, reflections are generally continuous and do not demonstrate any DHI. On the eastern side, however, the observed deformation of the previous sections maintains, and it becomes dominated by polygonal faults at different levels with a high degree of linkage, which subsequently leads to extensive deformation. Furthermore, there appears to be a deep fault that transects the Ormen Lange dome, but it is not easy to map due to the high degree of deformation in the area. At shallower depths, we observe continuous reflections with sparse polygonal faulting.

We can establish key trends by joining all the observations from the different cross-sections. First, faulting frequency and deformation have a northwest trend, meaning there is an overall degradation of facies in that direction. Second, East-West, the field is primarily defined by a lateral pinch out, while faults primarily contain North-South. The only expectation is the area around well 6305/5-3S, where there is a pinch-out in the South-North direction. Third, the reservoir is primarily continuous due south but increases in compartmentalization in the same direction as the increase in faulting (northwest). Fourth, around well 6305/5-1, the reservoir splits into two sections, with gas preferentially flowing along the western flank of the field. This trend follows the East-West shift in deformation, from being primarily due west in the south part of the field to being predominately due east in the northernmost sections field. Lastly, there is clear evidence of leakage from the reservoir unit due to the extensive presence of polygonal faults at that level. However, these faults seem to have a differential sealing capacity or a dependence on their linkage to the general deformation area. We can point out that gas migration does not always follow the path with higher deformation/fault linkage but instead follows a preferential path as outlined by the cross-sections. The final step is to use different seismic attributes to better outline the interplay between the abovementioned components.

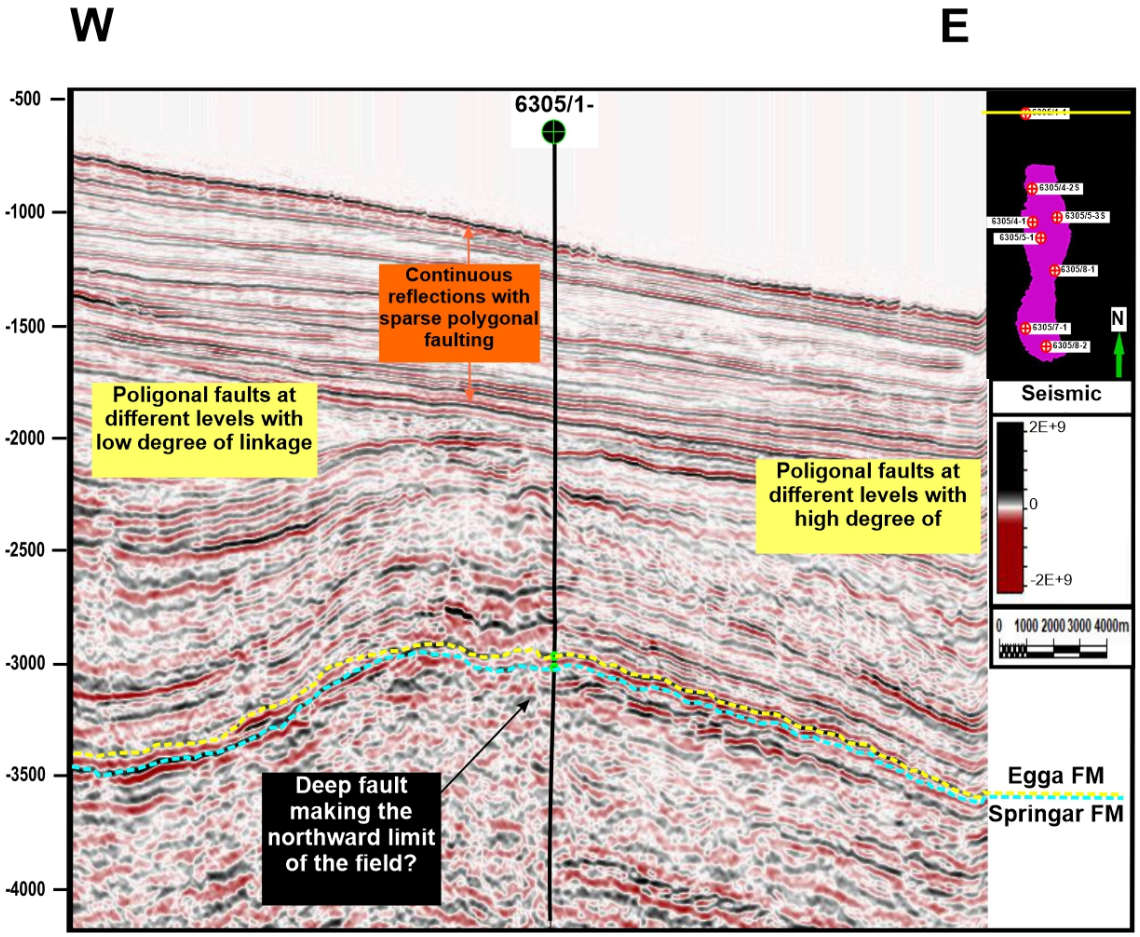

Figure 50: Interpreted cross line 6830, showcasing the primary East-West trends in the northernmost section of the field.

6.3.4 Seismic Attributes

This section aims to explore the aforementioned trends in the seismic sections and see how they are distributed at different depths. In Section 5 we discussed the potential impacts that the scarps in the seabed might have on the data, as they related to changes in velocity and potential pull-up effects. However, to this point, we have not explored not outlined potential areas where this effect might be present. Figure 51 showcases the evolution of the seabed geometry with depth to outline potential in-prints of the seabed at the reservoir level. Here I used the chaos to detect problematic areas and outline the seabed, but no clear in-print of the seabed was found in depth. Instead, a progressive transition into the reservoir area showcases its independent topography. However, a lack of sea bed in-print does not necessarily correlate to a lack of artifacts caused by the seabed. In this instance, it is hard to quantify the impact of changes in velocity caused by the shallow topography. Nonetheless, we can outline the areas where steep contrasts may exist and be careful during the interpretation of this section.

From the chaos sections (Figure 51) there is no indication that the seabed topography may cause chaotic zones by introducing unwanted artifacts in the data. Figure 52 shows the areas where we need to pay special attention to our interpretation. Seabed topography had no effect on most of the field, but we might see some effects on the eastern side of the field and points at the north and south ends of the field. However, based on the above section, this seems to pose no or negligible artifacts towards the seismic section.

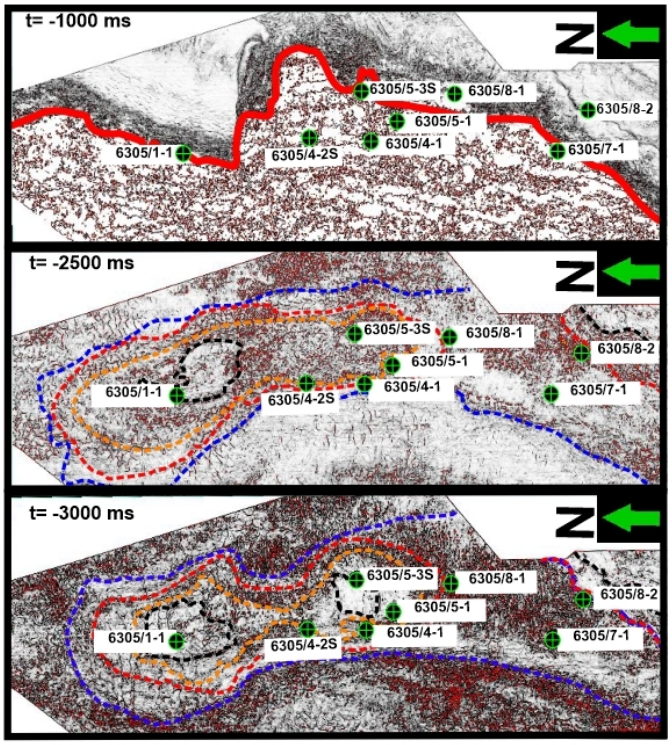

Figure 51: Seabed evolution with depth, chaos sections demonstrating the potential in-print of the seabed geometry at the reservoir level. The different lines serve as contour lines to outline changes in topography.

After delimiting the negligible effects of the seabed for our interpretation, we need to analyze the fault distribution across the reservoir. Such depiction is crucial, as our previous results demonstrated a close link between gas leaks, faulting, and overall reservoir compartmentalization. Looking at Figure 53 we observe a similar trend as that pointed by the seismic sections. First, there is an apparent South-North increase in faulting, with the north part of the field predominantly dominated by polygonal faults.

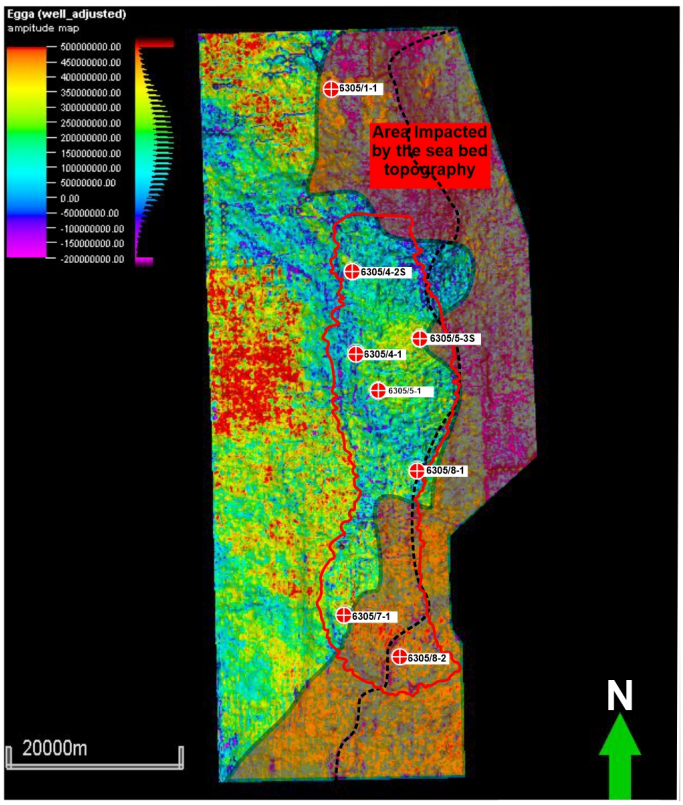

Figure 52: Amplitude map of the reservoir unit, showcasing areas where the seabed topography might introduce unwanted artifacts to the data. The doted black line showcases the eastern limit of the field and a progression into a different topographic structure. A 50ms time window from top egga was used

Moreover, there appears to have a northwest-southwest barrier that delimits an area with increased deformation due to an increase in polygonal fault degree. However, such a limitation is potentially topographic rather than fault-related, as there is no clear indication of a deeper fault in the middle of the field that would justify such a sharp contrast. Additionally, this separation is coincidental with the position of well 6305/5-3S, where we demonstrated a variation in the field termination in the cross-section. It is also possible that the chaotic nature of the northern part of the field limits a clear outline of the nature of this sharp contrast.

Furthermore, the middle of the field remains relatively continuous, with faulting predominately concentrated on the flanks. From the cross-sections, we know that clean sands are primarily compartmentalized at the flanks and remain relatively continuous in the middle of the field. Therefore, trends in the seismic section are also observed at this level, which gives more legitimacy to the leaking supposition posed above. Even though we do not see clear compartmentalization trends, we need to account for the trends mentioned above. More prominently is the East-West faulting trend that closely flows seismic sections.

As a whole, Figure 53 confirms the Southeast-Northwest degradation trend and its close relation to the degree of faulting and deformation. Furthermore, it emphasizes the impact of polygonal faults on the flanks of the field, primarily in the area between the dotted blue line and the previously mentioned delimiting structure. This is more prominent in the western flank, where polygonal faulting becomes more prominent and accompanies the facies degradation outlined in the well logs.

Another important aspect is the distribution of sands trough the field. In Section 2, we describe the Egga sands as turbidity deposits, which according to the literature, should have a lobe distribution due to the stacking of different turbidity currents. To investigate this, we can use the amplitude and RMS maps to outline the amplitude distribution field-wide for the reservoir unit, which is demonstrated by Figure 54.

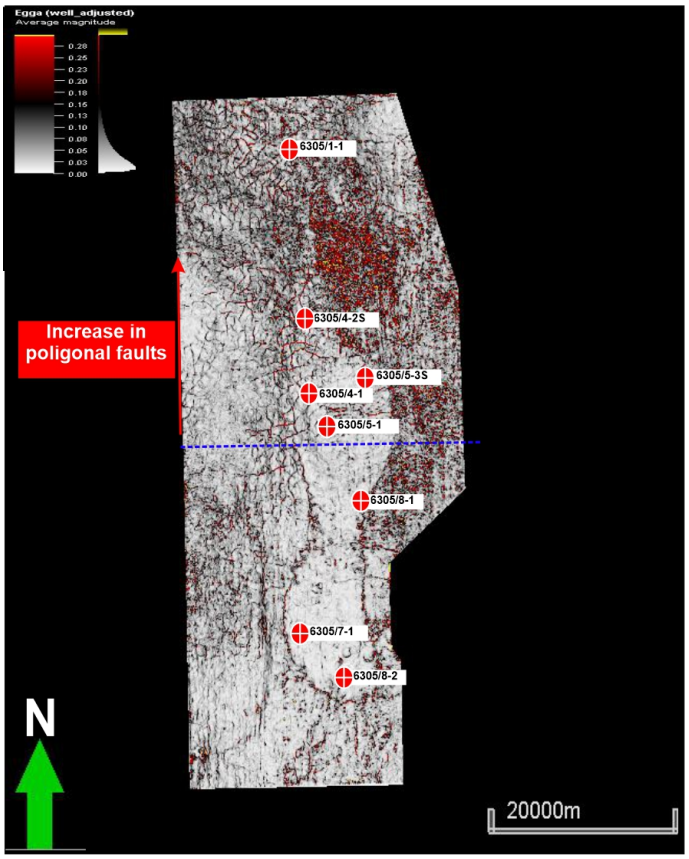

Figure 53: Average amplitude map for the Egga reservoir unit using a 50 ms time window. Depiction of polygonal faulting throughout the field at the reservoir unit. The dotted blue line marks the transition into a zone with higher polygonal fault occurrence

Here we still observe the extent of polygonal faulting, but more importantly, there is no clear evidence of several turbidity deposits. Instead we see the path for two distinct deposits. This is more consistent with the previous observation since we do not observe any stacking pattern for lobes in the cross-section.

On closer inspection, we see that both deposits steam from the Southeast end of the field. However, one flow extends to the saddle area of the field, while the other appears to encompass the remaining field areas. The interplay between both deposits is further explored in later sections as we develop a model for the field and determine the impact of all observations of volumetric calculations.

Furthermore, we can readily identify our DHI areas, which are consistently located at the flanks of the field. Also, we see that the DHI in the western flank of the field is more extensive, while on the eastern side, the trends around well 6305/5-3S delimit the extent of the field. Between well 6305/5-3S and well 6304/4-1, there is an area of low amplitude, which corresponds with the area where the reservoir is separated, and the gas tends to accumulate on the western flank of the field. Another observable trend is the overall decrease in amplitudes in the eastern and northern parts of the field. If we correlated this with prior trends, we see that it matches the distribution of HC in the field, as they are more readily located in the south and decrease towards the north. Such a trend can also be related to the overall degradation of facies as cleaner sands are located towards the south and western flank of the field and tend to degrade towards the north and eastern flank.

The amplitude and RMS surface attributes are helpful to understand how amplitudes are distributed across the field at the reservoir level. Nevertheless, it does not allow us to mark where and how our sands/ HC are distributed in the field. For this purpose, we will use volume attributes and see the progression from -2900 ms to 3400 ms using sweetness and RMS amplitude maps. The sweetness will allow us to understand the distribution of clean sands, and RMS amplitude will show how the HC is distributed. RMS amplitude is essential in this case as it will allow us to see

any potential leak patters

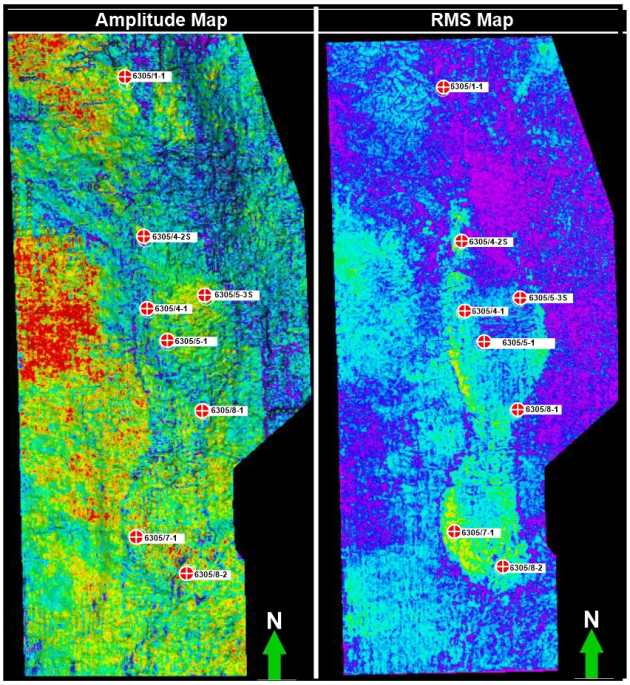

Figure 54: Amplitude and RMS map for the Egga reservoir unit using a 50 ms time window. Depiction of the overall distribution of sands, as to outline the extent of the turbidity deposits. Hot colors demonstrate high amplitude zones, while cold colors demonstrate low amplitude zones

Looking at sweetness maps in the areas around the reservoir unit, we can understand the distribution of clean sands in the reservoir. Figure 55 outlines some of the trends we observed above. Starting at -2900 ms, we see an accumulation of low-quality sands in the north part of the field above well 6305/5-1. This is consistent with the cross-section trends in the same areas, as we observed a general degradation of facies at the reservoir level and the accumulation of dirtier sand immediately above the reservoir. Moving to -3100, the northern segmentation of the field into isolated sand packages is precise.

At -3100 ms, the separation of the sand packages is evident. However, a different trend lies in the south of the field, as the clean sands for the region surrounding well 6305/8-2 are indicated to be at this level. Looking at the well logs and the seismic section, we would expect well 6305/8-2 to have clean sands at more profound levels or at a level that matches the sand accumulation for well 6305/7-1 and 8-1. However, there may be just a higher accumulation of clean sands in this section, and the selected time slices do not fully represent sand accumulation.

However, looking at -3200 ms, we see how the majority of the sands are distributed. Generally, clean sands are more concentrated on the flanks. Here the facies degradation is apparent as we move north; there is a clear decrease in sand quality following the abovementioned trends. Also, we can see that the extent of the clean sands all over the western ridge grated with decreased quality northward. At -3400, most clean sands are not present within the field, and we have predominately less clean sands primarily concentrated in the south of the field.

Additionally, we see an accumulation of clean sands southwest of the field. Looking at the previous trends, this could be because of the low degradation of facies in this area. Nevertheless, we do not have enough evidence to suggest that there is also an accumulation of HC in this area. We need to do the same exercise using RMS amplitude time slices for that investigation and the overall delineation.

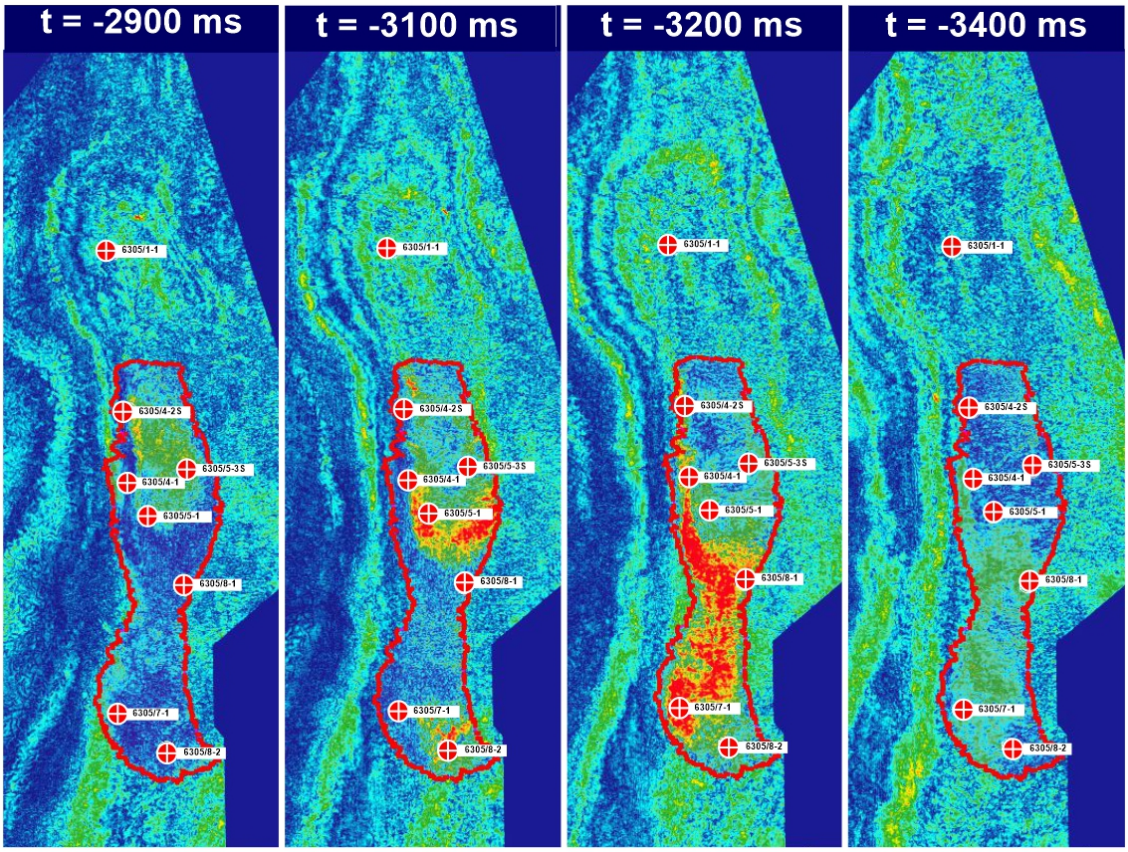

Figure 55: Sweetness time slices showcasing the distribution of clean sands around the reservoir unit

The RMS time slices in Figure 56 showcase a similar trend as that outlined by the sweetness. For this analysis, we will use high RMS amplitudes to indicate the presence of HC. Starting at -2900 ms, we see that the high amplitudes are primarily contained in the area around well 6305/5-3S, which relates to gas migration from the main reservoir area to overlaying layers. Also, we see relatively small amplitudes compared to the remaining time slices. Another observation is the high amplitude small areas around well 63045/1-1. These areas increase in size until time -3100 ms, after which they disappear. Based on previous observations, these areas might contain residual HC, and for this project, we will consider them to contain negligible amounts of HC.

Moving to -3050 ms, we see that HC accumulation matches with the sweetness sand distribution and the faulting/ compartmentalization trends discussed above. More noticeable is the area around well 6305/8-2, where we would expect the HC to be at deeper levels. However, as suggested by the sweetness, there is a more extensive accumulation of sands in this area, which translates to shallower HC showings relative to the neighboring wells. This observation does not change the o previous observations but introduces a level of caution while constructing the model and delimiting the impacts of the trap style for HC volumetric calculation.

At 3200 ms, we see the most significant extent of HC and its relative position to the available wells. The amplitude distribution in the north of the field matches well with all the previous trends. However, as we move south of the field, some discrepancies occur between the time slices and previous trends. First, previous trends show more HC concentration toward the field saddle. However, in the RMS time slices, we see that the HC accumulates primarily in the Eastern flank of the field before reaching the compartmentalization area. Additionally, we see a differential distribution of the amplitudes in the saddle area. Nonetheless, the north trends remain the same and do not vary from previous observations.

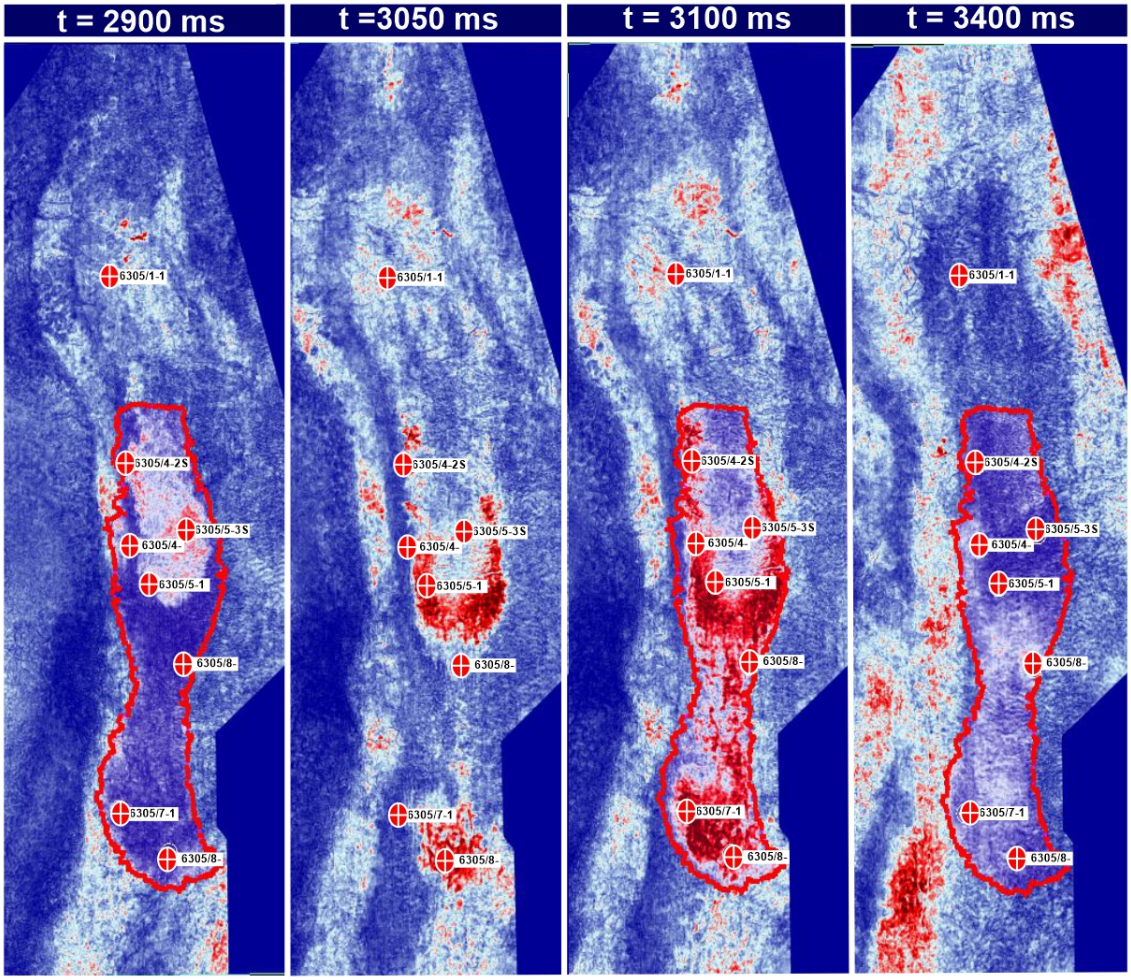

Figure 56: RMS amplitude time slices showcasing the distribution of HC around the reservoir unit

At -3400 ms, we see high amplitudes in the same area where clean sands were accumulating southwest of the field. However, our previous interpretation did not see any DHI indicators in this area. Therefore, we will assume it is a localized event with no direct correlation to the filed structure/disposition. At this point, we have outlined all significant features of the field and can proceed to make a model that describes the stratigraphic and structural components to characterize the trap style and define how the overarching trend impacts the calculation of HV volumetric calculations.

7 Discussion

7.1 General Observations

Here we will outline the primary observation for trap definition and the outline of its impact on volumetric calculations. Starting with the well logs, we observed a general decay in facies towards the North of the field. This is evident in the GR and the neutron-density logs. These logs show a northward increase in GR throughout the Egga RU and an overall decrease in sand indication in the density-neutron track. This trend is consistent with reports in the literature and helps define the extent of gas-bearing sands within the reservoir. AI and Vp/Vs curves are also helpful in defining some trends and the definition of potential stratigraphic changes within the reservoir.

Interpretation outlined the presence of a tight zone within the EGGA RU as per the "undulating" pattern in AI, which correlates to changes introduced by the tight zones. Based on the literature,

these tight zones can be classified as calcified sandstones due to their low porosity, high density, resistivity, and acoustic response. Based on the available well logs, we cannot establish a coherent analysis for permeability, and we can only assume the impact of these calcified sandstones is in the overall fluid distribution in depth. Extending our analysis to observed formation pressures, we can outline a potential relation between the barriers and the GWC.

Based on the literature, we know that the saddle area of the field (well 6305/4-1, 5-1, and 5-S) presents a gas down to effect. Furthermore, as we look into the pressure VS depth graphs, well 6305/4-1 presents an increase in pressure for the water column, indicating a hydrodynamic setting as the over-pressured water can move the GWC creating a tilted contact. However, if we account for the calcified sandstone layers, we observe a direct correlation between the depth of the layer and the shift in pressure linking the distribution of the GWC with the porosity and permeability properties of the calcified sandstones.

Moreover, the seismic sections, seismic attributes, and literature agree on the increase in polygonal faulting towards the North of the field and differential behavior in fault characteristics across the field. Through sweetness and the seismic sections, we see that faulting may segment/compartmentalize the reservoir unit and lead to some leakage. However, the seismic cannot solve the calcified sandstones as they are below the seismic resolution. Therefore, the interplay between the calcified sandstones, polygonal faults, and permeability distributions can only be inferred.

7.2 Model

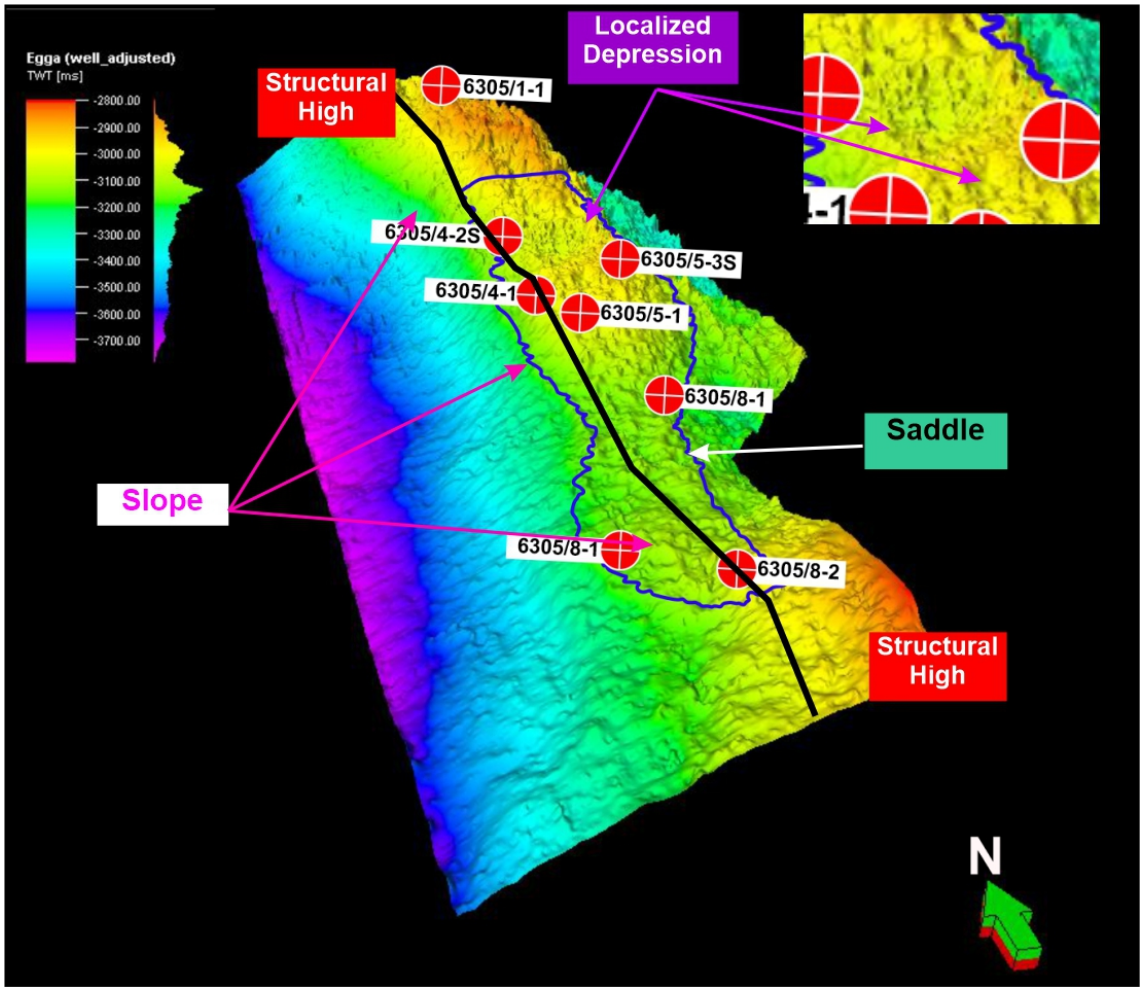

Figure 57: TWT 3D structure for the Egga RU. Depiction of important structural features for top of the Reservoir unit. The black line outlines the structure of the field.

From previous work, we have an idea of the distribution of the polygonal faults and their potential effect on fluid flow. However, no conclusive evidence exists on how they may impact the GWC. In this section, we will condense all the observations to propose two scenarios that explain the fluid distribution, alongside the structural, stratigraphic, and geomorphologic features of the field that all together may impact the HC volumetric calculations. First, we will explore the possibility of a hydrodynamic setting by considering the calcified layers to be permeable and contrasting them with the observed faulting trends. Second, we will assume that the layers are a baffle/barrier to fluid flow and significantly prevent vertical fluid flow. Afterward, we will discuss the impacts of both scenarios on volumetric calculations and present some considerations for future work.

The first step for our model definition is to describe the 3D structural outline of the field. Using the interpretation of the RU, we can construct a 3D model, which is illustrated in Figure 57. Here we see two structural highs at both extremes of the field, culminating in a saddle zone. The local depressions around well 6305/5-3S could explain the observed sand distribution and the sharp transition into the polygonal fault zone. The next step is to use the amplitude maps to delimit the deposition pattern of the turbidity sands of the Egga unit. The goal is to understand if the two interpreted flows are interconnected or independent.

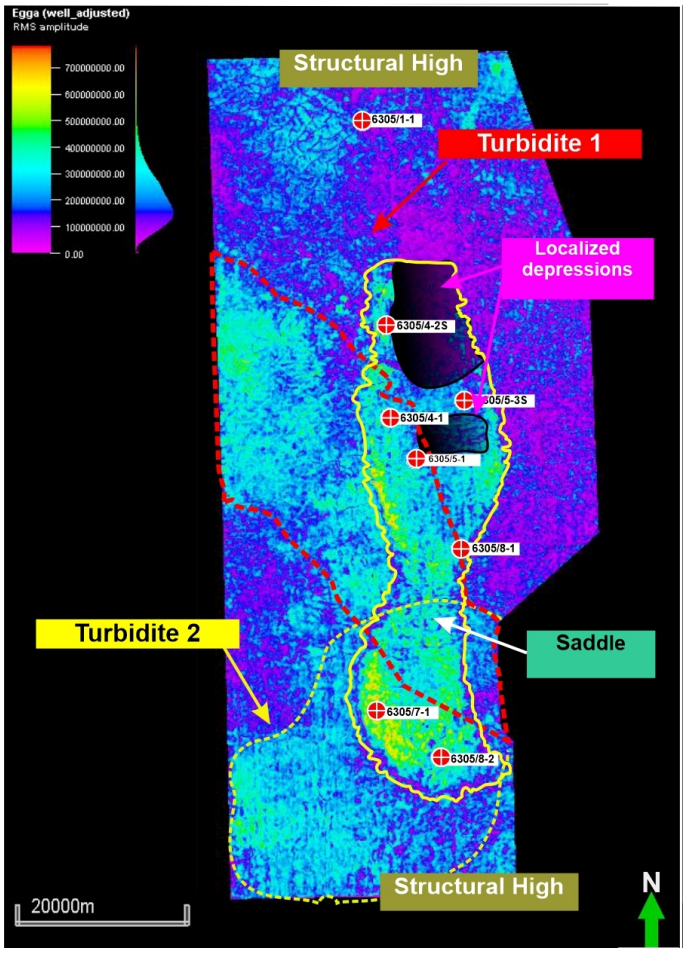

Figure 58: Amplitude map showcasing the flow pattern for the turbidity deposits

After understanding the 3D structure of the reservoir unit together with the well correlations, we can outline the sand distribution. First, we observe that two distinct amplitude anomalies can be associated with lobe-shaped deep marine deposits (figure 58), corroborating Gjelberg et al. (2005) previous model. Herein, the two lobe-shaped anomalies are further analyzed, with anomalies one and two (or turbidite one and two) covering the northern and southern parts of the field, respectively. Following the areal distribution of both lobe-shaped anomalies, we may infer that there is a small intersection area around the saddle zone. Furthermore, this intersection area is

relatively close to the fringe of the turbidites deposits, as previously shown on well correlations. Nevertheless, this area shows polygonal faulting, which could interfere with the seismic response, thus making it unclear. Also, turbidite one moved roughly southeast-northwest, which would help justify the preferential deposition of sands along the western flanks.

Furthermore, if we look at the areas with low amplitudes, we observe some overlap with areas with extensive polygonal faulting. These areas can be defined as the lobe fringes of turbidites one and two, which are clay-rich and would be susceptible to dewatering. Consequently, leading to a more extensive presence of polygonal faults in these areas, which is evident in Figure 53 and Figure 58. By considering the lateral extent of the lobe fringes, the structural outlay of the field, and the well log trends, we can delineate other observations.

Looking at Figure 5 we see that turbidite two has a relatively sizeable areal extent, with the turbidite lobe primarily concentrated in the southern part of the field before the Ormen Lange sub-basin. This preferential deposition corresponds with the position of the saddle area, indicating that the sands resulting from turbidite two would be primarily concentrated in this area and spill over through the remaining of the field. The good logs show an apparent decrease in reservoir thickness alongside facies degradation. Also, the northernmost wells (6305/4-2s and 5-3S) show isolated pockets of sand primarily towards the top of the reservoir. Furthermore, suggesting a mud-poor supply system where mud is distributed to the distal parts of the fan, accompanied by a weak decay in accumulation towards the North, according to toSmith and Møller (2003)

Based on this, we can start building our model and show the setting in which our hydrocarbons are distributed. Figure 59 is a simple cross-section illustration for the middle of the field and will be used in further discussions to outline the different scenarios and their impact on the distribution of the GWC. This model aims to give a general idea of the problem, but the above observations should be considered even though they might not be directly represented. At this point, the prominent trends that we want to outline are the presence of a shale layer in the southern part of the field within the reservoir unit, by accounting for the areal extent of the clean sands, the prevalent presence of shale in the North of the field and the degraded facies area marking the transition between both. The only assumption made in the presented model is that the tight calcified layer marking the GWC covers the entirety of the field. As we progress with the discussion, we will add to the model in Figure 59 to describe the nuances of the different scenarios.

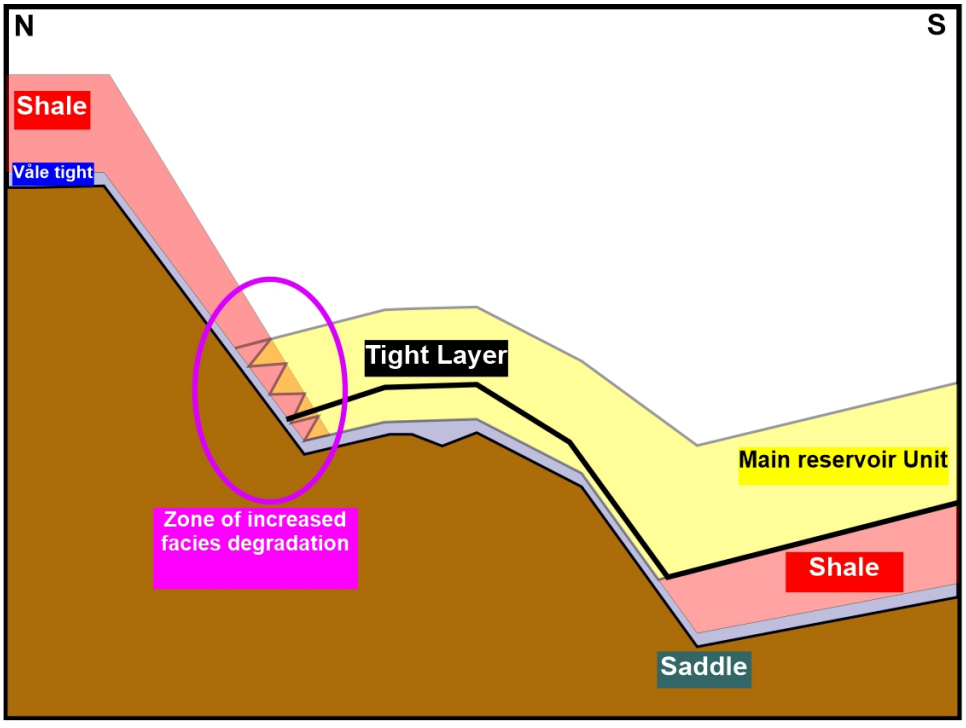

Figure 59: Simple model for the cross section of the middle of the field. Illustration of key stratigraphic and structural components. The model is not to scale.

7.3 Scenarios

The following scenarios build upon figure 59 to demonstrate how the trap style may have impacted the GWC and subsequently the calculation of gas-in-place. There are two main targets for our assumptions- the role of polygonal faults and the impact of the tight calcified zones on fluid motion through the field. The interplay between both aspects helps determine the position of the GWC as inferences about the above points help define the heterogeneities and barriers to fluid flow. To better discuss the impact of the above interpretations on the reservoir, we need to make a few alterations to Figure 59 primarily surrounding fault position at the top and base of the reservoir.

In this instance, we must represent the mechanisms through which water enters the reservoir. Given the area's slight structural relief, artesian flow is unlikely to contribute to water flow in the reservoir unit. Instead, an even contribution between artesian flow and inflow due to shale dewatering is the most plausible explanation. Due to extensive polygonal faults, the influence of dewatering shales is very plausible within the northern part of the field. Grecula et al. (2015) outlines the relation between the dewatering of underlying shales and the occurrence of polygonal faults, which increases in degree (larger throws) and volume as we move to the north side of the field. Therefore, we need to outline some of the characteristics of the polygonal faults to understand the circumstances in which they enter the reservoir.

Möller et al. (2004), provides a general overview of the characteristics of the polygonal faults. Faulting in the central areas of the field presents a different pattern than those in the flanks, which have smaller throws, less random orientations, and a prevalent East-West dipping component [Möller et al. (2004)]. Polygonal faults within the reservoir are syndepositional and are likely to have originated within the underlying smectite-rich Cretaceous shales. However, faults that originated this way may not reach the top of the reservoir. Möller et al. (2004) report evidence of the growth of up to one-third of the main reservoir unit, suggesting the syndepositional nature of the faults. Relative to sealing seal juxtaposition, clay smears and phyllosilicates frameworks are the most relevant components [Grecula et al. (2015), Möller et al. (2004)].

The extent of polygonal faulting within the reservoir indicates fault reactivation after deposition. Consequently, potential sealing mechanisms may have lost some efficiency due to it. Observed leakage points are evidence of that but do not necessarily indicate unconstrained fluid flow across the faults; somewhat, it might be baffled by remaining sealing mechanisms across the fault. A direct definition of such mechanisms is complex as polygonal faulting is not as well understood and defined as extensional tectonic faults. Nonetheless, we cannot neglect the effects that it may have on fluid flow. With all these considerations, we can use Figure 60 as we progress further in our discussion.

7.3.1 Tilted contact due to a Hydrodynamic Setting

Fluid contacts in the reservoir are conveniently defined as flat since the tilt in such contacts is often negligible. Nonetheless, the influence of heterogeneities in the distribution of the contacts is evident but does not solely define a contact as hydrodynamic. For a reservoir to be under a hydrodynamic regime, it needs to interplay between observed heterogeneities and pressure, with the latter having a more significant influence on the displacement of the HC. Equation 3 shows us how to calculate the tilt in the contact based upon the horizontal component of pressure. Based on DENNIS et al. (2005) work, we see that the contact tilt is dependent upon the horizontal component of the pressure gradient in the aquifer and the difference in vertical pressure gradients between the aquifer and HC phases. From our interpretation, we see that the horizontal component of the pressure gradient would be connected with the field heterogeneities.

Moreover, we would expect the horizontal component of the pressure gradient to be more prominent in the North of the field due to facies degradation and fluid flow through faults. Relative to the difference in vertical pressure gradients between the aquifer water and HC phase, the pressure graphs show a differential behavior across the fields.

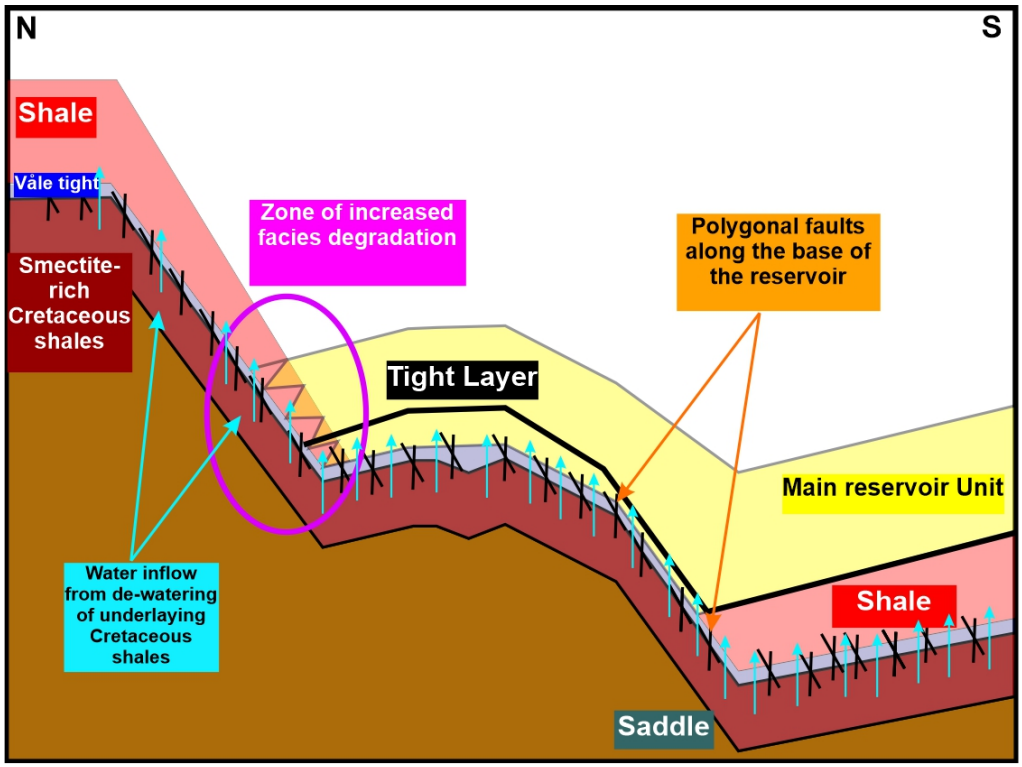

Figure 60: Updated simple model for the cross section of the middle of the field. Illustration of key polygonal faults along the reservoir base due to Smectite-rich Cretaceous shales de-watering, and associated water inflow into the reservoir.

In this instance, the Northern wells show a higher vertical difference than those at the South due to a south trending decrease in the pressure gradients. Even though the pressure profile of the field is not consistent with a hydrodynamic scenario, it becomes more plausible when paired with other factors.

First, we observe some reservoir compartmentalization due to polygonal faulting, but the seismic attributes show continuity in gas distribution through the reservoir sands (supported by a clear AVO class 2). Under a hydrodynamic setting, the polygonal faults acting as a permeability barrier and creating the apparent compartmentalization would be justified. Second, the GWC behavior across areas of differential permeability values is consistent with that observed in hydrodynamic settings. With the degradation of facies towards the North, reservoir fluids move from a low permeability zone to a zone with higher permeability values. Based on DENNIS et al. (2005) work, we would expect a contact flattening towards the South and a tilt in the contact towards the shalier, more tight zones in the North. Also, when a higher permeability reservoir overlays one with lower permeability, as we see in the South where the shallower parts of the Egga RU overlay a shale zone, we would expect the GWC to follow the bed boundary—looking at the good logs, we observe that these trends generally match the field observations. More important is that we would expect to observe hydrodynamic steps in areas with short discontinuous faults and a direct proportionality between the degree of tilt and the thinning of the GWC.

We can assume that the faults at the base of the reservoir create an apparent compartmentalization/segmentation of the reservoir, that the tight calcified sandstones do not hinder vertical fluid flow, and that the observed over-pressure in the northern water layers is sufficient to create a hydrodynamic setting and tilt the GWC. Under the given assumptions, the difference between the hydrostatic and a hydrodynamic setting is represented in the simplified model in Figure 61. Here we observe that the inflow of over-pressure water due to shale dewatering leads to the tilt of the water contact and a higher concentration of gas towards the South than the North, which is a general observation in the well logs. The hydrodynamic setting of the Ormen Lange is extensively discussed in the literature due to the inflow of water due to shale dewatering and the general depositional, structural, stratigraphic, and geomorphologic nature of the field.

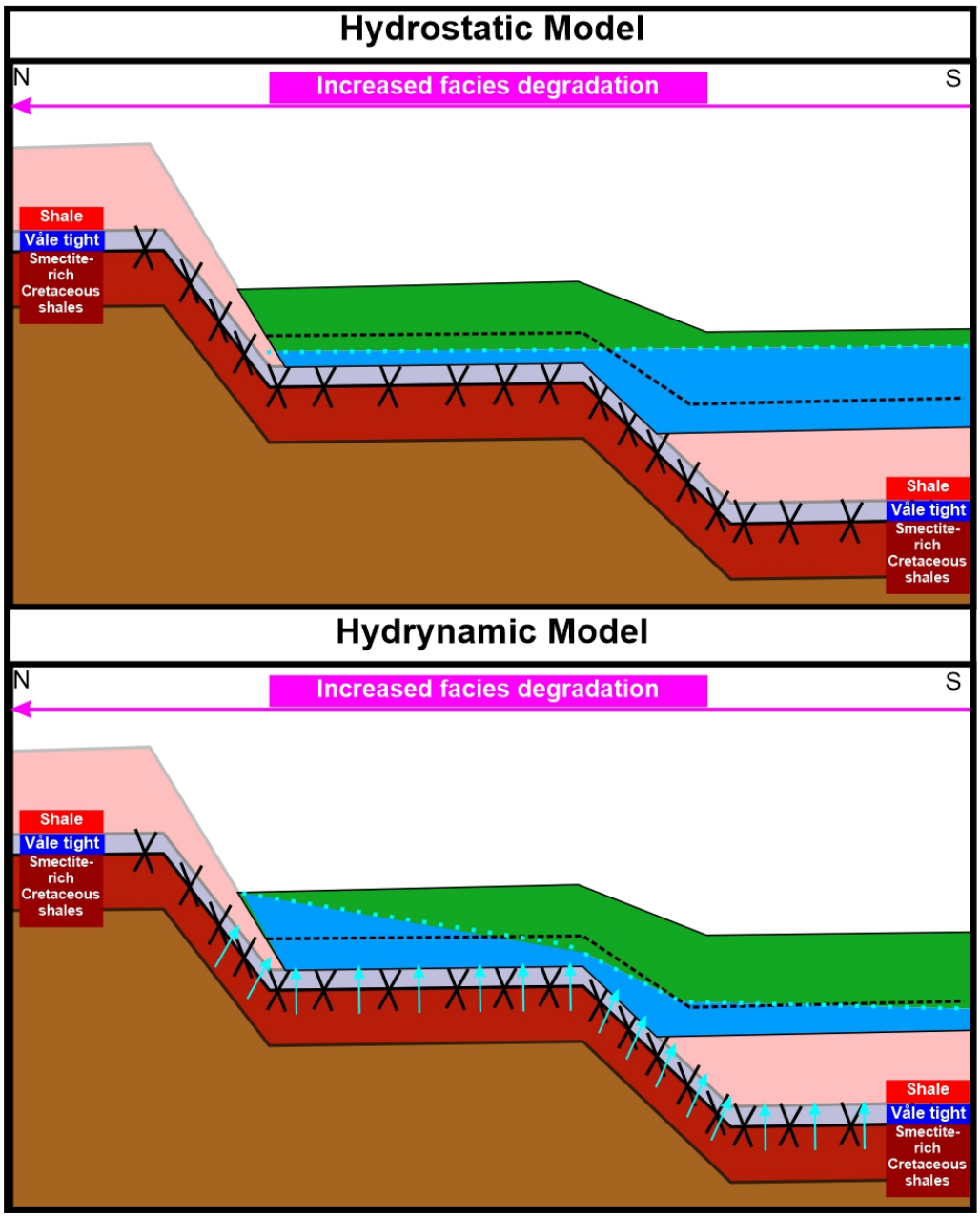

Figure 61: Simple model underlying the differences in GWC under a hydrostatic and hydrodynamic setting. The above model is not to scale.

The trends in Figure 31 show two key points, that the gas pressure regime is the same across the field but that there are differences in the water pressure regime. Moreover, water over-pressure is only present in the Northern part of the field, suggesting that a differential mechanism distributes pressure across the field. The rapid deposition of the reservoir helps justify why the water coming from the smectite-rich underlying layers is over-pressured, as suggested by Grecula et al. (2015). Under this assumption, we would expect some decrease in pressure as the water reaches the reservoir. However, the dynamic properties of the polygonal faults lead to baffled flow and help preserve the pressure, which justifies the pressure differential across the field.

Considering the well logs results, we could argue that the observed change in pressure is related to changes in stratigraphy. This premise could be extended by considering the over-pressured sands below the Egga RU. In such a scenario, we would consider the difference in pressure to be indicative of a hydrodynamic setting. However, the magnitude of the difference does not correlate with such a scenario and is more indicative of separate systems. Also, NPD outlines a gas down to situation

for well 6305/4-1, which is unlikely to be caused by a hydrodynamic setting when accounting for the stratigraphic trends outlined above. NPD further suggests that some faults found around the well present a dynamic sealing. Consequently, there is no evidence of a mechanism that prompts a hydrodynamic interpretation for the observation on well 6305/4-1.

In the southern part of the field, there is a shale zone below the clean sands, which serves as a baffle zone between the smectite-rich shales and the clean sands, while on the northern side of the field, such a baffle zone does not exist. Consequently, we can infer that the water is primarily entering the reservoir in the North and then artisanally flowing south due to structural relief, leading to a decrease in the water pressure regime in the South. However, even under this scenario, a tilted contact would be possible as long as the inflow velocity allows gas compression and contact tilting.

To discuss this point lets consider Darcy's law:

$$q = -\frac{k}{\mu}\Delta p \tag{6}$$

where q is the instantaneous flow rate, μ is the fluid's viscosity, and Δp is the pressure drop. First, let us assume that the instantaneous flow rate is directly proportional to the change in pressure ($\frac{k}{\mu}$ is constant). If we look at Figure 31, we observe small changes in pressure drops as we move between the gas pressure regimes across the field (approximately 2 bars). Therefore, suggesting that the water flow rate into the reservoir is relatively low, which is consistent with flow rates for dewatering shales. Furthermore, if we introduce the changes in permeability due to the degradation of facies and the dynamic outline of the polygonal faults and assume that the temperature is insufficient to change the water viscosity, we would still not have high enough flow rates to justify a tilted contact. This is due to the compressibility of gas, which would require flow rates comparable to those of mountainous areas to be compressed and tilt the contact. Additionally, there is evidence of leakage in the reservoir, which would help tilt the contact. Nevertheless, the natural low flow rates of shale dewatering are insufficient to compress the gas and tilt the contact, even with the leakages.

7.3.2 Flat Contacts between Reservoir Segments

Under normal circumstances, a flat contact is related to a hydrostatic scenario, where the contact is flat, or any variations are primarily justified by the heterogeneities in the reservoir. In our case, the inflow rate is relatively low and, based on the above discussion, has little to no effect on the tilt of the contact. Moreover, for this section, we will assume that the hydrodynamic influence of water inflow due to shale-dewatering is negligible and that the reservoir is predominantly under hydrostatic pressure. This assumption holds as our interpretation precedes production, and the hydrodynamic setting of the reservoir can change after production.

This section will primarily look at how the observed heterogeneities impact the GWC. We need to consider the following points:

- Given the increase in faulting due North, the inflow of water is expected to increase in the same direction.
- Water inflow maxima coincide with zones with high heterogeneities.
- Interpreted calcified sandstone layers to present a baffle to fluid flow, as their permeability is primarily connected to the presence of polygonal faults in the reservoir
- Polygonal faults segment the reservoir but do not compartmentalize it
- Pressure appears to be indirectly proportional to reservoir heterogeneities.
- The slope above the saddle area (between well 6305/8-1 and 6305/7-1) presents abnormal faulting patterns and appears to separate the North and South parts into distinguishable segments

By correlating the observations mentioned above, we can outline some essential aspects. First, the gas gradients are relatively the same, which indicates that despite the areal distribution, all wells have a common gas pressure regime. This indicates that the gas column across the field is under pressure, with slight variations caused by changes in stenography/structure. A similar observation can be extended to the water column, as the water gradients are relatively the same across all wells. Therefore, we can assume a common water pressure regime for the field. This is an important observation, as the observed shifts in pressure are not indicative of a hydrodynamic setting but are somewhat correlated with the presence of a tight calcified zone around the GWC. Furthermore, NPD reports a gas down to the effect on well 6305/5-3S, which combined with the observation on well 6305/4-1 would make the tight layers more prominent and a hydrodynamic setting more unlikely.

Additionally, if the main inflow is towards the North of the field due to increased faulting, we can draw a relation between the increased pressures in the North and the degradation in facies. As the water flows into the reservoir, we observe that it finds a zone with high shale content, which helps maintain its dewatering pressure. After, it flows into cleaner sands by following the structural relief and having an artesanal flow. However, as its flows towards the southern part of the field, it encounters different polygonal faults that segment the field and baffle flow. Also, vertical flow is delimited by the tight calcified zones, which help separate the water and the gas. Here we assume that the interpreted calcified tight zones have a large areal extent and a small vertical permeability in addition to low porosity. Thus, serving as a barrier to fluid flow, except in areas where polygonal faulting allows the scenario to change. We can substantiate this by looking at the interpreted GWC, as they tend to be below the calcified layers in the North and above the layers in the South, indicating a point at which the water can move to shallower parts.

Returning to the correlation between pressure, water inflow, and segmentation. The differential changes in pressure across the reservoir suggest that an increase in heterogeneities helps sustain pressure and that flow baffling across fault has little to no effect on pressure. This is evident by the decrease in water pressure from North to South despite the wide segmentation distribution across the field. Lets consider the scenario in figure 62. As we move from the North to the South, the pressure decreases alongside the inflow rate, which causes a proportional decrease in the water column. The baffling effects cause a more noticeable effect during horizontal flow. As the water moves across the fault between segments, the flow will be baffled, which, combined with the decrease in flow rate and pressure, leads to a slight decrease in the GWC. As we move south, the GWC decreases between each segment, creating an apparent tilt in the contact while it is overall flat.

Nevertheless, if our assumption about the calcified layers stands, we expect the GWC to remain below these layers across the field. However, we do not observe this; instead, the GWC remains within the same window across the field, as per Figure 62. Therefore, there must be a zone between wells 6305/7-1 and 8-1 where the layer is discontinuous, allowing water to laterally flow and set above that layer in the southern part of the field. Consequently, as the water flows above the tight cemented layer, the impact of changes in pressure becomes smaller as the low permeability layer contains the water. Consequently, even though baffled flow allows for slight changes in the GWC across the field and gives an overall sense of tilt, in reality, the contact is predominately flat, and heterogeneity rather than a hydrodynamic setting causes variations. Lastly, the structural setting of the field leads to a preferential flow towards the South, which in addition to the dewatering of shales, forces the water column to follow the field structure closely. Therefore, any significant shifts in GWC will be related to the structural relief rather than a hydrodynamic setting.

7.4 Impact on Volumetric Calculations

The above scenarios showcase the importance of the definition of the GWC as it would significantly change our understanding of the distribution of HC in the reservoir. Based on Section 3.5, we see that the calculation of gas in place is dependent on different aspects. Stratigraphic traps introduce different variability regarding the lithostratigraphic composition of the reservoir unit. Additionally, the structural outline of the field still plays a role in HC distribution. The Ormen Lange field is primarily a stratigraphic trap, with some structural components influencing the sand distribution

and HC. While the trap style defines the gross volume of sand in the reservoir, the intrinsic properties define the net pay.

For our purposes, volumetric estimations are based on the early stages of the field, where production did not impact the distribution of HC. In this instance, we need to estimate the original gas in place (OGIP) and how much of it can be economically extracted. Starting with the GIIP, this estimation depends on the area, net pay, porosity, water saturation, and the initial formation volume factor. Recoverable reserves are a fraction of the GIIP and are directly dependent on the recovery formation factor, showcasing that the volumetric HC estimations primarily depend on the reservoir's intrinsic properties.

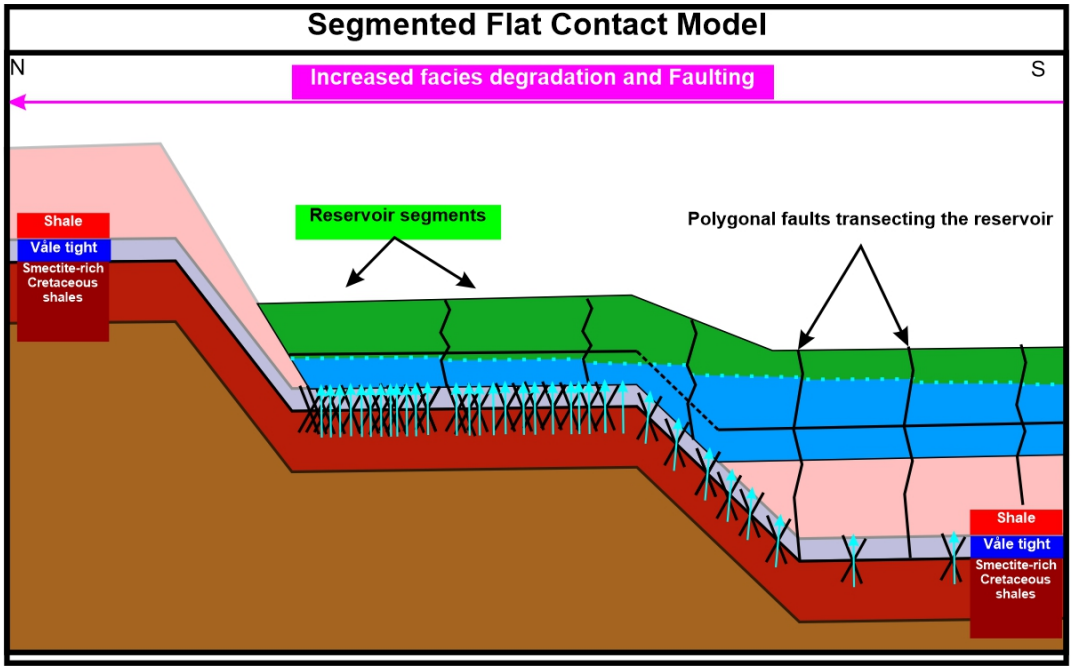

Figure 62: Simple model underlying the correlation between the decrease pressure and an increase in facies quality, and its impact in the GWC.

The north-trending facies degradation has the most significant impact on our calculations. As the reservoir becomes richer in shale, the net pay will proportionally decrease due to the reservoir's decreased ability to hold HC. Therefore, it is essential to accurately define the shale distribution, mainly in the North of the field, to understand how much sand we have and how much of it holds HC. Furthermore, facies degradation is often followed by a decrease in porosity and permeability, which increases the gross rock volume and decreases the net pay. Another aspect is clay's ability to hold water; if we increase the shale content in our reservoir (and with it clay), we are increasing the amount of water that our formation can hold, decreasing their ability to hold HC in the pore space and increasing the water saturation. Ideally, we would like to have a low water saturation to maximize the amount of HC in the formation. The recovery factor can directly observe the impacts of facies degradation. The formation recovery factor is dependent on the volume ability to flow fluid and how easy it is to extract it. Therefore, with higher levels of degradation, we decrease the amount of HC that the formation can hold and our ability to extract said HC.

For the Ormen Lange field, the influence of the polygonal faults is more relevant. As per the above discussions, we see that the approach to the impact of the polygonal faults alongside field heterogeneities helps us define the GWC. As a whole, the determination of the GWC is essential for the outline of the net pay and the areal extension of the field. For the Ormen Lange, the determination of the contact is relative to interpretation. We could consider it tilted in a first-order approximation, but it yields an uncertain result. Also, we could assume it to be flat and horizontally divide the reservoir into a gas and water zone.

Nevertheless, both approaches carry significant uncertainties are they do not accurately represent the outline of the field. The way we should approach this is to calculate the contact between fault reservoir segments, which are defined by the presence of major polygonal fault complexes. Nevertheless, the areal extent of the polygonal faults and the problematic mapping conditions make this approach unfeasible.

Moreover, for the Ormen Lange field is more prudent to divide the reservoir into two main sections, the southern and the northern part. In this division, the southern zone would be south of well 6305/5-1 and the northern part above this well. This way, we can group zone with similar structural—stratigraphic and geomorphologic characteristics. The goal is to separate the area with high facies deformation from relatively more homogeneous ones. Subsequently, the GWC can be determined for each section using their respective properties, leading to a better estimate of low and high cases. Overall, the stratigraphic trap has little impact on the volumetric estimates. Somewhat polygonal faults, extensive heterogeneity in the North of the field, and the surrounding geologic setting are the main risk factors for calculating volumetric estimations.

7.5 Future Work Considerations

The presented interpretation and subsequent discussion on the impacts of trap-style characterization on volumetric estimations and pre-production. The data used was primarily collected before production started in 2007. Therefore, any subsequent efforts to explore the field's evolution must consider production parameters.

Relative to seismic, 4D high resolution seismic would be the next step. Here we want to investigate the evolution of the DHI after production. Using the 1997 seismic data as the baseline, we could see how the fluid distribution in the field changes. Second, it would allow for a better interpretation of the impact of the dynamic profile of polygonal faults on fluid flow across the reservoir segments. However, more importantly, it would highlight the influence of pressure variation in the GWC. Here, we would monitor how the water column behaves due to the depletion of gas in the reservoir to understand which of the presented scenarios is more likely to occur. This is the most expensive approach and would require extensive efforts to outline concrete results.

A more direct approach would be conducting closed-hole surveys in the producing well. This approach is not as efficient as the original wire-line due to mitigation in the formation signal to the different tools. However, it should produce more data to delimit reservoir properties. The essential aspect of this approach is the measurement of formation pressures. Here we want to use our production information to progressively build a pressure map and better understand the water pressure regime across the field.

The seismic and the well logging information can be combined to create a detailed reservoir modeling. This approach gives a more comprehensive approach, using different data to build a model and represent that field properties. As with any subsurface approach, inherited uncertainty cannot be resolved. However, it presents the unique opportunity to test different scenarios and properties to explore the different postulated scenarios.

In all, the goal of future work should be to accurately understand the role of the polygonal faults and their relation to filed heterogeneities and the distribution of the GWC. Additionally, there is a need to investigate the deposition history of the field further to highlight the complex geologic evolution of the field and its relation to observed trends.

8 Conclusion

The Ormen Lange field is one of the largest gas producers on the Norwegian Continental Shelf, with a complex geologic definition, mainly when we consider the nuances of its structural, lithostratigraphic, and geomorphologic settings. Trap definition depends on the parameters above, as each impacts the overall reserves estimation. Of all, the structural complexity of the field is relatively

simple and can be defined as an anticline at the field scale. Moreover, the underlying Jurassic structures help define the field's position and play a role in fault propagation and reactivation. Furthermore, the Egga sands are the primary reservoir sands that become increasingly interbred with shale towards the end of the reservoir. Moreover, the Egga sands represent the deposition of different turbidity currents, which have two main depositional directions, one covering the North of the field and one the South.

The deposition of these turbidite currents influences the quality of the facies across the field. Here we observe an increase in facies degradation towards the North of the field due to an increase in shale content. Such differential areal distribution of sand and shale leads to a differential distribution of polygonal faults. Across the reservoir, polygonal faulting is directly proportional to the quality of the reservoir and the water influx from underlying smectite-rich shales. Polygonal faulting significantly affects fluid distribution due to its dynamic characteristics. Additionally, they segment the reservoir and dictate the lateral flow of gas/water and the reservoir's leakage rate. Another component is the calcified layers found across the reservoir, which dictate help dictate the GWC primarily as we transition into the South side of the field since their permeability is connected to the dynamic sealing properties of the polygonal faults transecting the reservoir.

Generally, we can define the trapping style of the Ormen Lange field as a lateral pitchout. East-West and at the South of the field, these hydrocarbons seem to be controlled by the structural spill point, whereas the North by the lateral pinchout. However, in the North of the field, trapping appears to be more closely connected with extensive facies degradation and the increase in faulting propagation. It is important to note that the chaotic setting in the North of the field prevents a clear outline of the trapping mechanism in this region. Nevertheless, the trap style of the field appears to dictate the areal distribution of the hydrocarbons and has a relatively small impact on the estimation of reserves. In this instance, the distribution of the GWC plays a more significant role in estimating reserves, at least after defining the overpressure zone northwards.

Extensive heterogeneities, primarily in the North of the field, require a conscious outline of the reservoir and the distribution of the GWC. Given the depositional history of the field and general faulting trends, it is beneficial to divide the field into the Northern and Southern regions, where we observe an increase in faulting (around well 6305/5-1). By dividing the field, we can have better lithostratigraphic control and a better definition of the Net to Gross in the different zones. Also, it gives us a better definition of the GWC. In the southern part, the GWC is flat and presents minor oscillation due to local heterogeneities and general field structure. However, in the North, the water influx is more prominent, the dynamic setting of segmenting faults is more evident, and facies degradation increases in complexity.

The influx of over-pressured water contributes to an increase in pressure in the water column. Under normal circumstances, over-pressure in the water column would lead to a hydrodynamic setting. However, a low inflow rate, a correlation between higher pressures and shale content, and the dynamic position of polygonal faults and the calcified sandstones make a hydrodynamic setting less likely. Instead, we have flat contacts within each compartment, deeper with depth, giving an apparent tilted contact when it is overall flat. Formation pressures for wells 6305/4-1 (represented above) show the correlation between the shift in the GWC, the increase in pressure, and the depth of the calcified sandstone. More importantly, this well presents a gas down-to effect, which helps justify the improbability of the hydrodynamic effect. Looking at Grecula et al. (2015) work and the distribution of wells with gas down to effects, we observe a similar pattern in the Northern region of the field. From the observed trends, the essential characteristic of the Ormen Lange field trap is the lithostratigraphic component and its correlation to the distribution of polygonal faults. While the stratigraphy impacts are relatively evident, their correlation to the dynamic position of polygonal faults requires further investigation and characterization. Relative to the implication for HC volumetrics, the characteristics of the trap increase the uncertainty for the delineation of net pay due to its dependence on the interpretation of the GWC and the influence of the facies degradation and polygonal faulting on fluid flow and subsequent distribution.

Bibliography

Biddle, Kevin T. and Charles C. Wielchowsky (1994). 'Hydrocarbon Traps: Chapter 13: Part III. Processes'. In: *AAPG*, pp. 219–235.

Bünz, Stefan et al. (2005). 'Fluid flow impact on slope failure from 3D seismic data: a case study in the Storegga Slide'. In: *Basin Research* 17(1), pp. 109–122. DOI: https://doi.org/10.1111/j.1365-2117.2005.00256.x. eprint: https://onlinelibrary.wiley.com/doi/pdf/10.1111/j.1365-2117.2005.00256.x. URL: https://onlinelibrary.wiley.com/doi/abs/10.1111/j.1365-2117.2005.00256.x.

Net Pay Determination for Primary and Waterflood Depletion Mechanisms (Sept. 1998). Vol. All Days. SPE Annual Technical Conference and Exhibition. SPE-48952-MS. DOI: 10.2118/48952-MS. eprint: https://onepetro.org/SPEATCE/proceedings-pdf/98SPE/All-98SPE/SPE-48952-MS/1929748/spe-48952-ms.pdf. URL: https://doi.org/10.2118/48952-MS.

Dalland, A., D. Worsley and K. Ofstad (1988). *A lithostratigraphic scheme for the Mesozoic and Cenozoic and succession offshore mid- and Northern Norway*. Oljedirektoratet.

DENNIS, H., P. BERGMO and T. HOLT (2005). 'Tilted oil–water contacts: modelling the effects of aquifer heterogeneity'. In: *Geological Society, London, Petroleum Geology Conference series* 6(1), pp. 145–158. DOI: 10.1144/0060145. eprint: https://pgc.lyellcollection.org/content/6/1/145.full.pdf. URL: https://pgc.lyellcollection.org/content/6/1/145.

Gjelberg, J. et al. (Jan. 2005). 'The reservoir development of the Late Maastrichtian–Early Paleocene Ormen Lange gas field, Møre Basin, Mid-Norwegian Shelf'. In: *Petroleum Geology: North-West Europe and Global Perspectives—Proceedings of the 6th Petroleum Geology Conference*. Geological Society of London. ISBN: 9781862391642. DOI: 10.1144/0061165. URL: https://doi.org/10.1144/0061165.

Grecula, M. et al. (Jan. 2015). 'Interplay of fan-fringe reservoir deterioration and hydrodynamic aquifer: understanding the margins of gas development in the Ormen Lange Field'. In: *Tertiary Deep-Marine Reservoirs of the North Sea Region*. Geological Society of London. ISBN: 9781862396562. DOI: 10.1144/SP403.7. URL: https://doi.org/10.1144/SP403.7.

Mahmud Butt, Furqan et al. (Jan. 2015). 'Gross Rock Volume Estimation And Petrophysical Analysis Of Lower Eocene Sui Main Limestone In Sara West Block Lower Indus Basin, Pakistan'. In.

Masoudi, Pedram et al. (2011). 'Estimation of in Place Hydrocarbon Volume in Multilayered Reservoirs Using Deterministic and Probabilistic Approaches'. In: *Energy Exploration & Exploitation* 29, pp. 543–557.

Möller, N.K. et al. (Jan. 2004). 'A geological model for the Ormen Lange hydrocarbon reservoir'. In: *Norsk Geologisk Tidsskrift* 84, pp. 169–190.

Muggeridge, Ann and Hisham Mahmode (Feb. 2012). 'Hydrodynamic aquifer or reservoir compartmentalization?' In: *AAPG Bulletin* 96(2), pp. 315–336. ISSN: 0149-1423. DOI: 10.1306/06141110169. eprint: https://pubs.geoscienceworld.org/aapgbull/article-pdf/96/2/315/3375403/315.pdf. URL: https://doi.org/10.1306/06141110169.

Nanda, Niranjan C. (2016a). 'Direct Hydrocarbon Indicators (DHI)'. In: *Seismic Data Interpretation and Evaluation for Hydrocarbon Exploration and Production: A Practitioner's Guide*. Springer International Publishing: Cham, pp. 103–113. DOI: 10.1007/978-3-319-26491-2_6. URL: https://doi.org/10.1007/978-3-319-26491-2_6.

Nanda, Niranjan C. (2016b). 'Shear Wave Seismic, AVO and Vp/Vs Analysis'. In: *Seismic Data Interpretation and Evaluation for Hydrocarbon Exploration and Production: A Practitioner's Guide*. Springer International Publishing: Cham, pp. 149–170. ISBN: 978-3-319-26491-2. DOI: 10.1007/978-3-319-26491-2_9. URL: https://doi.org/10.1007/978-3-319-26491-2_9.

NPD (n.d.[a]). *6305/1-1*. URL: https://factpages.npd.no/en/wellbore/PageView/Exploration/All/3555.

NPD (n.d.[b]). *6305/4-1*. URL: https://factpages.npd.no/en/wellbore/PageView/Exploration/All/4441.

NPD (n.d.[c]). *6305/4-2 S*. URL: https://factpages.npd.no/en/wellbore/PageView/Exploration/All/6441.

NPD (n.d.[d]). *6305/5-1*. URL: https://factpages.npd.no/en/wellbore/PageView/Exploration/All/3144.

NPD (n.d.[e]). *6305/5-3 S*. URL: https://factpages.npd.no/en/wellbore/PageView/Exploration/All/6118.

NPD (n.d.[f]). *6305/7-1*. URL: https://factpages.npd.no/en/wellbore/PageView/Exploration/All/3535.

NPD (n.d.[g]). *6305/8-1*. URL: https://factpages.npd.no/en/wellbore/PageView/Exploration/All/4109.

NPD (n.d.[h]). *6305/8-2*. URL: https://factpages.npd.no/en/wellbore/PageView/Exploration/All/7579.

Roe, Espen (1999). *Well Report: Well 6305/1-1*. Tech. rep. Norsk Hydro.

Smith, Ru and Nicola Møller (2003). 'Sedimentology and reservoir modelling of the Ormen Lange field, mid Norway'. In: *Marine and Petroleum Geology* 20(6). Turbidites: Models and Problems, pp. 601–613. ISSN: 0264-8172. DOI: https://doi.org/10.1016/j.marpetgeo.2003.03.004. URL: https://www.sciencedirect.com/science/article/pii/S0264817203001351.

Stirling, Eleanor, Edith Fugelli and Mark Thompson (Oct. 2015). 'The edges of the wedges: a systematic approach to trap definition for stratigraphic, combination and sub-unconformity traps'. In.

Wiki, SEG (2020). *Direct hydrocarbon indicators*. URL: https://wiki.seg.org/wiki/Direct_hydrocarbon_indicators.

Yongyu Li, Jonathan Downton and Yong Xu (2003). 'AVO Modeling in Seismic Processing and Interpretation Part 1. Fundamentals'. In: *Recorder* 28(10). eprint: https://csegrecorder.com/articles/view/avo-modeling-in-seismic-processing-and-interpretation-part-1-fundamentals. URL: https://csegrecorder.com/articles/view/avo-modeling-in-seismic-processing-and-interpretation-part-1-fundamentals.

Appendix

A Well Log Availability

The log availability for each of the used wells is as follows:

- **6305/1-1:**
  - DEPT.M - DEPTH
  - DENS.G/CC - Bulk Density
  - DTCO.US/F - Delta-T Compressional
  - DTSM.US/F - Delta-T Shear
  - CALI.IN - Caliper
  - DENC.G/CC - Density Correction
  - GRC.GAPI - Gamma Ray
  - MEDR.OHMM - Medium Resistivity
  - RT.OHMM - Deep Resistivity
  - RXO.OHMM - Micro Resistivity
  - SP.MV - Spontaneous Potential
  - NEUT.FRAC - Neutron Porosity
  - BITS.IN - Nominal Bit Size
  - BADH. - Bad Hole Flag
- **6305/4-1:**
  - DEPT.M - DEPTH
  - GRC.GAPI - Gamma Ray
  - CALI.IN - Caliper
  - RMED.OHMM - Medium Resistivity
  - RDEP.OHMM - Deep Resistivity
  - RMIC.OHMM - Micro Resistivity
  - AC. US/F - Sonic Transit time (Sloweness)
  - DENS.G/CC - Bulk Density
  - SP. - Spontaneous Pontential
  - BITS.IN - Nominal Bit Size
  - NEUT.M3M3 - Neutron Porosity
  - PEF. B/E - Photoelectric Factor
- **6305/4-2 S:**
  - DEPT.M - DEPTH
  - CALI.IN - Caliper
  - RMED.OHMM - Medium Resistivity
  - RDEP.OHMM - Deep Resistivity
  - RMIC.OHMM - Micro Resistivity
  - DENS.G/CC - Bulk Density
  - DENC.G/CC - Density Correction
  - PEF - Photoelectric Factor
  - NEUT.v/v - Neutron Porosity

- AC. US/F - Delta-T Compressional)
- ACS. US/F - Delta-T Shear
- K. v/v - Potassium Concentration
- TH. v/v - Thorium Concentration
- U. v/v - Uranium Concentration
- GR.API - Gamma Ray
- BS.IN - Bit Size
- ROP. M/HR - Rate of Penetration

- **6305/5-1:**
  - DEPT.M - DEPTH
  - CALI.IN - Caliper
  - RHOB.G/CC - Bulk Density
  - DRHO.G/CC - Density Correction
  - DTCO.US/F - Delta-T Compressional
  - DTSM.US/F - Delta-T Shear
  - GRC.GAPI - Gamma Ray
  - RT.OHMM - Deep Resistivity
  - RXO.OHMM - Micro Resistivity
  - MEDR.OHMM - Medium Resistivity
  - NPHI. FRAC - Neutron Porosity
  - BITS.IN - Nominal Bit Size
- **6305/5-3 S:**
  - DEPT.M - DEPTH
  - CALI.IN - Caliper
  - DEN.G/CC - Bulk Density
  - DENC.G/CC - Bulk Density Correction
  - RMED.OHMM - Medium Resistivity
  - RDEP.OHMM - Deep Resistivity
  - RMIC.OHMM - Micro Resistivity
  - PEF. B/E - Photoelectric Factor
  - NEUT.FRAC - Neutron Porosity
  - AC. US/F - Delta-T Compressional)
  - ACS. US/F - Delta-T Shear
  - K. v/v - Potassium Concentration
  - TH. v/v - Thorium Concentration
  - U. v/v - Uranium Concentration
  - GR.API - Gamma Ray
  - BS.IN - Bit Size
  - ROP. M/HR - Rate of Penetration
- **6305/7-1:**
  - DEPT. M - Depth
  - ETC2.IN - Unrecognised
  - PEFZ.B/E - Photoelectic Factor

- HLLS.OHMM - Medium Resistivity
- HLLD.OHMM - Deep Resistivity
- RXOZ.OHMM - Micro Resistivity
- RHOZ.G/CC - Bulk Density
- TNPH.% - Neutron Porosity
- HCAL.IN - Caliper
- NPHI.% - Neutron Porosity
- HRD.OHMM - Deep Resistivity
- HRM.OHMM - Medium Resistivity
- ETC3.IN - Unrecognised
- HRS.OHMM - Micro Resistivity
- HRHO.G/CC - Bulk Density
- HPHI.FRAC - Neutron Porosity
- HCAL1.IN - Caliper
- HDT.US/F - Sonic Transit Time (Slowness)
- SP.MV - Spontaneous Potential
- HGR.GAPI - Gamma Ray
- HDAR.IN - Caliper
- CHAM.DEG - Unrecognised
- HDMX.IN - Caliper
- HDMI.IN - Caliper
- RD1.IN - Unrecognised
- RD2.IN - Unrecognised
- RD3.IN - Unrecognised
- RD4.IN - Unrecognised
- RD5.IN - Unrecognised
- RD6.IN - Unrecognised
- CDF.LB - Unrecognised
- ETC1.IN - Unrecognised
- HDRA.G/CC - Density Correction
- GDEV.DEG - Deviation
- DF.LB - Unrecognised
- ECGR.GAPI - Gamma Ray
- BS.IN - Nominal Bit Size
- HMNO.OHMM - Micro Resistivity
- HMIN.OHMM - Micro Resistivity
- RSOZ.IN - Caliper
- DSOZ.IN - Caliper
- TENS.LB - Cable Tension

- **6305/8-1:**
  - DEPT.M - DEPTH
  - CALI.IN - Caliper
  - BITS.IN - Nominal Bit Size
  - GR.API - Gamma Ray

  - DEN.G/CC - Bulk Density
  - K. PPM - Potassium Concentration
  - TH. PPM - Thorium Concentration
  - U. PPM - Uranium Concentration
  - RMED.OHMM - Medium Resistivity
  - RDEP.OHMM - Deep Resistivity
  - RMIC.OHMM - Micro Resistivity
  - PEF. B/E - Photoelectric Factor
  - SP. - Spontaneous Pontential
  - AC. US/F - Sonic Transit time (Sloweness)
  - NEUT.FRAC - Neutron Porosity

- **6305/8-2:**
  - DEPT.M - DEPTH
  - AC. US/F - Delta-T Compressional)
  - ACS. US/F - Delta-T Shear
  - BS.IN - Bit Size
  - CALI.IN - Caliper
  - DEN.G/CC - Bulk Density
  - DENC.G/CC - Bulk Density Correction
  - GR.API - Gamma Ray
  - K. PPM - Potassium Concentration
  - TH. PPM - Thorium Concentration
  - U. PPM - Uranium Concentration
  - RMED.OHMM - Medium Resistivity
  - RDEP.OHMM - Deep Resistivity
  - RMIC.OHMM - Micro Resistivity
  - ROP. M/HR - Rate of Penetration
  - NEUT.M3M3‘ - Neutron Porosity
  - PEF. B/E - Photoelectric Factor

B Nomenclature

- **AI** - Accoustic Impedance
- **AVO** - Amplitude vs Offset
- **BP** - British Petroleum
- **CSF** - Clean Sand Fraction
- **ERU** - Egga Reservoir Unit
- **FWL** - Free Water Level
- **GRV** - Gross Rock Volume
- **GWC** - Gas-Water contact
- **HC** - Hydrocarbons
- **JML** - Jan Mayen Lineament

- **NST** - North Sea terminology
- **NH** - Norsk Hydro
- **NMO** - Normal move out
- **OWC** - Oil-Water contact
- **RF** - Recoery factor
- **STGIIP** - Stock-Tank Gas Initially In Place
- **STB** - Stock Tank Barrel
- **STOIIP** - Stock-Tank Oil Initially In Place
- **VHT** - Våle Heterolithic Unit
- **VT** - Våle Tight

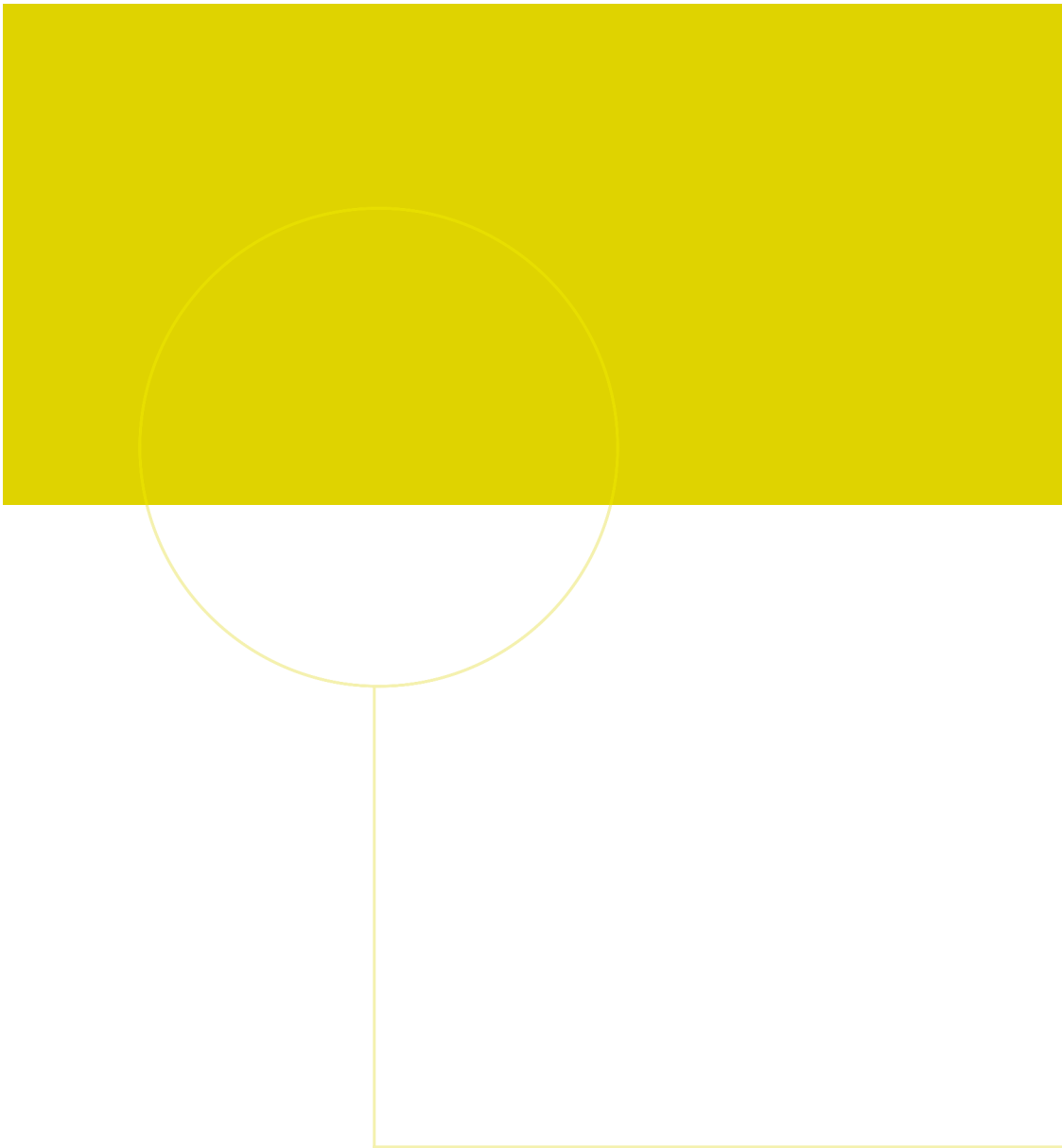

NTNU

Norwegian University of
Science and Technology